Long-lived Mesoscale Convective Systems over Eastern South Africa

by

Dedricks Monyai Morake

Thesis presented for the degree of DOCTOR OF PHILOSOPHY in the Department of Oceanography, University of Cape Town

July 2021

Dedication

This PhD thesis is dedicated to my parents Stephen and Christina Morake, my two sisters Mirriam Mdhlovu and Rebecca Morake, my brothers Ranchelo Mohosetji and Johanna Mdhlovu. To my three nieces Atlegang, Rirhanzo and Botlhale and my nephew Sandile Mdhlovu. Lastly, to my partner Tshegofatso Mokwena. I love you all, this is for you.

Ditebogo ke di lebisa go Modimo mong wa dithata tsotlhe, ke leboga diphuka tsa magodimo tse di mphuthetseng go fitlha mo nakong e. Batsadi, bonkgonne mmogo le ditsala ke lebogela tshegetso le tshusumetso ya lona. Noko!!!!!

Supervisors.

Prof. Chris Reason

Department of Oceanography, University of Cape Town, South Africa

Dr Ross Blamey

Department of Oceanography, University of Cape Town, South Africa

Funding

I am very grateful for funding from the National Research Foundation (NRF) through the Applied Centre for Climate and Earth System Science (ACCESS) and the University of Cape Town (UCT) Doctoral Research Scholarship.

Plagiarism declaration

I know the meaning of plagiarism and declare that all the work presented in this thesis is my own, save for that which is properly acknowledged. This thesis contains less than 80,000 words including appendices, bibliography, footnotes, tables, and equations, and has less than 150 Figures.

I confirm that I have been granted permission by the University of Cape Town's Doctoral Degrees Board to include the following publication in my PhD thesis, and where co-authorships are involved, my co-authors have agreed that I may include the publication:

D.M. Morake, R.C. Blamey, and C.J.C. Reason, 2021: Long-lived Mesoscale Convective Systems over Eastern South Africa. Journal of Climate, **34** (15), 6421-6439.

Signature: Date: 10 July 2021

Student Name: Dedricks Monyai Morake Student Number: MRKDED001

Abstract

Previous studies on severe weather in South Africa have often focused on synoptic-scale systems such as cut off lows, tropical extratropical cloud bands, and tropical cyclones, with little attention placed on the smaller mesoscale convective systems (MCSs). On a global scale, MCSs are not only important as key rainfall producers, but are often responsible for flooding, severe winds, hail and sometimes tornadoes. MCSs in South Africa remain poorly understood with there being little evidence of any long-term climatology studies of these systems over the region.

A climatology of large, long-lived MCSs over eastern South Africa for the extended austral summer (September-April) from 1985-2008 is presented. On average, 63 MCSs occur here in summer, but with considerable interannual variability in frequency. The systems mainly occur between November and March, with a December peak. This seasonal cycle in MCS activity is shown to coincide with favorable convective available potential energy (CAPE) and vertical shear profiles across the domain. Most systems tend to occur along the eastern escarpment with its sharp topographic gradients close to the warm waters of the northern Agulhas Current. The eastern escarpment can act as a convective trigger by mechanically uplifting sufficiently moist and unstable air masses. In addition, strong latent heat fluxes from the northern Agulhas Current help to create high-CAPE conditions. Typically, initiation begins in the early afternoon, MCS status is reached mid-afternoon, maximum extent early in the night and termination around midnight or shortly thereafter. The analysis also considered MCSs that developed over land versus those over the adjacent ocean. It is found that most MCSs initiate over land, but systems that initiate over the ocean tend to last longer than those that develop over land. The results also show that there are differences in the seasonal cycle between continental and oceanic MCSs, with oceanic systems containing two intraseasonal peaks (December and April).

There is a relatively strong positive relationship between the southern annular mode (SAM) and early summer MCS frequency. For the late summer, the frequency of MCSs appears related to the strength of the Mascarene high and Mozambique Channel trough, which modulate the inflow of moisture into eastern South Africa and the stability of the lower atmosphere over the region. The

results indicated that there is considerable variability in the long-lived MCS frequency on interannual time scales and such variability can have considerable impacts on regional rainfall totals during the summer months over eastern South Africa.

MCSs are known to produce heavy rainfall that is often associated with floods, which can be devastating to livestock, crops, infrastructure, and humankind. However, these systems also provide important rainfall within a short time span that is significant for rain-fed agriculture for a semi-arid country as South Africa. Using Climate Hazards Infrared Precipitation with Stations (CHIRPS) satellite rainfall data for 1985-2008, this study identified 38 daily extreme rainfall events which account for 40% of the top 50 extreme rainfall events over the two sub-domains of the eastern parts of South Africa that are linked to long-lived MCSs. Of the 38 events, systems duration ranged between 6-51 hours with 23 systems lasting for longer than 12 hours. Individual MCS-associated extreme daily rainfall events contribute between 21% - 54% to the total seasonal amount of rainfall over eastern South Africa. There is also noticeable interannual variability of seasonal rainfall over the northern and the southern domain, and considerable spatial variability in seasonal rainfall of MCS-related extreme rainfall events over the two sub-domains.

In general, the thesis has contributed to a better understanding of the wider group of large, long-lived MCS characteristics over eastern South Africa in terms of their distribution, frequency, life cycle, seasonal cycle and large-scale environmental conditions and the relationship between MCS frequency and interannual climate mode of variability such as El Niño-Southern Oscillation (ENSO), the subtropical south Indian Ocean dipole (SIOD), and SAM. The study also contributed to a better understand the role MCSs play in eastern South Africa summer rainfall and particularly extreme rainfall in the region.

Acknowledgements

I would give thanks to my supervisors, Professor Chris Reason and Dr Ross Blamey for their guidance, advice, input, support from when I was choosing my PhD research topic and through to completion of this thesis. I am very grateful for their assistance, mentorship, constant availability, patience and for giving me the opportunity to work with them. Sincere thanks to my family for their continual support, encouragements, and for making it possible for me to further my studies. The thanks also go to NRF, ACCESS and UCT Postgraduate Funding for financial support. Lastly, I would like to give thanks to my partner, friends, and colleagues from the department of Oceanography for their love, support, and encouragement in completing this thesis.

List of Figures

List of Tables

Table of Contents

Chapter 1: Introduction

Previous studies of the global distribution of favorable severe weather environments (e.g., Brooks et al. 2003) and of intense thunderstorms (e.g., Zipser et al. 2006) often identify southeastern Africa and the adjacent ocean as a "convective hotspot". In a recent example, convective storms along the east coast of South Africa during austral summer 2019/20 caused 44 deaths, destroyed 3000 houses, and led to considerable damage to infrastructure. This region as well as much of southern Africa receives most of its rainfall in summer through convective systems (Tyson and Preston-Whyte, 2000). The eastern South Africa region experiences the majority of its rainfall during the austral summer months (November-March), which is predominantly convective nature with warm sea surface temperatures (SSTs) over the east coast of South Africa acting as source of moisture during the late summer season (January – March) (**Fig. 3.1a**) (Tyson and Preston-Whyte, 2000). The rainfall peak over this region is during January and is greater than 100 mm per month from November to March with decrease in rainfall during winter (June and July) which is coincident with colder SSTs over the neighbouring ocean. The onset of the summer rains takes place as the Mascarene high retreats southeastward over the South Indian Ocean, the Saint Helena high moves southeast towards the southwestern tip of South Africa and the tropical convergence zones move poleward facilitating the inflow of relatively moist and unstable air into southern Africa from the western Indian and tropical southeast Atlantic (Reason et al. 2006). Elsewhere, southwestern South Africa is a winter rainfall region (Mediterranean-type climate) whereas the south coast receives rainfall nearly all year round (Weldon and Reason, 2014; Engelbrecht et al. 2015).

Studies of severe weather in southern Africa have mainly focused on synoptic-scale systems such as tropical-extratropical cloud bands (e.g., Hart et al. 2010, 2013), cut-off lows (e.g., Singleton and Reason, 2007ab; Favre et al. 2012) or landfalling tropical cyclones (e.g., Reason and Keibel, 2004; Mawren et al. 2020). Smaller systems, such as mesoscale convective systems (MCSs), are often overlooked. MCSs are convective storms that are organized, through induced mesoscale circulations, into a single cloud system (Zipser, 1982; Houze, 2004; Houze, 2018). Although there are various criteria to classify MCSs, they may be loosely defined as long-lived (≥3h)

cumulonimbus cloud systems that contain a precipitation area extending at least 100 km or more in at least one direction (Houze, 2004). There are numerous types of MCSs, but the most well-known are squall lines (linearly organized systems) and Mesoscale Convective Complexes (MCCs) defined as large, long-lasting quasi-circular systems (Maddox, 1980; Velasco and Fritsch, 1987; Fritsch and Forbes, 2001; Houze, 2004; Houze, 2018).

Occurrences of MCS activity are common in both tropical as well as mid-latitude land and ocean areas. This activity has been documented over parts of North America (Maddox, 1980; Ashley et al. 2003; Ashley and Ashley, 2008; Feng et al. 2019; Haberlie and Ashley, 2019; Cheeks et al. 2020), South America (Velasco and Fritsch 1987; Durkee and Mote, 2009; Durkee et al. 2009; Rasmussen et al. 2016), Europe (Laing and Fritsch, 1997; Morel and Senesi, 2002; García-Herrera et al. 2005; Kolios and Feidas, 2010), Asia (Laing and Fritsch, 1993b; Virtsa and Houze, 2016; Yang et al. 2019; Zhao et al. 2020), Australia (Keenan and Carbone, 1992; Cifelli and Rutledge, 1998; Perrin and Reason, 2000) and Africa (Laing and Fritsch, 1993a; Laurent et al. 1998; Mathon et al. 2002; Blamey and Reason, 2009, 2012; Liu et al. 2019). These systems mainly occur in summer but can occur during the transition seasons of autumn and spring.

The typical development of an MCS is through a single cell storm growing from the organization and triggering of secondary new cells or the amalgamation of smaller convective storms into a single cloud system. Understanding all the processes that result in convection being sustained and organized into an MCS remains a key scientific challenge. In general, the large-scale environments of such long-lived systems are associated with considerable horizontal temperature, moisture and stability gradients, along with considerable variations in both horizontal and vertical wind shear (Laing and Fritsch, 2000). Factors like environmental wind shear play an important role in the organization and maintenance of an MCS through influencing storm features such as updraft tilt and storm-relative inflow of moist unstable air (Parker and Johnson, 2000, 2004; Alfaro, 2017). Such environmental conditions can further be influenced by topography (e.g., Mulholland et al. 2019) with Fritsch and Forbes (2001) noting that most MCS populations occur downstream (typically within 1500 km) of north-south extending mountain ranges. Thus in the Americas, MCSs are often found on the leeward sides of the Rocky and Andes Mountains (Laing and Fritsch, 1997; Machado et al. 1998; Laing and Fritsch, 2000; Zipser et al. 2006; Rasmussen et al. 2016).

Mesoscale convective systems play a key role in the hydrological cycle and global circulation through the redistribution of energy, heat, and moisture in the atmosphere (Brooks and Dotzek, 2008; Yang et al. 2017; Feng et al. 2019). These systems often make large contributions to seasonal rainfall totals (e.g., Fritsch et al. 1986; Ashley et al. 2003; Nesbitt et al. 2006; Durkee et al. 2009; Blamey and Reason, 2013), producing rainfall that is important for sustaining people's livelihoods and the regional economy. Slow-moving or long-lasting MCSs often lead to extreme flooding, hail and strong winds (Maddox 1980; Maddox et al. 1986; Velasco and Fritsch, 1987; García-Herrera et al. 2005; Blamey and Reason, 2009; Durkee and Mote, 2009; Nuryanto et al. 2019).

Research on MCSs within Africa is mostly confined to the Sahel (e.g., Laurent et al. 1998; Laing et al. 1999; Mathon and Laurent, 2001; Mathon et al. 2002; Goyens et al. 2012; Vizy and Cook, 2018; Fitzpatrick et al., 2020; Klein et al., 2020) and the equatorial region (e.g., Taylor et al. 2018; Hartman, 2021). The southern Africa region has received relatively limited attention. Individual case studies of MCSs in South Africa have revealed that a single system can produce a considerable amount of rainfall (e.g., Rouault et al. 2003; Blamey and Reason, 2009). The only relatively long-term analysis of MCSs in southern Africa, based on Meteosat-7 data, was performed by Blamey and Reason (2012). In a subsequent study, Blamey and Reason (2013) showed that these MCSs can make a considerable contribution to warm season rainfall totals across eastern South Africa and southern Mozambique. However, two limitations to the Blamey and Reason (2012, 2013) analysis were that only a subset of MCSs, namely MCCs, were considered and that it only covered a 9-yr period (1998-2006). The limitation of a short study period of Blamey and Reason (2012) resulted in no clear evidence of any relationship between MCCs and the main modes of climate variability.

The El Niño-Southern Oscillation (ENSO) is considered the dominant driver behind interannual summer rainfall variability over southern Africa, with widespread drought typically occurring during El Niño events (Lindesay, 1988; Rocha and Simmonds, 1997; Reason et al. 2000; Cook, 2001; Reason and Jagadheesha, 2005). Other large-scale modes of climate variability that are known to influence regional summer rainfall include the southern annular mode (SAM) and the subtropical south Indian Ocean dipole (SIOD). The SAM, a zonally-symmetric mode of variability

in the Southern Hemisphere, consists of an out-of-phase geopotential height variations pattern between the mid-latitudes and high latitudes (Hartmann and Lo, 1998; Thompson and Wallace, 2000). Gillett et al. (2006) attribute the increase in summer rainfall in eastern South Africa during a positive phase in SAM (decrease in geopotential height over the Antarctic and increase in the midlatitudes) to anomalous easterly winds advecting more moisture from the Indian Ocean. The SIOD, on the other hand, is a regional mode of variability characterised by warm (cool) SST anomalies in the southwest Indian Ocean and cool (warm) in the southeast Indian Ocean together with anticyclonic (cyclonic) wind anomalies over the basin and has been linked with increased (decreased) summer rains over large areas of southeastern Africa during the positive (negative) phase (Behera and Yamagata, 2001; Reason, 2001, 2002).

This thesis uses data spanning 24 years and studies large, long-lived, intense MCSs, which is still a small subgroup of MCSs. Particularly defined minimum lifetime of 6 hours considerably decreases the range of sampled MCSs and will affect MCS lifecycle conclusions drawn from this study. The focus on long-lived (lasting at least 6 hours) MCSs represents a subgroup that includes the very important MCCs but may easily exclude shorter-lived MCSs that also typically occur in convective regions. The MCS sample analysed here will much more be active into the evening and nighttime hours and will develop certain characteristics that will not necessarily apply to the shorter-lived MCSs which are excluded from this study. Although shorter-lived MCSs produce less rainfall in total, their instantaneous rainfall can sometimes be just as extreme in some local areas.

Numerous flood and drought events, including multi-year droughts (Blamey et al. 2018), have occurred during this period so it is of considerable interest to investigate variability in MCS characteristics in this region. Furthermore, the nearby location of the Drakensberg Mountains and warm Agulhas Current (**Fig. 3.1**) with its large latent heat fluxes (Rouault et al. 2003), have been previously found to be favorable for severe weather (Rouault et al. 2002; Singleton and Reason, 2006; Blamey and Reason, 2009; Blamey et al. 2017), hence the focus on this domain, leaving the tropical southern African region for future work.

This thesis comprises the following chapters: An overview of the literature on the general atmospheric circulation and rain-producing weather systems over southern Africa during austral summer, and a brief overview of MCSs and tracking methods that are used to identify/track these systems in **Chapter 2. Chapter 3** contains the data and methods that were used in the study. **Chapter 4** presents analysis of the long-lived MCSs climatology produced during the extended summer (September-April) over eastern South Africa for 1985-2008. **Chapter 5** deals with the insight on the long-lived MCSs and extreme rainfall events over two sub-domains over eastern South Africa, and their rainfall contribution to seasonal rainfall and monthly rainfall totals. Finally, summary and conclusions are presented in **Chapter 6**.

The main aims of this thesis are twofold, with the first relating to the development of the long-lived MCS climatology for the period 1985-2008, based on which we can gain a better understanding of seasonal and interannual MCS variability and the large-scale circulations that are favouring the development of long-lived MCSs in the region during extended summer months (September-April). Secondly, an attempt is made to investigate the impact of long-lived MCSs over part of eastern South Africa by examining the links between long-lived MCSs and extreme rainfall events, and their contribution towards regional summer rainfall totals. To achieve these aims, the following questions are addressed:

Chapter 4:

- What are the spatial distribution, frequency, life cycle, and seasonal cycle of long-lived MCSs over eastern South Africa?
- What are the favourable large-scale environmental conditions for development of long-lived MCSs?
- What is the role of the ocean in the development and intensification of long-lived MCSs over eastern South Africa?
- Are there any relationships between long-lived MCS frequency and the main climate modes of variability such as ENSO, SIOD, and SAM?

Chapter 5:

- What is the role of large, long-lived MCSs in extreme rainfall events over eastern South Africa ?
- What is the contribution of extreme rainfall events that are associated with large, long-lived MCSs towards seasonal and monthly rainfall totals?

Chapter 2: Literature review

2.1. Introduction

Southern Africa experiences strong climate variability on a range of time scales, and it is prone to occurrence of floods and droughts (Mason and Jury, 1997; Cook et al. 2004; Reason et al. 2006; Singleton and Reason, 2007; Dieppois et al. 2016; Reason, 2016; Driver and Reason, 2017). Its regional climate is influenced by multiple factors including topography, semi-permanent atmospheric circulation systems, geographical location in the subtropics and tropics, the air-sea interaction of the highly dynamic and variable oceans to its west, east and south (**Fig. 2.1**).

Rainfall over southern Africa has strong seasonality; most of southern Africa receives the majority of its rainfall during austral summer (and particularly in December-February, DJF) (**Fig. 2.2**). Along the west and southwest coasts of South Africa and adjacent inland areas is a winter rainfall dominated region while further east along the south coast there is an all season rainfall region (Blamey and Reason, 2013; Weldon and Reason, 2014; Engelbrecht et al. 2015; Reason, 2016). A bimodal rainfall regime exists in northeastern Tanzania and Kenya with the short rains during October-December and the long rains during March-May on average.

The main atmospheric circulation features that affect southern Africa are the semi-permanent, high pressure systems over the subtropical South Indian and South Atlantic Oceans, the Inter-Tropical Convergence Zone (ITCZ) and the Circumpolar Trough over the Southern Ocean (Reason and Rouault, 2005; Reason et al. 2006). The relationships between these features and the regional climate variability are still not completely understood.

2.2. Regional atmospheric circulation

Southern Africa is strongly influenced by the position and strength of the subtropical South Atlantic high pressure (SAHP) and South Indian high pressure (SIHP) systems (Tyson and

Preston-Whyte, 2015). The SAHP is semi-permanent anticyclone cell over the South Atlantic Ocean that shifts 6^{o} meridionally and has a zonal shift of about 13^{o} within the seasons (Reason et al. 2006). This anticyclonic feature drives southerly winds along the west coast of southern Africa producing upwelling, along the South African west coast in summer but throughout the year along the Namibian coast (Reason et al. 2006). The zonal movement and intensification of the SAHP near the subcontinent, particularly during the summer, is linked to formation of a coastal low level jet along the Namibian coast (Nicholson, 2009; Lima et al. 2018). Further north, a warm pool of SST develops over the tropical southeast Atlantic during summer from which moisture flows towards the Congo basin and Angola (Reason et al. 2006; Reason, 2016). This inflow converges with that from the tropical western Indian Ocean where strong convergence of moisture occurs. On average, the tropical southeast Atlantic is considered to be less important than that from the tropical western Indian Ocean (Reason et al. 2006) but it can make important contributions during some summers (Rouault et al. 2003; Reason and Smart, 2015; Rapolaki et al. 2020) or on shorter scales (Cook et al. 2004).

Low-level westerlies from the tropical southeast Atlantic converge with the low-level easterly winds from the Indian Ocean in the Congo Air Boundary (CAB) convergence zone (Torrance, 1979). The seasonal migration of the CAB has been identified as a key process that indicates the southward shift of the African tropical rain belt (Howard and Washington, 2019). Another convergence zone exists over tropical southeastern Africa which merges in with the ITCZ over the low latitude Indian Ocean where surface northeasterly and southeasterly trade winds converge (**Fig. 2.1**). The ITCZ is found in all tropical oceans and is known as a key component of the general circulation of the Earth (Yan, 2005). It shifts strongly north and south of the equator over the Indian Ocean and neighbouring land masses with associated strong monsoonal wind reversals in this region. After crossing the equator over the western Indian Ocean by November, the ITCZ is at its southernmost position over the Mozambique Channel and Madagascar in February with northeast monsoonal flow towards Tanzania which then recurves across northern Mozambique and the Channel as northwesterlies towards Madagascar. In March it retreats northwards and by May it is established north of the equator with strong southeasterly flow along the northern Mozambique and Tanzanian coasts. As these winds strengthen in May and June, they recurve as the Findlater jet blowing along the Kenyan / Somali coast to bring the SW monsoon to India in northern summer.

Over the South Indian Ocean, the SIHP is semi-permanent anticyclone cell typically located somewhere between 20ºS and 35ºS. One of the centres of the anticyclonic activity in the Southern Hemisphere, this high-pressure system is thought to play a crucial role in the evolution of subtropical south Indian Ocean dipole (SIOD) events (Behera and Yamagata, 2001; Hermes and Reason, 2005). The SIHP results in easterly and northeasterly flow along the eastern coast of South Africa and Mozambique (**Fig. 2.1**). During summer, the SIHP migrates southeastward away from South Africa allowing frontal systems to track closer to southeastern South Africa and potentially link up with disturbances in the easterlies to form tropical-extratropical cloud bands (Hart et al. 2013). The South Indian Ocean is regarded as a major source of moisture for summer rainfall due to its warm SST and because many of the summer rain-producing weather systems have a substantial easterly component to their track (Rouault et al. 2003; Hansingo and Reason, 2009).

Midlatitude westerlies exist on the southern margins of the SAHP and SIHP (as well as in the midlatitude South Pacific) and extend to near the Antarctic continent. The core of this westerly regime forms the Circumpolar Trough over the Southern Ocean. During the winter season, this trough and associated westerly winds shift equatorward bringing rainfall to the southwestern tip of South Africa. In the summer months, they retreat poleward together with the SAHP shifting south-eastwards, resulting in dry conditions over western South Africa.

On more regional scales, the Mozambique Channel trough (MCT) is a cyclonic feature that is characterised by a low-pressure area over central and southern Mozambique which is prominent in austral summer (**Fig. 2.1)** (Cook et al. 2004, Munday and Washington, 2017). The MCT is generated by a dynamical adjustment of the easterlies flowing over the high topography of Madagascar (reaching over 2000 m – **Fig. 2.1**) and can also be sustained by local air-sea interaction of relatively warm SST over the Mozambique Channel (Barimalala et al. 2018, 2020). The role of the MCT in southern Africa climate is not well understood. In recent studies, Barimalala et al. (2018; 2020) have shown that variation in the MCT can strongly impact the moisture transport coming from the southwest Indian Ocean (SWIO) into the subcontinent and trigger an increase in rainfall over the southern African mainland. These authors confirmed that a weak (strong) MCT strengthens (weakens) the South Indian Ocean Convergence Zone (SICZ; Cook, 2000) and favours

(weakens) the transport of moisture from the SWIO into the subcontinent which promotes an increase (decrease) in local rainfall (Barimalala, et al. 2020).

Another regional circulation system is the Angola Low (denoted AL in **Fig. 2.1**) which is a low to mid-troposphere cyclonic system found over southern Angola and northern Namibia (Reason et al. 2006; Munday and Washington, 2017). Munday and Washington (2017) defined the mean state of the Angola Low as a heat low during austral spring (October-November; ON), that is driven by strong surface heating whereas in summer (December-February; DJF) it is more like a tropical low and is associated with moist instability. The Angola Low is found to dominate lower to mid-troposphere atmospheric circulation, and to be one of the important regional circulation systems that influence the interannual and synoptic variability of summer rainfall over southern Africa (Cook et al. 2004; Reason et al. 2006; Fauchereau et al. 2009; Hart, et al. 2010).

In addition, a continental heat low develops in summer over the central Kalahari Desert. The heat low helps to induce a weak cyclonic circulation, which can divert the low-level northeasterlies further south (Hart et. al. 2010). The Angola Low starts to develop around October each year at low levels, and it strengthens during January and February (Munday and Washington, 2017). It can act as a tropical source region for the tropical extra-tropical cloud bands or tropical-temperate troughs (TTTs) which bring a substantial contribution to the summer rainfall over sub-tropical southern Africa (Harrison, 1984; Reason et al. 2006; Hart et al., 2010, 2013).

The Botswana high is a prominent circulation system in the mid-level of the troposphere centred over central Namibia and western Botswana that occurs during austral spring, summer, and early summer (October-April) (**Fig. 2.1)** (Driver and Reason, 2017; Reason, 2016). The Botswana high is well known to the weather and long-term forecasters in the region, but it has not been given much attention in the research literature except in connection with rainfall over Zimbabwe (Matarira, 1990; Ratna et al. 2013). Its seasonal cycle, low frequency variability, and impacts on southern Africa summer rainfall and temperature were examined by Reason (2016) and Driver and Reason (2017). While some of its rainfall impacts may be related to the El-Niño Southern Oscillation (ENSO), the Botswana High may also affect variability in summer rainfall and temperature directly. Furthermore, the variability in the Angola Low and the Botswana high have

been associated with summer rainfall anomalies over southern Africa (Cook et al. 2004; Reason and Jagadheesha, 2005; Reason, 2016; Driver and Reason, 2017). In general, the strengthening (weakening) of the Angola Low is associated with above (below) average rainfall over southern Africa, while strengthening (weakening) of the Botswana high is associated with below (above) average rainfall over southern Africa.

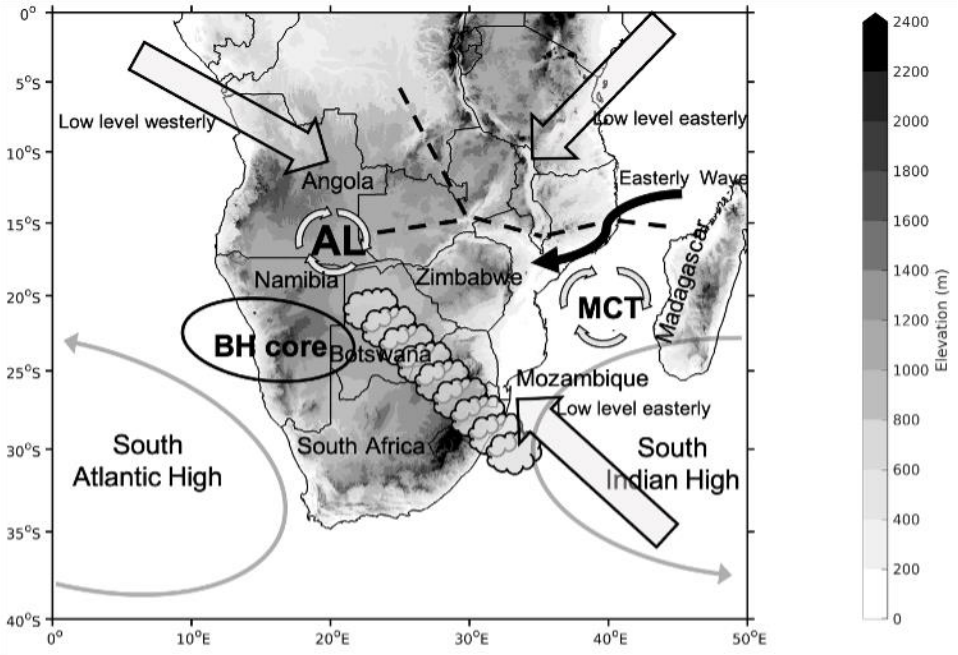

Figure 2.1: A schematic showing the important atmospheric features of southern African climate during austral summer. The AL (Angola Low) and cyclonic circulation over the Angola region donate the Angola Low. The core of the Botswana high at the 500 hPa level is shown by a black ellipse, as a black short line the ITCZ over the western Indian Ocean, and its meridional arm through the Congo Basin and stretching toward the Angola Low. The cloud bands lying diagonally from the Angola Low across subcontinent represent the mean position of the tropical extra-tropical cloud bands in the region. The high-pressure systems over the two oceans and the three light shaded arrows represent the three-primary low-level moisture streams and the black arrow represents easterly waves (Adapted from: Driver and Reason, 2017).

2.3. Large-scale climate modes and southern African rainfall

The regional circulation of southern Africa is not only influenced by its surrounding oceans, but it is also strongly affected by SST variability in the Pacific Ocean, particularly due to ENSO, the Southern Ocean Mode, known as the SAM, and the SIOD.

2.3.1. El-Niño Southern Oscillation

The El-Niño Southern Oscillation is a coupled ocean-atmosphere phenomenon which involves oscillation of atmospheric pressure between the tropical eastern and western Pacific Ocean, affecting the climate of the tropics and subtropics on interannual time scales (periodicity ranging between two and seven years) (Nicholson and Entekhabi, 1987; Preston-Whyte and Tyson, 1988; Philander, 1983). The positive (negative) phases of ENSO are defined as an El Niño (La Niña) characterised by anomalously warm (cold) waters in the tropical eastern and / or central Pacific Ocean. This variation in ocean temperatures is due to changes in the winds which then alters atmospheric circulation, rainfall patterns and distribution of clouds on a global scale. The shift in position of warm / cold in the western SSTs of the tropical Pacific leads to change in deep atmospheric convection and then generation of planetary waves that propagate the impacts to the mid-latitude and high latitudes of both the Northern and Southern Hemisphere (Wallace and Gutzler, 1981; Ropelewski et al. 1986; Kiladis et al. 1989; Colberg et al. 2004).

In southern Africa, ENSO has the greatest impact on the summer rainfall regions during its mature phase of the ENSO events, by altering the position of cloud bands which are the major summer rain-producing systems in the region (Fauchereau, 2009; Mason and Jury, 1997). During the positive phase - El Niño, the major convergence zone shifts to the east, causing the tropical extra-tropical cloud bands to form offshore over the South Indian Ocean which leads to reduced rainfall over the mainland of southern Africa (Hart et al. 2013). In addition, high pressure anomalies and increased subsidence over the region during El Niño events tends to result in less convection over southern Africa and drought (Lindesay, 1988, Reason et al. 2000; Cook, 2001). On the other hand, during the negative phase - La Niña, the primary zone of convergence is situated over land, leading to above average summer rainfall over southern Africa. Hart et al. (2018) showed that El Niño

seasons are characterised by a reduced number of cloud bands, and they tend to move offshore during El Niño events, while La Niña years typically experience a climatological number of cloud bands and those that do occur are likely to be more intense. However, reduced rainfall over southern Africa during strong El Niño events does not always occur (Reason and Jagadheesha, 2005; Lyon and Mason 2007; Blamey et al. 2018). For example, the strongest El Niño event of 1997/98 did not lead to the expected rainfall anomalies. While the relatively weak El Niño events of 1991/1992 and 2002/2003 were associated with widespread and severe drought, the dry conditions were less intense during the El Niño event of 1997/1998 (Reason and Jagadheesha, 2005). These rainfall patterns highlight the nonlinear relationship between El Niño events and southern Africa summer rainfall, which has been well documented (Reason and Jagadheesha, 2005; Fauchereau et al. 2009; Boulard et al. 2013). However, it has been suggested that the lack of severe drought during 1997/1998 may be due to the Angola Low that had not been weaker than average during this summer (Reason and Jagadheesha, 2005; Lyon and Mason, 2007). A similar lack of an impact on the Angola Low was attributed by Driver et al (2019) to the lack of widespread drought during the 2009/10 El Niño. Better understanding of how ENSO influences southern African summer rainfall is needed because of the varied and nonlinear nature of the associated impacts over the region.

2.3.2. Southern Annular Mode

The Southern Annular Mode (SAM) is the leading mode of climate variability in the extratropical Southern Hemisphere, with opposing geopotential height perturbations of opposite signs between the mid-latitudes near about 40ºS and Antarctic near 65ºS (Marshall, 2003; Gillett et al. 2006). This mode leads to hemispheric-scale changes in mid-latitude wind and SST and has been shown to have impact on both summer (Gillett et al. 2006) and winter (Reason and Rouault, 2005) rainfall regions of South Africa. The positive phase of the SAM is associated with negative geopotential height anomalies over polar latitude and positive geopotential height anomalies over the mid-latitudes which leads to easterly wind anomalies over east and southeast of South Africa (Thompson and Wallace, 2000). The easterly flow hinders the advection of moisture into the coastal regions of southwestern South Africa in winter and weakens approaching cold fronts, leading to reduced rainfall over western South Africa (Reason and Rouault, 2005, Mahlalela et al.

2019). The anomalously wet winters in the South-Western Cape region of South Africa have been linked to the negative phase of the SAM (Reason et al. 2002; Reason and Rouault, 2005, Mahlalela et al. 2019). However, little work has considered its potential influence on the rest of southern Africa (Reason et al. 2006).

2.3.3. Subtropical South Indian Dipole

The subtropical South Indian Ocean dipole (Behera and Yamagata, 2001) is defined as the SST anomaly difference in SSTs between one pole over the southeastern Indian Ocean south of Madagascar and the other one over the southwestern Indian Ocean near Western Australia, has been shown to have a relationship with summer rainfall over large parts of southern Africa. The SIOD usually develops in December-January and reaches its peak in February (Behera and Yamagata, 2001). The SIOD has positive phase characterised by unusually warm SST in SWIO south of Madagascar and anomalously cool SST in the SWIO off Australia and it is associated with the occurrence of high-pressure anomalies in the mid-latitude South Indian Ocean. When the SIOD is in positive phase, above average summer rainfall tends to occur with the reverse during the negative SIOD events (Behera and Yamagata, 2001; Reason, 2001, 2002).

2.4. Rainfall producing weather systems

The summer rain-producing weather systems over southern Africa result from the disturbances in the general atmospheric circulation over the tropical and the mid-latitudes (Blamey and Reason, 2012), ranging from short-lived single cell thunderstorms to large-scale systems. In low latitudes, African easterly waves (AEWs) are waves in the atmosphere that move from east to west over the Sahel region of Africa and they are the largest in the mid-levels of the atmosphere (Russell et al., 2017). AEWs initiated through convective heating in the central and eastern Africa (Hsieh and Cook, 2008; Crétat et al., 2015), propagate westward and interact with convection (Hsieh and Cook, 2008; Crétat et al., 2015). Numerous studies associated the generation of waves with an instability of the Africa easterly jet, while according to Schubert al. (1991) easterly waves are a result of zonal flow instability associated with ITCZ. However, easterly waves over southern

Africa (**Fig. 2.1**) are semi-stationary and are almost exclusively a summer phenomenon with an annual cycle peaking between December and February (Tyson and Preston-Whyte, 2000). Easterly waves occur over the north-western desert and semi-desert areas of southern Africa in response to strong surface heating in summer (Tyson and Preston-Whyte, 2000). Consequently, they are shallow and hardly extend to the 500 hPa level. Unlike their counterparts over north of the Equator, they are not travelling waves in the easterlies (Tyson et al., 1996). On average, the easterly waves dissipate near Madagascar, where a standing wave over the steep orography is found. However, in some years when climatic conditions are suitable, easterly waves penetrate further westward (Jury and Elvis, 2000). Easterly waves play a more important role for rainfall over southern Africa in the late summer (e.g., Tyson and Preston-Whyte, 2000). Widespread heavy rainfall north of about 25^{o} -30^{o} S can occur due to the passage of easterly waves across southern Africa without cloud band development (Dyson and Van Heerden, 2001).

Tropical-extratropical cloud bands (also referred to as TTTs in earlier literature) result from interactions between a westerly disturbance passing south of South Africa and a tropical disturbance over the low latitude interior. These cloud bands are known to be the main synoptic rainfall producing system over subtropical southern Africa during summer (Harrison, 1984; Reason et al. 2006; Hart et al. 2010). They are characterised by convective activity and clouds that extend in a northwest-southeast direction that stretches from the tropical disturbance (e.g., the Angola Low in many cases – **Fig. 2.1**), which transport heat and moisture to the mid-latitudes. Such cloud bands can often lead to high rainfall in the region (Hart et al. 2010). These authors found that the cloud band events that occurred in January 1998 contributed more than 40% of the rainfall during that summer season over South Africa.

Additional weather systems associated with significant rainfall over southern Africa during summer include mesoscale convective systems (MCSs), cut-off lows (COLs) and tropical lows. COLs are important weather systems defined as cold cored systems that form when the upper troposphere troughs become cut-off from the westerly waves and are displaced equatorward of the polar jet streams (Singleton and Reason, 2007; Nieto et al. 2008; Favre et al. 2012). These weather systems are often associated with deep moist convection, which can lead to significant amounts of

rainfall over a short period of time, resulting in flash-flooding (Singleton and Reason, 2007). On occasion, these systems can produce more than 100 mm rainfall within a day. COLs are often seen throughout all seasons but seem to be more frequent over South Africa during winter, showing two peaks in occurrence near the west coast and near the east coast (Omar and Abiodun, 2020). Tropical lows are middle level cyclonic vortices that form in the tropical easterlies and are regarded as a weather system that contributes rainfall in the tropical edge (from west to the east coast of southern Africa between 12-22^{o} S) (Howard et al. 2019). In the ocean when conditions are favourable, tropical lows may intensify into tropical cyclones. However, tropical lows that exist over land and do not intensify are much less catastrophic than tropical cyclones, but more frequent (Hunt and Fletcher, 2019; Howard et al. 2019).

Coastal areas of South Africa and southern Mozambique can receive rainfall during summer from cold fronts (particularly in early summer) and ridging anticyclones. Cold fronts are defined as the baroclinic boundary between cold and warm air masses, where temperature decreases by at least 3^{o}C (Tyson and Preston-Whyte, 2015). Cold fronts are associated with transition zones between relatively warmer and colder air at a frontal zone (cold air replacing warm air) (Tyson and Preston-Whyte, 2015; Lennard, 2019). These systems tend to bring rainfall over the south-western, north-western Cape (predominantly winter rainfall region), as well as the south coast and east coast (Lennard et al. 2017). Ridging anticyclones are high pressure systems that often originate from budding of anticyclones from the South Atlantic Ocean and are subsequently responsible for the transport of moisture from the SWIO into the southern Africa (Dyson, 2015; Landman et al. 2017; Ndarana et al. 2020). This weather system is common during the summer half of the year with a peak in occurrence during austral spring (September-October) (Tyson et al., 1996) and is known to produce widespread rainfall over the eastern part of southern Africa (Crimp and Mason, 1999; Tyson and Preston-Whyte, 2000). In this region, ridging anticyclones are associated with 60% of rainfall days during the summer rainfall season per year (Ndarana et al. 2020).

Daily latitudinal shifts in the position of the SAHP can strongly affect the subcontinent's weather. The SAHP may ridge eastward and south of the subcontinent, extended ridging leads to budding of a separate high which then drifts eastward into the SWIO before merging into the South Indian high. The newly formed ridging anticyclone with westerlies may strongly affect the weather of

South Africa (Tyson and Preston-Whyte, 2015). Briefly, the weekly synoptic cycle and its relationship with the ridging anticyclone following passage of a cold front is described. On the first day, the circulation is dominated by subtropical highs, thereafter a low emerges in the midlatitude westerlies south of South Africa which as it drifts eastward, trails its associated cold front across the southern part of South Africa on the third day (Tyson and Preston-Whyte, 2015; Ndarana et al., 2018). On the fourth day, the front moves off the east coast, at the same time the Atlantic high begins to ridge eastward towards Cape Town. By the fifth day, a large ridging anticyclone has broken off from its parent SAHP and is drifting around the tip of the subcontinent and into the SWIO. Then on the sixth day, the ridging high has merged into the SIHP and the circulation patterns become like day one again to complete the synoptic cycle (Tyson and Preston-Whyte, 2015, Ndarana et al., 2018).

Since ridging anticyclones, cold fronts and the midlatitude part of the cloud bands all track along and south of the coast, the presence of the warm Agulhas Current near the east and south coasts of the country play an important role in rainfall generally over South Africa (Reason, 2001b) as well as in the diurnal cycle of the rainfall over South Africa (Rouault et al. 2013). Highest rainfall occurs near the east coast (**Fig. 2.2**), where SST is at its warmest, and is further enhanced by orographic effects such as the Drakensberg mountains in eastern South Africa. The close proximity of the warm Agulhas Current to the east coast has been shown to not only result in high latent heat fluxes, transferring more moisture to the atmosphere than the surrounding waters (Rouault et al. 2003), but also result in local storm intensification (Rouault et al., 2002). Garstang et al. (1987) described how the interaction between the topography of the northeastern escarpment with that of westerly waves propagating across the southern tip of Africa has been shown to assist in the development of convective storms that lead to high rainfall over eastern South Africa. The topographic lift along the eastern escarpment and westerly wave dynamics lead to the strong ascent of moist air (Garstang et al., 1987; De Coning et al., 1998). Previous studies done on diurnal cycle of the rainfall in other parts of the world have shown a midnight to early morning maximum in the frequency of rainfall events in coastal areas, a late afternoon to early evening maximum over the continental interior, and a nighttime maximum in mountainous areas. All of the above-mentioned spatial patterns are predominantly the result of convection, local land / sea breeze circulations, orography, and convection and important for eastern South African rainfall (Rouault et al. 2003).

2.5. Extreme rainfall events over southern Africa

Southern Africa may experience extreme rainfall events during the austral summer that are related to convective storms, ranging from single cell storms through to organised systems such as mesoscale convective complexes (MCCs) (Blamey and Reason 2012, 2013), squall lines (Rouault et al. 2002) and tropical storms (Reason and Keibel, 2004; Rapolaki and Reason, 2018). Other rainfall producing systems that can also lead to extreme rainfall events over the region include tropical extratropical cloud bands (Harrison, 1984; Reason et al. 2006; Hart et al., 2010, 2013) and COLs (Singleton and Reason, 2007; Nieto et al. 2008; Favre et al. 2012). Extreme rainfall events over southern Africa are often associated with major socio-economic impacts and sometimes loss of life. These extreme rainfall events may induce floods that collapse small dams, reservoirs, and severely road infrastructure. Severe-weather-producing systems over the region include tropical cyclones (e.g., Dyson and Van Heerden, 2001; Reason and Keibel, 2004; Rapolaki and Reason, 2018), COLs (e.g., Singleton and Reason 2006, 2007; Favre et al. 2012) and MCSs (e.g., Blamey and Reason, 2009, 2012).

Studies have shown considerable spatial and temporal variability in the intensity of extreme rainfall over many regions of South Africa (Groisman et al., 2005; Kruger, 2006; Rapolaki et al., 2019), while low frequency changes in rainfall are less clear (Lennard et al., 2013). Dyson et al. (2015) noted that there is an apparent transition in atmospheric conditions over South Africa from an extratropical nature in early summer, thus the region experiences more intense / strong sheared thunderstorms that produce strong winds and hail, and more tropical nature in late summer, producing slower moving but heavier rainfall type thunderstorms. It is essential to understand the changing nature of extreme rainfall events in the country and weather systems linked to these extremes. In order to mitigate or prepare for extreme rainfall events it is necessary to understand the spatial and temporal characteristics of extreme rainfall events in terms of frequency, intensity, seasonality, and understand any changes that may have occurred within these attributes.

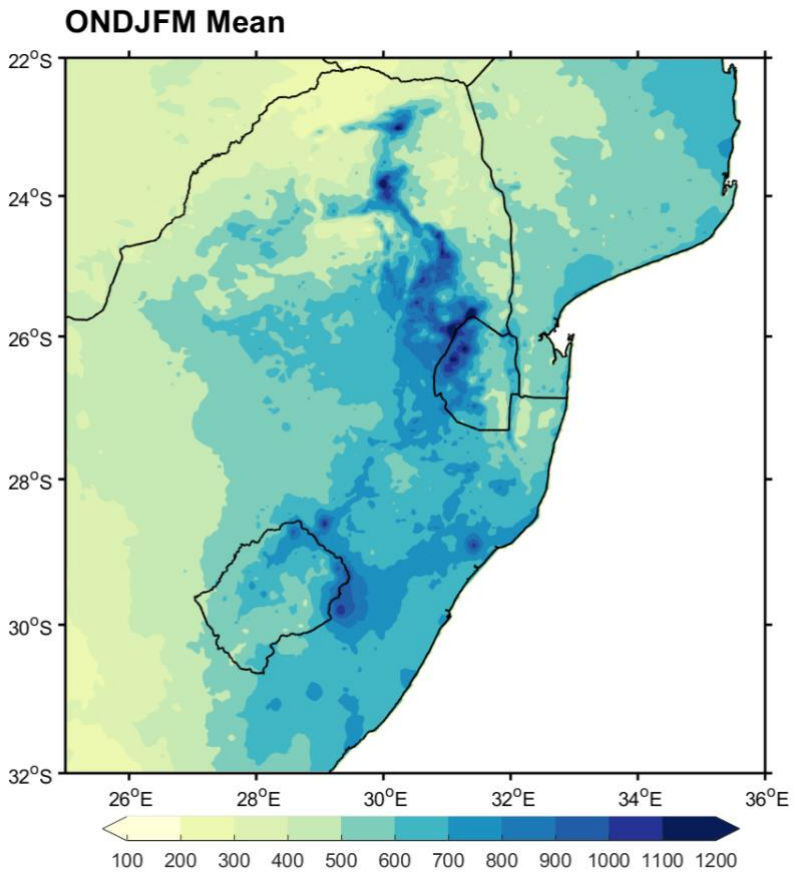

Figure 2.2: The extended austral summer (October to March) seasonal Mean rainfall (shaded; mm) over the Southeast Africa. The mean is based on CHIRPS daily data from 1985-2008. cell n.

2.6. Mesoscale convective systems

Mesoscale convective system is a term used to describe an ensemble of thunderstorms that satisfy certain spatial and temporal criteria. These large convective storms result when smaller convective storms merge and organize into a single cloud system. Mesoscale refers to the size (km^2) of the weather system, while convective refers to the type of storm, and systems simply mean that they are organised into one cloud system. There are various criteria to classify MCSs, they are given a general definition as a long lived (≥3 hours) cumulonimbus cloud systems that contain a precipitation area of roughly 100 km or more in at least one direction (Houze, 2004; Liu et al., 2019). The formation of MCSs is typically associated with weak mid-tropospheric short-wave

troughs and weak surface fronts, and their growth is often supported by low level thermal forcing and convective instability (Maddox et al. 1986; Yang et al. 2019). The organisation of MCS is typically characterised by different processes, operating on range of different scales which include, namely strong heating of sufficiently moist and unstable air masses over land, available moisture sources (e.g., warm ocean), a lifting mechanism (e.g., flowing over high topography), and favourable wind shear (Hodges and Thorncroft, 1997; Laing et al., 2008; Rehbein, 2018; Houze, 2018). These systems are not only classified based on the size, but also in terms of the geometry of the system and the relative arrangement of the convective and stratiform rainfall regions.

In general, there are two categories of these systems, which are linear systems and quasi-circular systems. There are numerous types of MCSs, but most common are squall lines (Cotton, 2000), which are classified under the category of linear systems and are found in the tropics and mid-latitudes. These systems are usually dominated by a line of convective cells in the front, followed by stratiform rainfall and some authors (e.g., Parker and Johnson, 2004) suggested that linear systems could be considered as a development phase for many MCSs. Another specific type of MCS are MCCs, which are among the largest of the MCSs defined by Maddox (1980). These systems are defined as large systems extending to about 350 000 km^2 in area of a cloud shield exhibiting a quasi-circular organised system and lasting for more than 10 hours (Maddox, 1980; Laing and Fritsch, 1997; Blamey and Reason, 2009; Blamey and Reason 2012, 2013; Houze, 2018). MCCs require additional features to satisfy the conditions favourable for their formation. Laing and Fritsch (1997) through a global study of MCCs noted that these systems have a strong tendency to occur in certain regions of the world where there are low-level jets occurring in the lee (relative to prevailing mid-level flow) of major mountain ranges (evaluated terrain). The eccentricity is used to differentiate the specific systems from the other MCSs, some systems can obtain the size and duration of MCC but fail to show a quasi-circular appearance. These large more linear type systems are given the name Persistent Elongated Convective Systems (PECS, Anderson and Arritt, 1998).

Environmental conditions that are favourable for the development of MCSs include low static stability, CAPE, baroclinic frontal zone, vertical wind shear, low level convergence, and upper-level divergence (Laing and Fritsch, 1997; Coniglio et al. 2010; Yang et al. 2017). MCSs are

typically associated with a low-level jet (LLJ) which provides low level advection of equivalent potential temperature and vertical wind shear (Cheeks et al. 2020). MCSs require favorable synoptic environments, they can also initiate from local forcing, such as a land-sea breeze or lifting mechanism (e.g., mountain-plains solenoid). MCSs occur in the presence of CAPE and wind shear, however there is evidence that too much shear limits MCS duration (Yang et al. 2017), and environments with more CAPE and shear favor development of Supercells rather than MCSs (Thompson et al. 2012). MCSs typically initiate with a group of convective cells that are organised by their proximity or shared initial forcing (**Fig. 2.3**). MCSs take on the form of organisation shown in **Fig. 2.3**, where a new cell forms on or just ahead of the leading edge of the storm. As cells move through the storm, they undergo their life cycles. New cells form, the older cells weaken and evolve into larger, contiguous region of stratiform precipitation (Cheeks et al. 2020). At n + 1 and n, the cells are in a developing stage, with updraft air lifting the cells and precipitation particles developing aloft but not yet raining. Precipitation particles are initiated near cloud base at n +1 and grow by collecting cloud water (**Fig. 2.3**). The convective component of MCS requires a continuous inflow of moisture, while the stratiform component is comprised of leftover of ice particles from convection that are aloft by a larger, mesoscale updraft (Cheeks et al. 2020).

2.6.1. Global distribution of MCSs

Mesoscale convective systems are distributed over the tropical and mid-latitude areas (both land and ocean) in all continents except the Antarctic (Maddox, 1980, Laing and Fritsch, 1993a, Houze, 2004). The use of different satellite images enables researchers to locate the global distribution of MCSs using features such as lighting distribution, ice in clouds and regions of convective versus stratiform precipitation (Houze, 2004). These intense systems occur primarily over land, where they can benefit from the peak of low-level buoyancy that is generated by daytime heating (Houze, 2004). Previous studies have shown that conditions over land often favour the rapidly moving squall line MCSs, especially in regions of strong shear (e.g., sub-Saharan Africa which is influenced by the African easterly jet) (Houze, 2004). Huang et al. (2018) have also shown that globally MCSs occur more frequently and are more intense over land than over oceans.

Previous studies on MCSs have mostly been conducted outside Africa with a few studies that have included Africa being focused on Sahel Region (e.g., Laurent et al. 1998; Laing et al. 1999; Mathon and Laurent, 2001; Mathon et al. 2002; Goyens et al. 2012; Vizy and Cook, 2018; Fitzpatrick et al., 2020; Klein et al., 2020), East Africa (Vemado et al., 2021) or subtropical southern Africa (e.g., Blamey and Reason, 2012, 2013). On average, about 9 MCCs events occur over southern Africa per year and can contribute up to 20% of the total summer rainfall (November-March), with some producing about a third of total monthly rainfall over the region (Blamey and Reason, 2012, 2013). However, the processes behind the occurrence of MCSs over southern Africa are still not well understood including their contribution to seasonal rainfall totals and extreme rainfall in the region (Blaney and Reason, 2012). The geographic setting of the region, in particular the location of the Drakensburg / eastern escarpment and the warm SSTs of the Agulhas Current region in relation to the prevailing mid and upper-level flow is likely important for the development of MCSs (Blamey and Reason, 2009, 2012, 2013). A previous study (Blamey and Reason, 2009) has shown that an individual MCS event can produce more than 100 mm of rainfall in a day over eastern South Africa.

Although not much research has been done on MCS in South Africa, earlier work suggests that systems over this region appear to follow the mechanisms of MCS drivers that were found in other regions globally (Laing and Fritsch 1993, 1997; Blamey and Reason, 2012, 2013). It is important to note that studies on the global distribution of favourable severe weather environments (e.g., Brook et al. 2003) and of intense thunderstorms (Zipser et al. 2006) have identified southeastern Africa and the Agulhas Current as a convective “hotspot”. Garstang and Tyson (2000) suggested that the occurrence of MCSs over South Africa is typically the result of many interacting processes, operating on different scale ranging from the synoptic scale to local conditions. These authors noted that the possible controls of cumulus convective development appear to be the atmospheric stability and availability of moisture in the lower levels. The impact of MCSs on the south and east coast of South Africa, has already been highlighted by Rouault et al. (2003) and Blamey and Reason (2009; 2013).

2.6.2. Life cycle of MCS

Mesoscale convective systems have three key moments of their life cycle namely: initiation, maturity, and dissipation. Initiation refers to the moment when the first thunderstorms generally develop, maturity refers to the moment when the area of continuous cloud top reaches a maximum extent in size, and dissipation refers to the moment when the definition of MCS is no longer met (Liu et al. 2021). The moments of MCSs life cycle may occur at any time of the day, but the occurrence frequency at each moment shows an obvious diurnal variation (Chen and Houze, 1997; Kolios and Feidas, 2010). The differences in the diurnal variation of MCS over land and ocean have been noted in many previous studies (e.g., Chen and Houze, 1997; Tsakraklides and Evans, 2003; Kolios and Feidas, 2010; Huang et al. 2018). The MCSs over land occur in the afternoon, they initiate between 1500 – 1700 LST, followed by the maximum extend which takes 2-4 hours to organise into a MCS status, hence the largest MCS number exist between 1800-2000 LST and last for 3-4 hours before dissipating around midnight (Huang et al. 2018). In contrast, there is no distinct diurnal variation or preferred initiation time of MCSs over the ocean areas. Oceanic MCSs have two peaks in the maximum extent of spatial coverage, one occurring at 0500 – 0600 LST, and the other occurring in the afternoon at 1400-1600 LST (Tsakraklides and Evans, 2003; Huang et al. 2018). The Oceanic MCSs tend to dissipate more frequently in the afternoon between 1500-1700 LST.

The reason behind the distinct differences in the diurnal variation between the land based and ocean based MCSs are related to the large diurnal thermal variations over land than over the ocean. MCS activities over the coastal areas are also regulated by the local occurrence of land / sea breezes (Goyens et al. 2012; Huang et al. 2018). In terms of duration of these convective systems, it has been found that there is a near linear relationship between the average convective systems radius and its life cycle (Machado et al. 1998). MCSs are defined to have duration of longer than 3 hours but the largest MCSs subset MCC usually last for around 10-13 hours from storm initiation to the time they shrink to below the minimum MCC size criteria (Laing and Fritsch, 1997; Jirak et al. 2003; Ashley et al. 2003). Laing and Fritsch (1997) noted that MCCs with large cold cloud shield usually last longer than those with small cloud shield. However, factors that determine how these systems attain these large dimensions (maximum size)

are not fully understood, it is believed to be the combination of dynamic and thermodynamic properties that determine the limitation on the ultimate size and duration of an MCS, and in some cases it appears to be dynamic rather than the thermodynamic (Cotton, 2000; Houze, 2004). MCS with short during tend to initiate later in the afternoon than MCSs with longer duration and this is explained by the fact that systems that initiate later in the afternoon when the diurnal heating is decreasing, most of these short-lived systems do not have enough time to develop and establish mesoscale circulation which could allow them to last longer before instability disappears later at night (Morel and Senesi, 2002).

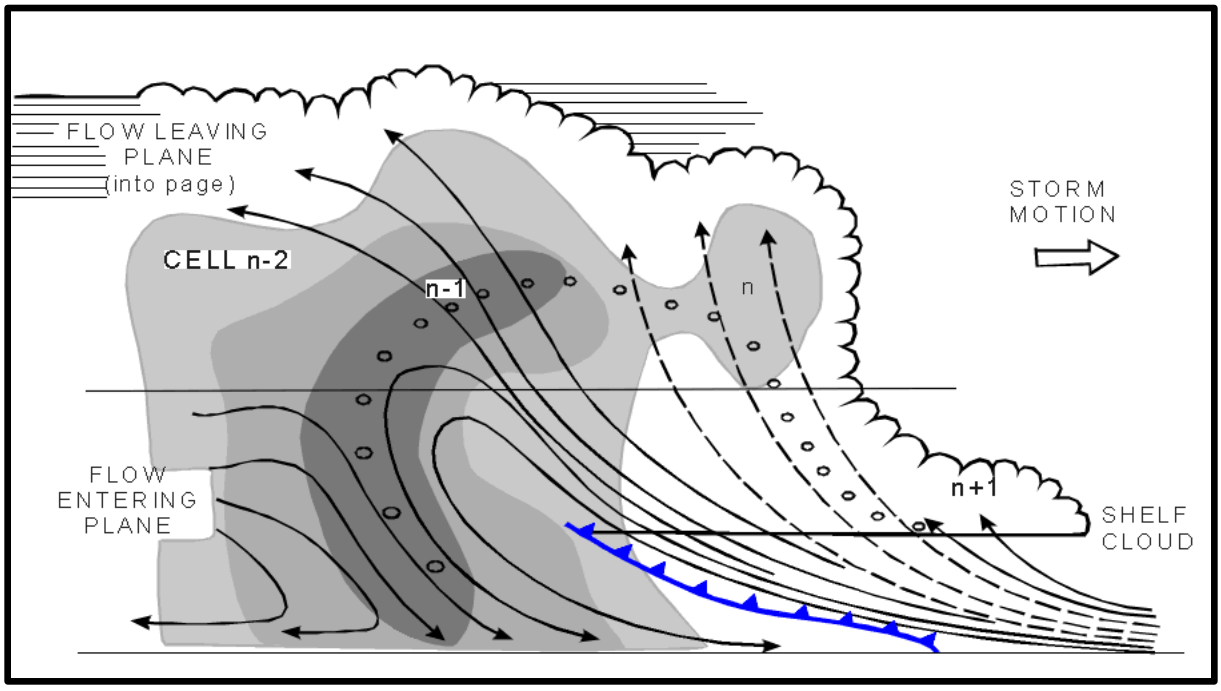

Figure 2.3: A schematic showing a model of a multicell thunderstorm. It shows a typical vertical cross section through a multi-cell storm, grey shades represent radar reflectivities of 35, 45 and 50 dBz. There are four successive cells in different stages of development. Cell n-2 is already in dissipating stage, cell n-1 is in mature stage and forms the centre of the storm, cell n is in development stage and a shelf cloud n+1 flat base indicating an active updraft form ahead of the cell n.

2.7. MCS tracking methods

Detecting MCSs using satellite data has a long history and involves two major steps: the identification of MCSs and the tracking of their evolution (e.g., Machado et al., 1998; Hennon et al., 2011; Fiolleau and Roca, 20113; Huang et al. 2018). In the early studies, researchers used manual tracking which required labour intensity with large uncertainties (Huang et al. 2018). The advancement in technology and increase in availability of satellite imagery has allowed researchers to study and observe convective systems over vast regions at regular time intervals. The use of radar has also allowed researchers to study and investigate the structure of MCSs in identifying the distribution of convective cells with stratiform precipitation (e.g., Bluestein and Jain, 1985; Parker and Johnson, 2000). The identification of MCSs from various types of meteorological data is crucial for studying their properties, characteristics, and in building their climatology (Whitehall et al. 2015). Research related to the seasonality of MCS has been limited by previous methodology such as dealing with the big data of identifying these systems in automated methods and other datasets (Whitehall et al. 2015).

In the beginning of the 1980s, the tracking and identification of MCSs became more automated using either infrared (IR) images that provided the cloud-top brightness temperature (BT), or a combination of IR and visible images that provided information on cloud characteristics, to obtain characteristic temperatures and areas defining a cloud cluster (Velasco and Fritsch, 1987; Augustine and Howard, 1991; Laing and Fritsch, 1993a; Laing and Fritsch, 1997; García-Herrera et al. 2005). The identification of MCS using IR image is based on a set of predefined criteria of the cloud-top BT threshold, and minimum area coverage of the cloud-top at respective BT threshold. Low BTs are generally used as a representation of the cold cloud shield of convective systems (used to allocate areas of deep contiguous convection). However, it is always a challenge for MCS identification due to the lack of agreement on the threshold to be used for the identification and tracking of these systems. In the literature, BT thresholds ranging from -18ºC and -65ºC (255 and 208 K) have been proposed (Chen et al. 1996; Machado et al. 1998). It has been noted that imposing stricter MCS identification criteria will certainly exclude some potential MCSs and using a less strict threshold may result in the inclusion of some spurious MCSs (Huang et al. 2018). Goyens et al. (2012) reviewed the criteria used for MCS identification and suggested

a broad adoption of BT threshold of -40 ºC (233 K) as a reasonable threshold and has been adopted globally and in Africa (mostly in West Africa).

Automatic tracking algorithms have then been proposed to overcome the limitations of the previously manual identification/tracking (Fiolleau and Roca, 2013), including the area-overlapping method (Williams and Houze, 1987; Mathon and Laurent, 2001), the overlap of ellipsoidal equivalents (Boer and Ramanathan, 1997), the centroid tracking method (Johnson et al. 1998), and the maximum spatial correlation method (Carvalho and Jones, 2001). The automated method is seen to be more efficient and allows for a larger, more complete climatology to be developed (Machado et al. 1998; Carvalho and Jones, 2001). However, it has been documented that one disadvantage of fully automated method includes the manner in which this method handles the evolution of MCS, particularly in the case of splitting and merging of systems (Machado et al. 1998, Durkee and Mote, 2009).

The use of IR and visible radiance is due that geostationary satellite produce IR images from the same position every about 30 minutes and tracking of MCSs needs high temporal resolution. Additionally, MCSs are associated with very cold cloud-top temperatures since these systems are associated with deep convection. Williams and Houze (1987) introduced the area-overlapping technique for tracking individual cloud clusters through time using IR satellite data. This technique tracked clusters by first identifying individual cloud-top areas with equivalent blackbody temperature less than -60ºC (213 K) to identify deep convection. If the area identified meets the size criteria of being sufficiently large (e.g., exceeding 5000 km^2), then it is deemed to be an MCS. Then overlap between consecutive satellite images is calculated. If overlap is at least 50 %, the two features are judged to be the same MCS. This method assumes that the MCSs in successive frames represents the same entity if there are sufficient common overlapping pixels in their images.

Evans and Shemo (1996) made use of the area-overlapping methods and in addition, they assigned rainfall to each system using two different IR-based rainfall algorithms. Tsakraklides and Evans (2003) improved this tracking algorithm whereby they included calculations of the complete set of system characteristics for warm cloud regions -38ºC (235 K) as well as information on the growth in vertical, and horizontal extent of the system. Mathon and Laurent (2001) introduced the

improvement of interpolating cluster life cycle in the case of missing data. Other methods have been developed to improve the technique that relies on minimisation of a cost function to solve the correspondence problem and these methods were used in multiple studies (Núñez Ocasio et al. 2020).

Carvalho and Jones (2001) identified and tracked convective systems using the magnitudes of the spatial correlation between consecutive satellite images and the change in horizontal areas of convective systems. In recent years, Fiolleau and Roca (2013) developed fully automated Tracking of Organised Convection (TOOCAN) algorithm for identification and tracking of MCSs. TOOCAN used the most convective cores of the cloud-top, identified by the low BT, and through clustering methods that associated cloud clusters through time. This method enabled the study of MCSs decomposed into their many small-scale features, which allowed for an earlier detection in life cycle (Núñez Ocasio et al. 2020). Whitehall et al. (2015) created automated algorithm "Grab 'em Tag 'em, Graph 'em" (GTG) using a graph theory. The algorithm identifies the cloud cluster with IR cloud-top brightness temperature approach, creates a corresponding graph node, then using area-overlap, the edges of the cloud cluster in consecutive satellite images and is weighted according to percentage overlap. The algorithm also assigns rainfall using Tropical Rainfall Measuring Mission (TRMM) 3-hourly product, 3B42. Application of GTG showed that the high overlapping percentage criterion (90%) in GTG makes the detection of small systems more difficult and inherently puts into question its ability to account for splits and mergers when small systems separate from bigger one and the data are regridded to a coarse resolution (Núñez Ocasio et al. 2020).

The area-overlapping tracking technique has been used widely to track MCSs using IR imagery (e.g., Williams and Houze, 1987; Chen et al., 1996; Mathon and Laurent, 2001). Some methods use a searching radius (Johnson et al. 1998) to find MCS in the next image rather than searching for overlapping pixels. The problem with fixed search radius is that MCSs can move at different speeds and thus a fixed radius is not reliable for all MCSs. However, these previous methods are unable to effectively identify, classify, track, and assign rainfall to MCSs over northern Africa without showing weakness either through methodology or by restricting resolution of satellite data. Núñez Ocasio et al. (2020) developed Tracking Algorithm for Mesoscale Convective Systems

(TAMS) algorithm that can effectively identify, track, classifies and assigns rainfall to MCSs throughout their entire lifespan. TAMS combines area-overlapping and projected-cloud-edge tracking technique to maximise the detecting progression of convective systems throughout their evolution, accounting for spits and mergers.

2.8. Summary

The focus of this chapter was to review existing background literature on the climate variability of southern Africa, and weather systems that bring most of the rainfall over the region. South African rainfall is subjected to interannual rainfall variability that may be linked to large-scale climate modes of variability. Most of the rainfall over the region occurring during the austral summer is linked to cloud bands, tropical lows, cut-off lows and MCSs.

This chapter has presented an overview of the climate of southern Africa in which organised convective systems play a large role during the summer half of the year. A very important category of these convective systems which have not been much studied over South Africa are mesoscale convective systems (MCS). Gaps in the existing literature on the variability, impacts and distributions of these systems over South Africa have been discussed within the context of what is known about them elsewhere. It is clear that the study of MCSs and their influence on southern Africa rainfall needs considerably more research. The only studies of MCSs in southern Africa, were done by Blamey and Reason (2012, 2013) on a particular subset of MCSs, namely MCCs. These authors provided evidence that MCCs can make a considerable contribution to warm season rainfall totals across eastern South Africa and southern Mozambique. However, there were limitations since the studies focused on MCCs only and the available dataset represented a rather short period which was insufficient to assess the potential influences of ENSO, the SIOD or SAM. Since a much longer-term global tropical (30^{o}S-30^{o}N) MCS data set (Huang (2017) is now available for 1985-2008, the objective in this thesis is to derive a climatology of MCSs over South Africa and to study their variability. This chapter also provided a platform to understand the algorithms and methods used for tracking and detecting MCSs, and how the advancement in technology and increase in available satellite imagery has allowed researchers to observe and study MCSs over vast regions at regular time intervals.

Chapter 3: Data and Methods

3.1. Domain

Figure 3.1 shows the study domain with Drakensberg and Maluti Mountains rising to about 2500-3500 m within a few hundred km of the warm Agulhas Current. In the interior of these mountains are mainly plains with interspersed low mountain ranges that gradually slope up towards the escarpment. In the east of the Drakensberg mountains, in KwaZulu-Natal (KZN) province contains a narrow coastal plain with numerous stepped terraces, steep valleys and smaller mountain ranges before the slope rises sharply up to the eastern edge of the Drakensberg escarpment.

The study region (Domain 1, the dark blue polygon in **Fig. 3.1**) extends from 38°E (offshore of the Agulhas Current) to well inland of the Drakensberg Mountains and from 23°-30°S. The southern latitude is determined by the limit of the available data (30°S-30°N) whereas 23°S is roughly the northern extent of the Drakensberg. The western boundary of Domain 1 was subjectively determined by first getting the longitude of the highest point along the entire stretch of the eastern escarpment and then moving 2 degrees further west. MCSs that are initiated outside the domain but then subsequently track through the domain are excluded from the analysis.

Within Domain 1, two smaller regions (the green polygon in **Fig. 5.1**) are defined to highlight the importance of MCSs for extreme daily rainfall totals. Extreme rainfall events in this region are poorly understood and little researched despite the region containing a large rural population and making substantial agricultural and tourism contributions to the national economy. These two smaller domains are defined based on South Africa Water Management Areas (see **Fig. 3.1**). The northern domain is the basin that feeds the Pongola/Phongolo River. This river flows into Pongolapoort/Jozini Dam, mainly used for irrigation and domestic use, before joining the Maputo River in Mozambique. Further motivation for choosing the northern sub-domain is that it lies south of the typical landfall location of tropical cyclones/storms in central Mozambique but north of the coastal region that typically gets significant rainfall from onshore flow associated with ridging anticyclones, thus it represents an interesting transition zone. The domain contains high

biodiversity including the World Heritage Site of iSimangaliso Wetland Park on the coast. The only previously documented MCS case study for southeastern Africa occurred in this sub-domain (Blamey and Reason, 2009). The southern domain is a merge of the Thukela and Mvoto to Umzimkulu Water Management Areas and contains the largest city in eastern South Africa (Durban, population of around 3.5 million). and tracking

3.2. MCS Database

The Huang et al. (2018) MCS identification and tracking are based upon combining the area-overlapping method with Kalman Filter (KF) based approaches. The area-overlapping method is conceptually straightforward and works reasonably well for tracking large and slow-moving MCSs (Huang et al. 2018). However, the method tends to fail small and fast moving MCSs, especially when the temporal resolution of satellite observation is low (Huang et al. 2018). The failure is because of the area-overlapping method assumes that the location and the area of MCSs do not change significantly with time. To solve the limitations of conventional area-overlapping methods, KF based methods were used in Huang et al. (2018) work. KF is an optimal estimator that can predict the state of a process and use measurement to correct its prediction (Huang et al. 2018). One of its many successful application is object tracking (Xing et al. 2009). In terms of estimating the speed and direction of the target systems, the KF method can robustly track small and fast-moving systems, which is not well-represented or even missed by conventional area-overlapping methods (Huang et al. 2018). As the results, the complete life cycles of MCSs can be better capture. The KF method first predicts the movement states of the potential MCS, then updates its estimation by maximising the posterior probability of the target potential MCS (Huang et al. 2018). The distance between the position of the potential MCS at time are then calculated to determine the most appropriate potential MCS for the continuation (Huang et al. 2018). One uncertainty of the KF algorithm stems from the measured position of the potential MCSs. The position of a potential MCS is determined by averaging the coordinates of the coldest 10 pixels inside the cold cloud shield (Huang et al. 2018). Then if the potential MCS contains fewer pixels, then the geographic information of the pixels is average to provide the position. Both methods have uncertainties into the position determination because of the irregular shapes and inhomogeneous spatial distribution of cloud systems (Huang et al. 2018).

Huang et al. (2018) used the European Union Cloud Archive User Service (CLAUS) project data (Hodges et al. 2000), a global dataset based on the calibrated International Satellite Cloud Climatology Project (ISCCP) B3 radiance data (Rossow and Schiffer, 1999) was used in this work. The CLAUS dataset has been widely used to detect convective activity (e.g., Nguyen and Duvel, 2008; Dias et al. 2012; Dong et al. 2016) and the available CLAUS data provides a 3-hourly global brightness temperature (BT) with intervals sampled at a 30 km (1/3 degree) resolution, which provides a good indication of convection.

A system is first identified in an image (based on a set of criteria), then using the geographic overlapping (with overlap thresholds) between the original identified system and cloud clusters on a subsequent image, the systems are matched and linked. Initiation is determined when no overlapping occurs in the preceding image and termination occurs when no cloud cluster is found in the next image. During this process, if the convective system satisfies the various criteria (discussed below) for a set amount of time, it is defined as an MCS. Various automated methods are used in the literature for MCS detection/tracking incluing but not limited to centroid tracking (e.g., Johnson et al. 1998), maximum spatial correlation (e.g., Carvalho and Jones, 2001), clustering methods (e.g., Fiolleau and Roca, 2013) and graph theory (e.g., Whitehall et al. 2015).

A challenge for MCS identification is the lack of consensus on the thresholds used to track the system as it evolves. The main defining criteria for MCS identification are based on the cold cloud shield BT and the size of the cold cloud shield at the respective BT threshold. A low BT is used as a proxy for convection taking place (i.e., used to delineate areas of deep, continuous convection) and this threshold varies between -18ºC and -65ºC (255 and 208 K) in the literature (Machado et al. 1998). Even colder BT thresholds are at times used to identify the convectively active areas of a particular system and can reveal the presence of overshooting tops. For most MCS studies in Africa (mostly West Africa), slightly narrower BT thresholds ranging from -40°C (233 K) to -60°C (213 K) have been used, with the lower threshold (-40°C) being commonly used (see Table 1 of Goyens et al. 2012). In the Huang et al. (2018) methodology, MCSs are identified as convective systems with a brightness temperature (BT) less than -40ºC (233 K) and a size threshold of 5000 km^2. However, because the focus of this study is on long-lived, intense MCSs, a filter is applied to the Huang (2017) database to extract such systems. Here, only systems that contained

BT values colder than a threshold of -52°C (221 K) and contain a corresponding area covering at least 10,000 km^2 are considered. Furthermore, the system is required to meet these two thresholds for at least 6 hours. These are very strict thresholds to define a larger group of MCSs other than MCCs, as mentioned in the aims of the thesis in the beginning. This more constrained BT threshold is similar to that applied to MCSs in the Americas (e.g., Maddox, 1980; Cotton et al. 1989; Anderson and Arritt, 1998, 2001; Durkee and Mote, 2009; Cheeks et al. 2020) and has previously been applied to MCCs in South Africa (Blamey and Reason, 2012). The 10,000 km^2 size threshold has previously been used in the literature (e.g., García-Herrera et al. 2005; Rafati and Karimi, 2017). Various size thresholds are used in the literature ranging from 100 km^2 through to 100,000 km^2 (Hitchens et al., 2012). These subjective thresholds can impact the MCS climatology developed for a particular domain. The focus of the study is on large, long-lived, intense MCSs, which is why a stricter set of thresholds were used, namely: a BT threshold of -52°C (221 K), a corresponding area covering at least 10,000 km^2 and lasting for a minimum of 6 hours. Given such thresholds and 3-hourly temporal resolution of the data smaller, short-lived MCSs and the timing of the storms that become an MCS are omitted from the analysis although they may sometimes produce substantial rainfall. This study uses the Huang (20117) MCS dataset, which extends over the domain (30ºN-30°S) for 1985-2008 and contains basic trajectory information along with the intensity, area, eccentricity, speed, direction, and duration of each MCS. MCSs identified in January 1985 or December 2008 are excluded since those two months lie outside the period covered by the CLAUS dataset.

3.3. Environmental conditions

CAPE and u and v winds from the high resolution ERA5 reanalysis (Copernicus Climate Change Service (C3S), 2017) are used to better understand seasonal conditions favouring MCS development. CAPE is a nonlinear combination of two of the ingredients described by Doswell et al. (1996) in identifying deep, moist convection, which are moisture and conditionally unstable lapse rates. In the ECMWF Integrated Forecasting System (IFS), CAPE is calculated by considering parcels of air departing at different model levels below the 350-hPa level. The maximum CAPE produced by the different parcels is the value retained. The calculation of this CAPE in ERA5, due to computational efficiency considerations, assumes: (i) the parcel of air does

not mix with surrounding air; (ii) ascent is pseudo-adiabatic (all condensed water is instantaneously removed by precipitation) and (iii) other simplifications related to the mixed-phase condensational heating. It is recognized that the quality of ERA5 derived CAPE remains untested for southern Africa due to the lack of sounding observations. Elsewhere, biases in the predecessor of ERA5, ERA-Interim, with some of the convective parameters, possibly related to boundary layer representation, have been identified in parts of Europe (Taszarek et al. 2018). For the same domain, ERA5 appears to produce a better agreement between pseudo-soundings and radiosonde data (Ukkonen and Mäkelä, 2019).

The development and evolution of an MCS and associated severe weather is also dependent on the vertical shear profile (Weisman and Klemp, 1982, 1984; Bluestein and Jain, 1985; Parker and Johnson, 2000; Coniglio et al. 2006; Coniglio et al. 2010). ERA5 u and v winds are used to calculate the 0-6 km (deep layer) wind shear. For the surface, winds at 100m above ground level are used, while for the 6 km level, winds from two pressure levels (400-hPa and 500-hPa) are used. A caveat with using reanalysis derived winds and not radiosonde observations (not available for the domain) is that the model may not be able to resolve orographically induced mesoscale circulations that may modify the environment around mountains (e.g., Púčik et al. 2017). As described earlier, eastern South Africa contains a narrow coastal plain, rising sharply up towards the eastern escarpment (2500-3500 m), while the interior of South Africa is a plateau, sitting around 1.6 – 1.9 km above sea level. Given the topography, the upper level to calculate the vertical wind shear in the coastal area was determined using the 500-hPa level and 400-hPa for the high lying regions. Only data covering the MCS period (1985-2008) is used and the 15h00 UTC (17h00 LST) data are presented here since local convective activity in South Africa typically occurs in the afternoon (Tyson and Preston-Whyte, 2000).

To better understand variability in MCS frequency, conditions favorable for MCS development are analysed through a composite analysis using monthly ERA5 data for years with anomalously high MCS activity. Given that there is an apparent transition in atmospheric conditions over South Africa from an extra-tropical nature in early summer [October-December (OND)] to a more tropical nature in late summer [January-March; (JFM)] (Dyson et al. 2015), the composite analysis is divided into OND and JFM. Moisture fluxes were computed from the horizontal winds and

specific humidity. The National Oceanic and Atmospheric Administration (NOAA) daily Optimum Interpolation Sea Surface Temperature (OISST), which is available from 1981 to present on a 1.0° × 1.0° horizontal grid (Reynolds et al. 2007), are used to analyse seasonal SST anomalies in the Indian and Atlantic Ocean for the composites. The statistical significance of the composite anomalies was determined using a two-tailed nonparametric Monte Carlo bootstrap statistical significance test. Monte Carlo method is one approach to numerically approximate an integral using a random sample from the domain of the integrand (Tofighi and MacKinnon, 2016, Hope, 1968). The nonparametric Mento Carlo bootstrap technique, the sample data set is treated as a population and the sampling distribution is approximated by taking a number of the repeated sample from the original sample (Tofighi and MacKinnon, 2016). The quantity of interest is estimated from the original sample as well as the bootstrap samples by fitting the SEM model for each sample resulting in estimates of the quantity of interest (Tofighi and MacKinnon, 2016).

The Oceanic Niño Index based on SST anomalies in the Niño 3.4 region (5°N-5°S, 120° - 170°W) from OISST data is used to identify ENSO events. The Marshall (2003) index is used for the SAM while the SIOD index is defined as the SST anomaly difference between the eastern Indian Ocean (90˚E-100˚E; 18°S-28°N) and the southwestern Indian Ocean (55°E-65°E; 27°S-37°S) (Behera and Yamagata, 2001). The Mozambique Channel Trough (MCT) index used in this study is based on the area-average of the relative vorticity at 850-hPa over 35°-44°E; 16°-26°S (Barimalala et al. 2018).

The Gridded Satellite data (GridSat-B1; Knapp et al. 2011) cloud top temperature was used to identify the top cloud temperature of the MCS events linked to the top 50 extreme rainfall events over eastern South Africa discussed in **Chapter 5**. The dataset is available at 0.07^{o} (~ 8km) spatial resolution which extends over the domain (70^{0} N to 70^{0}S), for period 1981 – near present. Both relatively high spatial and temporal resolutions of GridSat-B1 data make it suitable to analyse and track a wide range of convective systems which could last for few hours to days and weeks. This dataset is derived from the International Satellite Cloud Climatology Project-B (ISCCP B; Knapp, 2008). GridSat-B1 is freely and easily accessible from the NOAA National Centers for Environmental Information (NCEI; https://www.ncdc.noaa.gov/gridsat/).

3.4.1 Identification of extreme rainfall events

Climate Hazards Infrared Precipitation with Stations (CHIRPS) version 2 (Funk et al. 2015), daily data are used to identify daily extreme rainfall events over the KZN province. CHIRPS combines multiple data, including those from rain gauges and satellites, to provide the best currently available estimates of daily rainfall at a 0.05° (~5 km) spatial resolution on a quasi-global (50°S-50°N) domain. CHIRPS is primarily based on GridSat data, which is why those datasets are not at all independent. CHIRPS uses a statistical algorithm to translate IR cloud top temperatures into rain rates based on cloud top temperature / rain radar (TRMM / GPM) relationships, followed by a bias correction of using a monthly ratio method of aggregated rainfall from station data. Thus, GridSat becomes the centre piece of CHIRPS data. Here, CHIRPS data are analysed over eastern South Africa for 1985 to 2008 period that the MCS data are available.

3.4.2. Daily extremes ranking method

The ranking of daily extremes is based on (Ramos et al. 2014) and is used to characterize and rank each summer day, taking into account the severity of the rainfall anomaly and its spatial extent. However, instead of being based on the normalized departure for each day at each grid point, as in the original method, the 95th percentile threshold value is rather used for each Julian day. Only grid points with rainfall amounts above 1 mm.day^{-1} (wet days) for the austral summer season (October-March) are considered. A 7-day running mean is applied to the 95th percentile threshold for each grid point to smooth the daily climatological noise. Ramos et al. (2014) note that the length of the smoothing filter (e.g., 7 days versus 21 days) does not significantly alter the ranking of the days. An anomaly value was then calculated by subtracting the rainfall of each day from this daily climatological 95th percentile threshold. A new value ('R') was computed, which is the magnitude/extent of the event and is obtained by:

1. Determining the percentage of grid points that contained a positive anomaly value on each given day (hereafter N and in percentage, %).
2. The mean value of anomalies across the grid points that contained a positive value (hereafter M and in millimeters, mm).

3. The extent and magnitude of the extreme ('R') is determined by multiplying N x M, with the higher the R value, the more extreme the daily event. The highest value of R then corresponds to the first day in the extreme ranking.

This method for identifying daily extreme rainfall events has previously been applied to other parts of southern Africa (e.g. Blamey et al. 2018; Rapolaki et al. 2019). Top extreme daily rainfall events linked to long-lived MCS were determined by matching MCSs from the database with that of the ranked days of extreme rainfall. It should be noted that this method does not take into account whether actual flooding occurred with the extreme rainfall day identified. This is because other factors, such as antecedent rainfall or topography of the basin, are not considered here. The contribution of MCSs to eastern South Africa rainfall is defined as the ratio of MCS related extreme daily rainfall events at each grid point to the seasonal and monthly rainfall. The contribution of MCS rainfall A (in percentage, %) was calculated as follows:

Equation 1: $\mathrm{A} = \mathrm{Td}/\mathrm{T} \ * \ 100;$

Where Td is the daily rainfall produced during the MCS events; T is the seasonal or monthly rainfall total for the individual summer of the event over eastern South Africa. The rainfall contribution of MCS events is calculated from the rainfall produced by an MCS over eastern South Africa domain on MCS days (**Fig. 3.1b**).

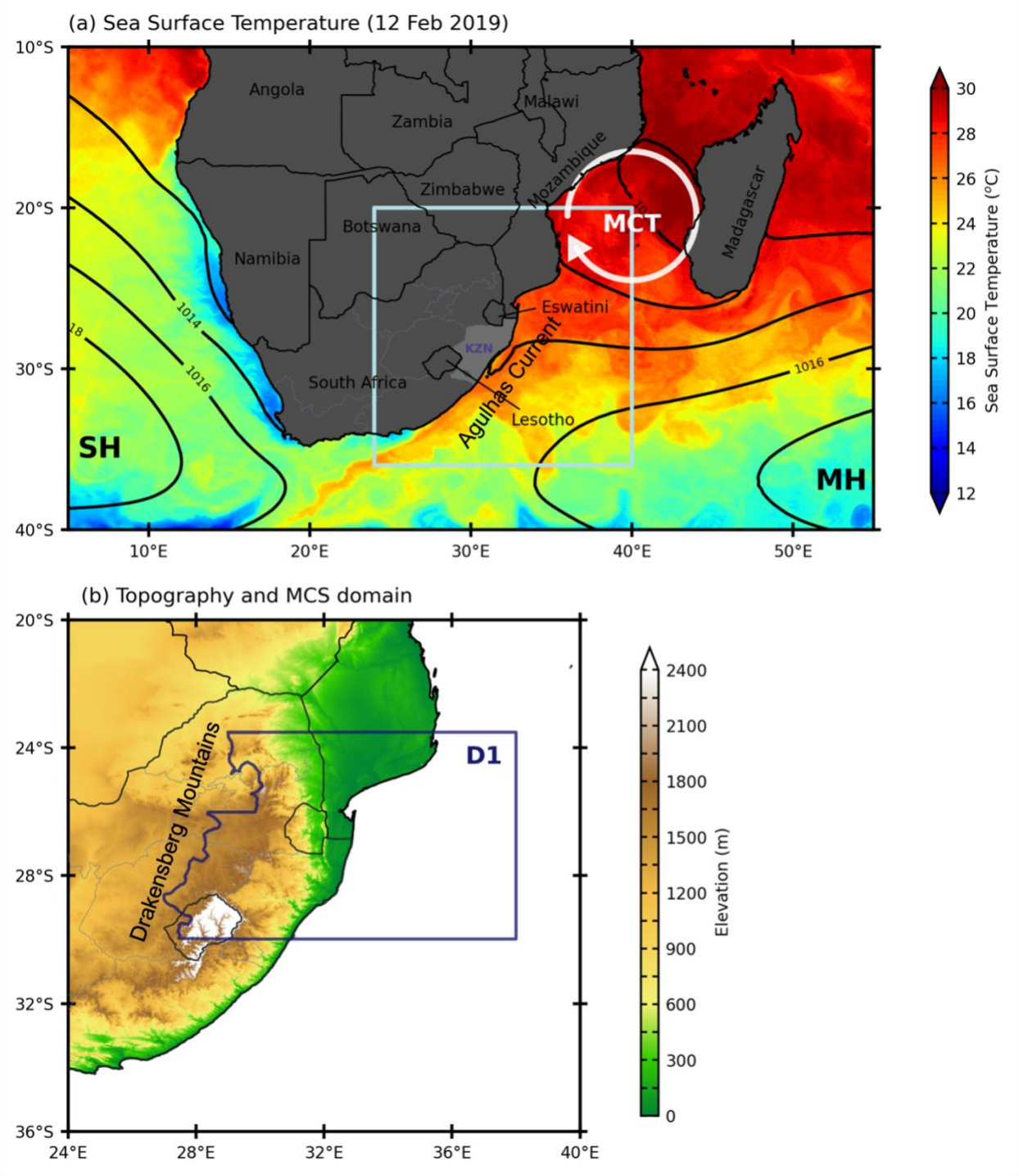

Figure 3.1: (a) SSTs (°C; based on the Multi-scale Ultra-high Resolution (MUR) SST) surrounding southern Africa for a particular summer day (12 February 2019), with extremely warm SSTs along the east coast and cold upwelled water along the west coast. JFM mean sea level pressure (hPa), for the period 1985-2008 and based on ERA5 reanalysis, is shown in black contours (over ocean only) and used to illustrate the location of the St. Helena high (SH) and Mascarene

high (MH). The approximate location of the Mozambique Channel trough (MCT) during JFM is depicted by the white circle. The location of the KwaZulu-Natal (KZN) province (eastern South Africa) is shaded in light grey. The light blue box shows the domain used for panel **(b)**. **(b)** Topography over eastern South Africa (shading, m) which is derived from ETOPO2. The blue polygon (D1) depicts the domain used in this study (referred to as Domain 1 in the text) to build the MCS climatology.

Chapter 4: Long-lived mesoscale convective systems over eastern South Africa

This chapter develops a climatology of large, long-lived MCSs over eastern South Africa. These systems are of great research interest because of they often lead to extreme flooding, hail, lighting, strong winds and sometimes even tornadoes. However, these systems remain poorly understood with relatively little to no evidence of any long-term climatological study of South Africa MCSs. The systems are of importance as they often make large contributions to seasonal rainfall totals, producing rainfall that is important for semi-arid countries such as South Africa, particularly since most of the agriculture in the region is rain-fed. In this chapter, we investigate the spatial distribution, frequency, life cycle, and seasonal cycle of large, long lived MCSs in this region and investigate the favourable large-scale environmental conditions for the development of long-lived MCSs. The chapter further investigates the role of the ocean in the development and intensification of large long-lived MCSs over eastern South Africa, and the relationships between these systems frequency and the main climate modes of variability such as ENSO, SIOD, and SAM.

4.1. Spatial distribution

Figure 4.1 shows that south of 15°S, there are two regions in southern Africa where MCSs preferentially develop. One is the eastern South Africa/Lesotho/Agulhas Current region focused on in this study and the other is the tropical belt (except over the northern Namibian/southern Angolan coast with its cool offshore SST due to upwelling). The South African/Lesotho maxima is clearly associated with topography with most systems tending to initiate near the eastern escarpment where there are sharp topographic gradients. Garstang et al. (1987) described how the interaction between topography of the northeastern escarpment and the upper air westerly waves propagating across the southern tip of Africa can lead to the development of strong convection over the east coast of South Africa.

A total of 1461 large, long-lived MCSs were identified and tracked in Domain 1 (green Polygon in **Fig. 4.1** and covers the South African/Lesotho maxima) for the period 1985-2008. Of these

MCSs, the majority were located over land during the developing stage of their evolution compared to those found over the adjacent ocean, this will be further analysed in the continental versus oceanic MCSs section. This distribution is comparable with the global population of MCSs, with the most frequent occurrence being on land (e.g., Mohr and Zipser, 1996; Zipser et al. 2006; Huang et al. 2018) and also for MCCs, a subset of MCSs (Laing and Fritsch, 1997; Durkee and Mote 2009; Blamey and Reason, 2012). It is likely that more systems occur on land than over the ocean due to more favorable thermal instability, orographic lift, and large diurnal thermal variations over land, related to land cover and topography (Houze, 2018; Huang et al. 2018).

4.2. MCS life cycle

Figure 4.2 shows the diurnal cycle of MCSs through three key stages of their lifespan, the developing, mature and termination stages. The developing stage represents the time when the system is first identified in the data, the mature stage refers to when the system reaches the maximum spatial extent, and the termination stage is the last time step in which the systems are last identified. Given the low temporal resolution of the data, the timing of the first storms (i.e., before system becomes classified as an MCS) is not easily identified and therefore not included. The stages are also restricted to intervals of three hours due to the temporal resolution of the data.

Based on the coarse temporal resolution, MCSs along the east coast and adjacent ocean tend to develop in the mid-afternoon (1500 UTC), reach a maximum spatial extent during the evening (between 1800 and 2100 UTC) and then mainly terminate during the night (2100 - 0300 UTC) (**Fig. 4.2**). Over 60% of the systems reach MCS status during the period between 1200-1500 UTC (a peak of 38% at 1500 UTC). Meanwhile, around 50% reached maximum spatial extent between 1800 and 2100 UTC, and over 50% terminated between 2100 and 0300 UTC. The timing of MCSs over eastern South Africa, also identified by Blamey and Reason (2012) using a higher resolution dataset, is consistent with the diurnal cycle of MCSs in other domains (Chen and Houze, 1997; Machado et al. 1998; Morel and Senesi, 2002; Kolios and Haralambos, 2010; Huang et al. 2018; Yang et al. 2019; Cheeks et al. 2020; Núñez Ocasio et al. 2020).

The duration of MCSs over the east coast of South Africa ranges from a minimum of 6 hours (threshold) to over 24 hours (**Fig. 4.3**). Just over half the MCSs (53%) over Domain 1 last between 6 and 9 hours, with ~27% lasting between 12 to 15 hours, and the remainder longer than 18 hours. Around 7% of the systems (103 out of 1461 MCS in the entire climatology) last longer than 24 hours. Climatological studies of MCS in other regions (e.g., Velasco and Fritsch, 1987; Machado et al. 1998) have also found cases where the systems last longer than 24 hours if the environmental conditions and moisture inflows remain favorable over the storm region.

4.3. The seasonal cycle of MCSs

Figure 4.4 plots the monthly variability of MCS frequency over Domain 1. There is a sharp increase through the early summer to reach a maximum in December followed by a gradual decrease through the late summer. It is also evident that considerable variability can occur within the different months, with December and January showing the largest range (**Fig. 4.4b**). The spatial distribution of the origins of the MCSs during the different summer months is shown in **Fig. 4.5**. In general, there are more systems near and downstream of strong topographic gradients or the Agulhas Current. There is a clear preference for systems to develop over land during the core summer period (November-February) compared to that over the ocean.

To highlight the seasonal evolution of favorable conditions for MCSs development, CAPE and deep layer vertical wind shear distributions produced with ERA5 data are analysed. **Figure 4.6** depicts the mean number of days per summer month exceeding 1000 $J.kg^{-1}$ across South Africa at 15h00 UTC. This threshold choice follows since it has previously been identified as an indicator of extreme rainfall events over inland South Africa (Dyson et al. 2015). Two hotspots are evident in eastern South Africa, one along the northern part of the Drakensberg near the border with Eswatini, and the other along the southeast coast around 30-32°S. Although high CAPE values in the two domains appear simultaneously at the start of the summer (October/November), high values of CAPE are more frequent along the northern parts (around Eswatini; ~31°E,27°S) during the early/core summer months (November-January) reducing during the late summer as solar insolation weakens. In contrast, the maximum along the southeast coast (~30°-32°S) contains high values of CAPE which increase from October through February followed by a small decrease in

spatial extent but not obviously in magnitude in March and April. Over the Agulhas Current region, the areas of high CAPE increase in extent through the summer as SSTs warm with the maximum occurring in March-April, the time of warmest SSTs.

The summer cycle of vertical wind shear is presented as the mean number of days per month when deep layer vertical wind shear between 12 - 25 m.s.$^{-1}$ at 15h00 UTC (**Fig. 4.7**). Although southern South Africa generally experiences more days with favorable wind shear than the domain, revealing the presence of the subtropical jet stream, it does not contain the same convective activity as found along the east coast due to cooler adjacent SSTs and a more stable atmosphere there (Weldon and Reason, 2014; Engelbrecht et al. 2015). Over the east coast of South Africa, favorable wind shear days are most frequent during early summer months (September-November) with a north – south gradient along the coast (more days with favorable shear in the south). The shear subsequently decreases in strength over the northern part of the east coast as the summer progresses, with the lowest values occurring between January and March. Due to the escarpment and the interior being at an altitude greater than 1000 m, vertical wind shear using a 400-hPa upper level was calculated leading to a very similar spatial pattern as **Fig. 4.7** but with more days with wind shear between 12 - 25 m.s.$^{-1}$. Overall, the favorable storm environments seen throughout the summer period over the southern part of the domain (immediately east of Lesotho and over the southern part of the east coast) help explain the maxima seen in MCS activity in this region (see **Fig. 4.1**) compared to the rest of the domain.

4.4. Continental versus Oceanic MCSs

To better understand the potential role of the ocean in the development and intensification of MCSs over eastern South Africa, the systems have been categorised into being either continental or oceanic. The motivation for undertaking such a classification is that MCSs have been found to have different properties, such as in size and duration, based on the underlying environmental conditions over the land and ocean (e.g., Durkee et al. 2009; Yuan and Houze, 2010; Kolios and Feidas, 2010; Liu and Zipser, 2013; Huang et al. 2018). Continental (oceanic) MCSs are defined here as systems that are located over land (ocean) during the developing stage of their evolution.

It should be noted that, unless stated below, results do not differ substantially if continental/oceanic MCSs are defined based on the location of the system at the mature phase (maximum extent).

It is found that the majority of MCSs were located over the land during the developing phase, whereas fewer systems were found over the adjacent ocean (**Fig. 4.5**). Out of the 1461 MCSs over the domain, the majority were located over land with 73% of the systems being categorized as continental and 27% as oceanic. Continental (oceanic) MCSs are defined here as systems that are located over land (ocean) during the developing stage of their evolution. If continental/oceanic systems are defined based on the location of the MCS at the maximum extent, then 892 systems are classified as continental and 569 as oceanic, almost a 60% continental - 40% oceanic split. Thus, MCSs in eastern South Africa typically initiate over the land and then track eastward towards the South West Indian Ocean, which is described in more detail below.

The differences in the diurnal variation of the three MCS stages over land and ocean are shown in **Fig. 4.8**. MCSs over land display a prominent diurnal cycle with almost 50% of the systems first identified in the afternoon (1500 UTC), reaching maximum spatial extent in the evening (1800-2100 UTC) before terminating during the night (2100-0000 UTC) (**Fig. 4.8a**). By contrast, MCSs over the ocean contain a less obvious diurnal cycle. Systems over the ocean appear to contain two favourable initiation times, one occurring at about 0300 UTC, and the other occurring in the afternoon near 1500 UTC. The latter corresponds to the typical time of maximum SST in the diurnal cycle. It is not obvious what factors might contribute to the early morning initiation time. In general, SST is coolest around dawn and shortly thereafter but whether or not there is much of a diurnal range in SST depends on both dynamic (e.g., wind-induced mixing and Ekman pumping) and thermodynamic (short and long-wave radiation and latent heat fluxes) factors. Most of the oceanic MCSs reach their maximum spatial extent in the late morning between 0900 and 1200 UTC before they terminate during the afternoon (1200-1500 UTC) (**Fig. 4.8b**).

Both land and ocean based systems tend to be relatively short-lived with about 45% and 38% of systems lasting for 6 hours, respectively (**Fig. 4.9**). An obvious difference between the two populations is that continental systems are shorter lived than the oceanic systems (**Fig. 4.9**). This is evident by the higher percentage of the oceanic systems having a duration longer than 18 hours

compared to the continental systems. Around 13% of oceanic systems have a duration longer than 24 hours. Previous studies have documented that MCSs that develop over oceans are generally larger, slower, and longer lasting than those over the continent (Mohr and Zipser, 1996; Laing and Fritsch, 1997; Mathon and Laurent, 2001; Huang et al. 2018).

Another major difference between continental and oceanic MCSs over Domain 1 appears to be the different seasonal cycle (**Fig. 4.9b**). Land based systems reveal a single peak in the season (December), due to favourable thermal instability over land during this period (Blamey et al. 2017), whereas there appears to be two minor peaks in ocean-based systems (December and April) (**Fig. 4.9b**). A December peak may arise because this is the month of maximum insolation while the circulation over eastern South Africa is still influenced by midlatitude systems, thus leading to relatively large airmass contrasts and baroclinicity in the environment within which the MCS develops. Over the ocean, April is close to the month (March) of maximum SST as well as the time when midlatitude circulation systems start to dominate over tropical influences. The transitional months also show a tendency to have fewer systems in the northern land or ocean regions of the domain whereas a large number of systems are found in these areas in the main summer months.

4.5. Interannual variability and large-scale circulation favouring MCS development

On average 63 MCSs occur per summer, ranging from a minimum of 45 (1995/96) to a maximum of 81 (1987/88) with a standard deviation of 10 (**Fig. 4.10a**). To investigate whether there is relationship between MCS frequency over Domain 1 and large-scale circulation favouring MCS development such as ENSO, SAM, SIOD and MCT detrended correlations method is used. Detrended correlations of MCS frequency over Domain 1 are only significant with SAM during early summer (OND; $r = 0.64$, $p < 0.01$) and SIOD during late summer (JFM; $r = -0.53$, $p < 0.01$). The link between SAM and MCS frequency is consistent with the summer rainfall region of South Africa being typically wet (dry) during the positive (negative) phase of the SAM (Gillett et al. 2006). Thus, the shift in mid-latitude westerlies linked to SAM could play a key role in MCS development in eastern South Africa (discussed in more detail below). Although ENSO is

considered the dominant driver behind interannual rainfall variability over southern Africa during summer, there is no conclusive relationship with MCS frequencies over eastern South Africa. This inconsistency between ENSO and MCS activity may reflect the non-linear relationship between ENSO and southern African climate previously documented (Reason and Jagadheesha, 2005; Fauchereau et al. 2009; Boulard et al. 2013; Blamey et al. 2018; Driver et al. 2019).

To better understand variability in MCS frequency, conditions that are favorable for MCS development are analysed using composites based on ERA5 data. Only years with anomalously high MCS activity (seasons containing a standard deviation above 1 in **Fig. 4.10b**) for OND (1985, 1987, 1998, 1999 and 2001) and JFM (1987, 1990, 1992, 2005 and 2006) are included. Since some summers show OND and JFM with opposite signed anomalies (e.g., OND 1986 and JFM 1987 in **Fig. 4.10b**), early and late summer composites are derived. To gauge whether there is any difference in MCS location during these chosen OND/JFM composites, the domain is divided into four quadrants, roughly dividing it into a southern/northern and land/ocean quadrant (**Fig. 4.11a**). In OND, the northeast quadrant shows a large percentage increase in mean anomaly of the number of systems with the southwest quadrant also showing a significant increase. Most of the latter (26% or ~4 more systems than average) mostly occur over land across KZN. For the northeast quadrant increased (60% or ~2 more systems than average), these changes occur over land/coastal areas in southern Mozambique. For JFM composite, there is a larger percentage increase in MCS development in the southwest quadrant (mean is 13) compared to the other three (**Fig. 4.11c**). Although the other three quadrants have similar sized percentage increases, only that in the northwest is significant.

Figure 4.12 shows that there are significant increases in the number of days with favorable CAPE (**Fig. 4.12a**) and wind shear (**Fig. 4.12b**) for the JFM composite, particularly over the mainly land-based southwest and northwest quadrants which contained the largest increase in MCS frequency (**Fig. 4.11c**). For OND, the largest increase in MCS frequency occurred over parts of southern Mozambique in the northeast quadrant. **Figure 4.12c** shows a significant increase in favorable CAPE days over southern Mozambique as well as nearby land and ocean areas. While the CAPE changes are consistent with an increase in MCS numbers here, there is no obvious change in the

number of shear days in this region (**Fig. 4.12d**). It is possible that in addition to CAPE, some other factors may have also influenced MCS frequency in the northeast quadrant.

All five cases in the OND composite coincide with positive SAM (**Table 4.1**) and with significant positive height anomalies over the east coast of South Africa and neighbouring ocean (**Fig. 4.13a**). Associated with the positive SAM pattern is a weakening of the subtropical jet, particularly near 25-30°S over South Africa and the southwest Indian Ocean (**Fig. 4.13b**), and a strengthening of the polar jet near Antarctica. These changes in the jet streams impact on extra-tropical cyclones originating in the southwest Atlantic which provide the mid-latitude input to the dominant summer synoptic rainfall producing system in southern Africa, tropical-extratropical cloud bands (Harrison 1984; Hart et al. 2013). Visual inspection of satellite imagery indicates that MCS systems are often embedded within these cloud bands, implying that if conditions are favorable for cloud bands, then they may also be for increased MCSs. During wet summers over subtropical southern Africa, these cloud bands are aligned northwest-southeast across the mainland (Fauchereau et al. 2009). **Figure 4.14a**, which shows composite anomalies in 500-hPa vertical velocity, indicates a northwest-southeast swath of relative upward motion extending from southeastern Angola, across Botswana and northern South Africa/northeastern South Africa to the northern Agulhas Current region, consistent with enhanced convection and cloud band activity there including most of the northern part of the MCS domain. The stronger upward motion is accompanied by a decrease in OLR (increased cloud cover) for much of the domain and particularly over the northern half of the MCS domain (**Fig. 4.14c**), consistent with increased MCS activity.

For JFM, the correlation between the SIOD and MCS variability appears to be partly explained through the relationship between SSTs in the Indian Ocean, the Mascarene high, and the MCT. Of the five JFM seasons with anomalously high MCS frequency, four experienced SST anomalies that were too weak to be classified as a SIOD event (**Table 4.1**). Of the five JFMs, four (1987, 1990, 1992, and 2006) are associated with a weaker MCT, while JFM 2005 experienced a near-average MCT (**Table 4.1**). Barimalala et al. (2020) show that the MCT, which is most pronounced in JFM (see **Fig. 3.1a** for general position of the MCT), is correlated with the strength and position of the Mascarene high over the Indian Ocean, and typically leads to more (less) moisture flux from the Mozambique Channel and from the south of Madagascar towards mainland southern Africa

when both circulation features are weak (strong). Composite 850-hPa geopotential height and 850-hPa moisture flux anomalies confirm a weaker Mascarene high and weaker MCT in periods with high MCS activity (**Fig. 4.15a**). The weaker low-level winds and reduced cloud cover over the channel during these weak MCT late summers are favorable for warmer than average SSTs here, as well as in the oceanic parts of the northern MCS domain (**Fig. 4.15b**). These warm SSTs are conducive to increased convection and MCS activity over the domain since the flow will remain onshore, albeit weaker, but with more moisture than average. Indeed, low level specific humidity anomalies (**not shown**) during the five JFMs reveal positive anomalies (moisture gain) within most areas of the MCS domain, particularly land areas and northern Agulhas Current, and negative anomalies over the Mozambique Channel (moisture loss). This anomalous specific humidity pattern also creates sharper than average gradients between the Agulhas Current and further offshore which may assist MCS development. The westerly moisture flux anomalies over Botswana extending into northern South Africa also imply more moisture flux convergence over the MCS domain with the onshore flow. Reason and Mulenga (1999) and Reason (2001) have previously demonstrated through a set of idealised experiments using an atmospheric general circulation model that this anomalous circulation and convergence, linked to warm SST anomalies in the southwest Indian Ocean, plays a key role in above average rainfall in eastern South Africa. Furthermore, Blamey and Reason (2009) presented model evidence that SSTs and associated surface heat fluxes in the northern Agulhas Current were important for the development of an MCS over northern KZN.

Lastly, the favorable environmental conditions and increased MCSs activity during the OND composite seasons coincide with above average rainfall over the MCS domain and neighbouring areas (**Fig. 4.16b**). For JFM, **Fig. 4.16d** shows that most of southern Africa experienced well below average rainfall. However, over much of the MCS domain, rainfall was average to above average suggesting that the increased MCS numbers here in these late summers played an important role in preventing drought conditions. This suggestion is consistent with a detailed synoptic classification of extreme rainfall events over the Limpopo River basin, which lies mainly to the northwest of the MCS domain as well as covering the far northern part of it, in which MCSs contributed 14% of these events (Rapolaki et al. 2019). The following Chapter is aimed to

investigate the impact of long-lived MCSs events on regional rainfall and quantify the long-lived MCS rainfall contribution towards summer rainfall over eastern South Africa.

4.6. Summary

Based on the quasi-tropical (30°N-30°S) MCSs dataset covering the period 1985-2008 developed by Huang et al. (2018), an analysis of long-lived MCSs over eastern South Africa during the extended summer (September-April) was conducted. The identification of the MCSs is based on CLAUS 3-hourly global brightness temperatures (BTs) with intervals sampled at a 30 km (1/3°) resolution. A few of the limitations of Huang et al. (2018) are that it has a low temporal resolution of 3 hourly and spatial resolution of 30 km, and that it is restricted to 30°N and 30°S. Therefore, the southern part of South Africa (30°-34°S), which has very strong topographic gradients and is also strongly influenced by the Agulhas Current, is excluded. However, the earlier study of Blamey and Reason (2012) on MCCs over southern Africa which was based on only 9 years of satellite data found no MCCs south of about 32°S. Overall, the results presented here which are based on 24 years of data are consistent with those of Blamey and Reason (2012).

It is clear that over southern Africa between 15°S and 30°S there is a pronounced local maximum in frequent MCS activity over the relatively small region extending from the Drakensberg to the Agulhas Current. A total of 1461 long-lived MCSs were identified over eastern South Africa and the adjacent ocean for the extended summer (September-April). Although it is not possible to make direct comparisons with other regions given the much smaller domain used in this study and the variations in the literature in MCSs threshold criteria used, it is apparent that the number of systems identified here is generally less than that compared to MCS regions in North America, Europe, Asia, and West Africa.

Mesoscale convective systems in eastern South Africa occur most frequently between November and January with a peak during December. The larger frequencies in November and December, particularly over land, compared to late summer could be linked to the large-scale environment since temperature and moisture gradients over South Africa tend to be stronger in early summer than in late summer (Todd et al. 2004). Our results reveal that more favorable CAPE and vertical

shear profiles occur across the wider domain during November – December. Previous studies have highlighted the dominance of organized convection in early summer over eastern South Africa, for example through large-scale cloud bands (Hart et al. 2013), MCCs (Blamey and Reason, 2012) and the frequency of days with favorable severe weather conditions (Blamey et al. 2017). In the late summer months (February-March), favorable CAPE and shear environments are more restricted to the southern parts of the east coast of South Africa and over the Agulhas Current. Relatively few MCSs occur during the transitional months of September/October and March/April (less than 10 per year in these months on average).

The systems generally reach MCS status (i.e., developing phase) during the mid-afternoon, a maximum extent during the evening hours and subsequently terminate in the middle of the night. This MCS life cycle closely matches the diurnal cycle of rainfall over the east coast of South Africa (Rouault et al. 2013) and is consistent with MCS timing in the US Great Plains and South America. The possible role of nocturnal low-level jets or land-sea breezes over eastern South Africa on MCS characteristics remains to be investigated. Although CAPE and deep layer vertical shear parameters have provided some insight into the distribution and frequency of the MCSs here, it is noted that further work is needed to understand upscale convective growth, where systems transition from isolated deep convection into organized MCSs, over eastern South Africa.

The results presented here suggest that most of the MCSs initiated over land as opposed to over the adjacent ocean. The tendency of systems to preferentially initiate over land has been noted in previous studies (e.g., Kolios and Feidas, 2010; Durkee and Mote, 2009). For eastern South Africa, the systems typically develop over land (near the escarpment) and then track eastwards to the adjacent warm ocean (Agulhas Current). A similar pattern was documented in the limited climatology of MCCs over southern Africa by Blamey and Reason (2012). Although not completely understood, the complex terrain of the eastern escarpment could influence MCS development or evolution directly (e.g., modifying cold pool structure) or indirectly (e.g., changing vertical wind shear and CAPE) like that in the north–south running Sierras de Córdoba Mountain range in Argentina (Mulholland et al. 2019). As indicated earlier, the northern Agulhas Current has been shown to contain favorable conditions (high latent heat fluxes), for local storm intensification. Although the findings here provide evidence that the northern Agulhas Current

plays an important role in the development and intensification of MCSs, model simulations are required to investigate the exact mechanisms through which it does so. This extends to examining general climatological differences between ocean based versus land based MCSs in the region. For example, the results presented here also show that there is difference in the seasonality between continental and oceanic MCSs. Land based systems reveal a single peak in the season (December), likely due to favourable thermal instability over the land then. On the other hand, ocean-based systems appear to have two peaks; namely, December and April. The latter may relate to this month being near maximum SST as well as the start of increasing baroclinicity over the region.

Considerable interannual variability in the frequency of MCSs within the domain was also found, with an average of 63 systems occurring per season with the least in 1995/96 (45) and the most in 1987/88 (81). There is little to no evidence of any robust relationship between MCS frequency and the main modes of climate variability that influence the region, such as ENSO, the SIOD and SAM. The only significant correlations observed were between MCS frequency and SAM during OND (early summer) and the SIOD in JFM (late summer). The relationship between the SIOD and MCS activity in JFM appears to be linked through the strength of the Mascarene high and MCT. Late summers with more MCSs typically occurs when the Mascarene high is weaker, which as a result weakens the MCT. With a weaker MCT, warmer SSTs occur in the Mozambique Channel which leads to a moister airmass being advected over the MCS region by the prevailing easterly winds. Westerly wind anomalies extending from west and northwest of the MCS domain lead to increased low level convergence over the domain with this moister easterly inflow. Thus, favorable conditions occur for MCS development, which is illustrated with more days with sufficient CAPE and more favorable wind shear during these late summers.

Lastly, a composite analysis revealed that an increase in rainfall often occurred in regions containing anomalously high MCS activity during OND and JFM. To what extent MCSs influence the local hydrological cycle remains uncertain and warrants further investigation. It further highlights the need to better understand local environmental factors that play a role in the frequency, intensity, and evolution of these systems. Here, different environmental factors played a role in the increase in MCS activity between OND and JFM.

Table 4.1: The phase or strength of ENSO, SAM, SIOD and MCT for the different OND and JFM periods with anomalously high frequency of MCSs within Domain 1. Note that MCT strength is only shown for JFM. Years with a strong phase of the respective index is indicated in bold text.

	Early Summer (OND)				
	1985	**1987**	**1998**	**1999**	**2001**
ENSO	Neutral	El Niño	La Niña	La Niña	Neutral
SAM	**Positive**	Positive	**Positive**	**Positive**	**Positive**
SIOD	Neutral	Positive	Positive	Negative	Negative
	Late Summer (JFM)				
	1987	**1990**	**1992**	**2005**	**2006**
ENSO	El Niño	Neutral	**El Niño**	El Niño	La Niña
SAM	**Negative**	Positive	Negative	Positive	Neutral
SIOD	Neutral	Neutral	Neutral	Neutral	**Positive**
MCT	Negative	Negative	Negative	Neutral	**Negative**

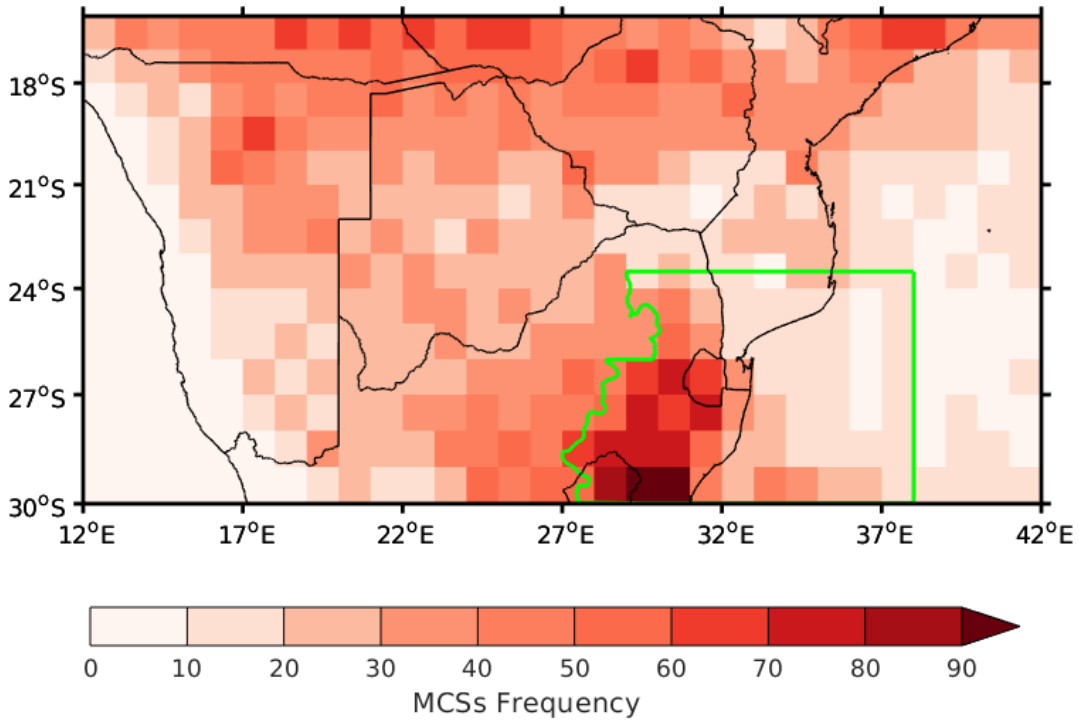

Figure 4.1: A heat map showing the mean location of all MCSs over southern Africa between 15°S and 30°S during the developing phase (first identification of the system in the dataset) for the extended summer of the period 1985-2008. The grid spacing is at 1° resolution. The domain used for the study is highlighted again by the green polygon, with no data available south of 30°S.

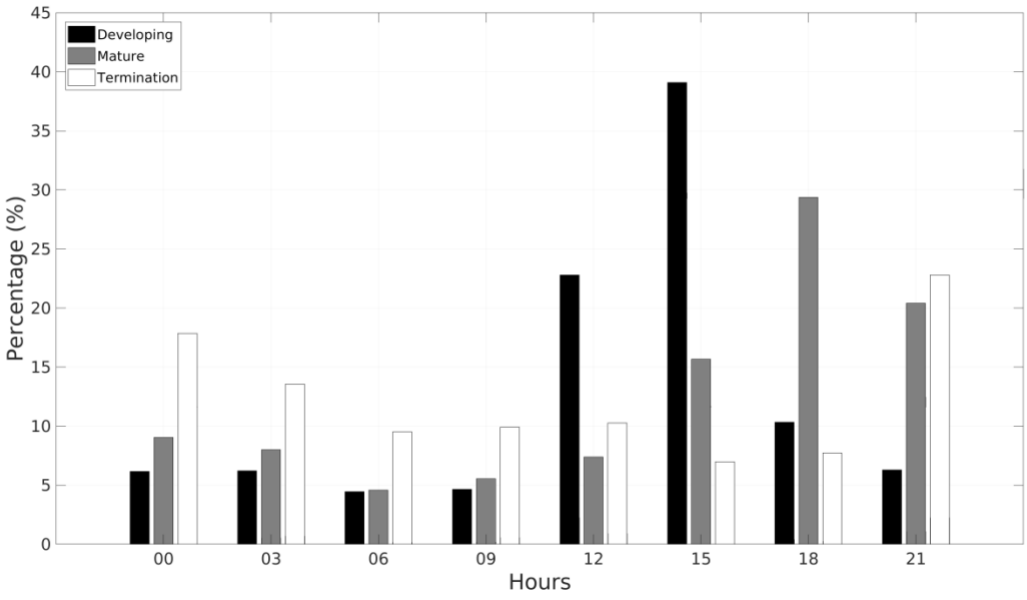

Figure 4.2: Diurnal variation of MCS occurrence (in percentage) over eastern South Africa for the extended summer. The key stages of the MCS life cycle denoted in the legend and the times are in Universal Time Coordinated (UTC; Local time is UTC+2).

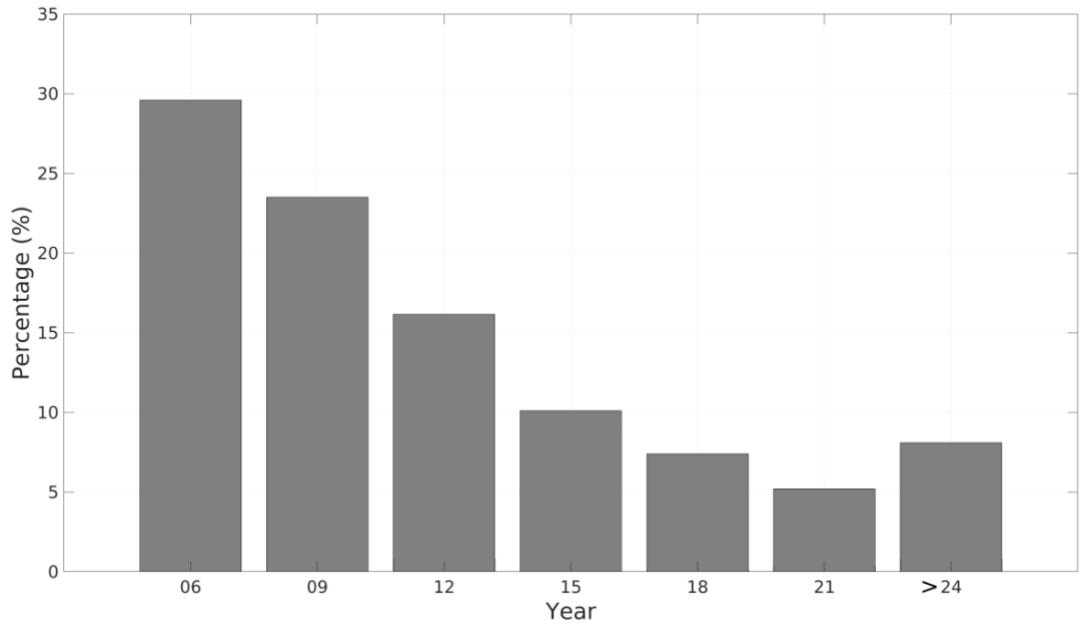

Figure 4.3: The duration of warm season MCSs (given in percentage) over the eastern South Africa.

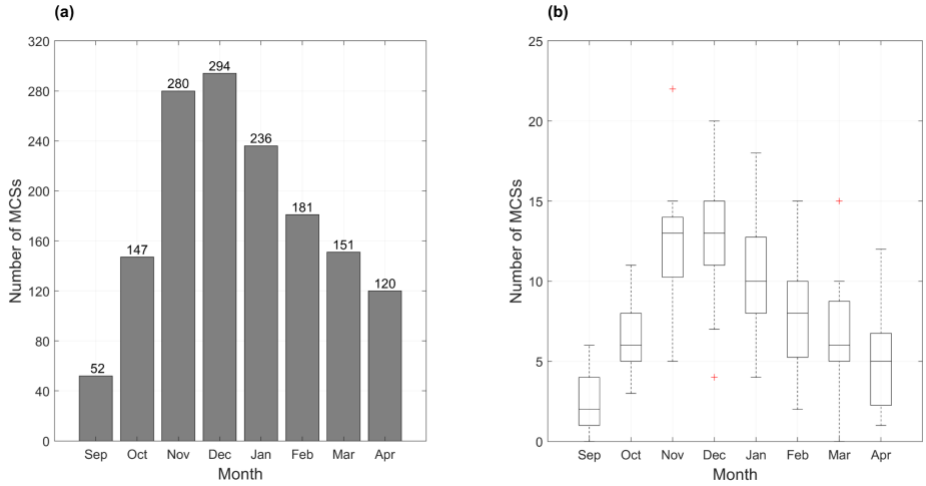

Figure 4.4: (a) The total number of MCSs within the domain for each month over the period 1985-2008. The number above each bar represent the total number of systems for that month and **(b)** box plots illustrating the monthly mean and range in MCS activity for the period 1985-2008. The horizontal line in each box (shows the 25%-75% range) is the mean and outliers are denoted by +.

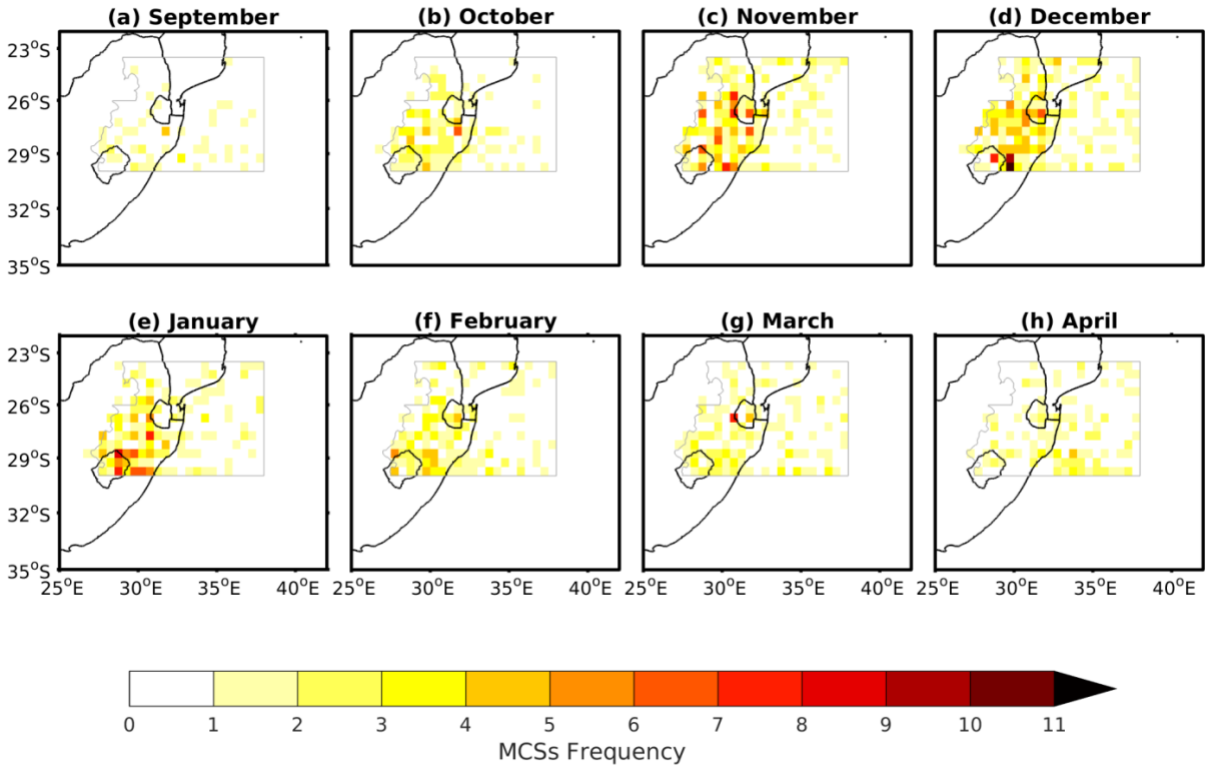

Figure 4.5: Spatial distribution of the origin of all MCSs for the extended summer starting in **(a)** September and ending in **(h)** April for the period 1985-2008. The grid spacing is 0.5° resolution, while the grey polygon is the outline of the domain.

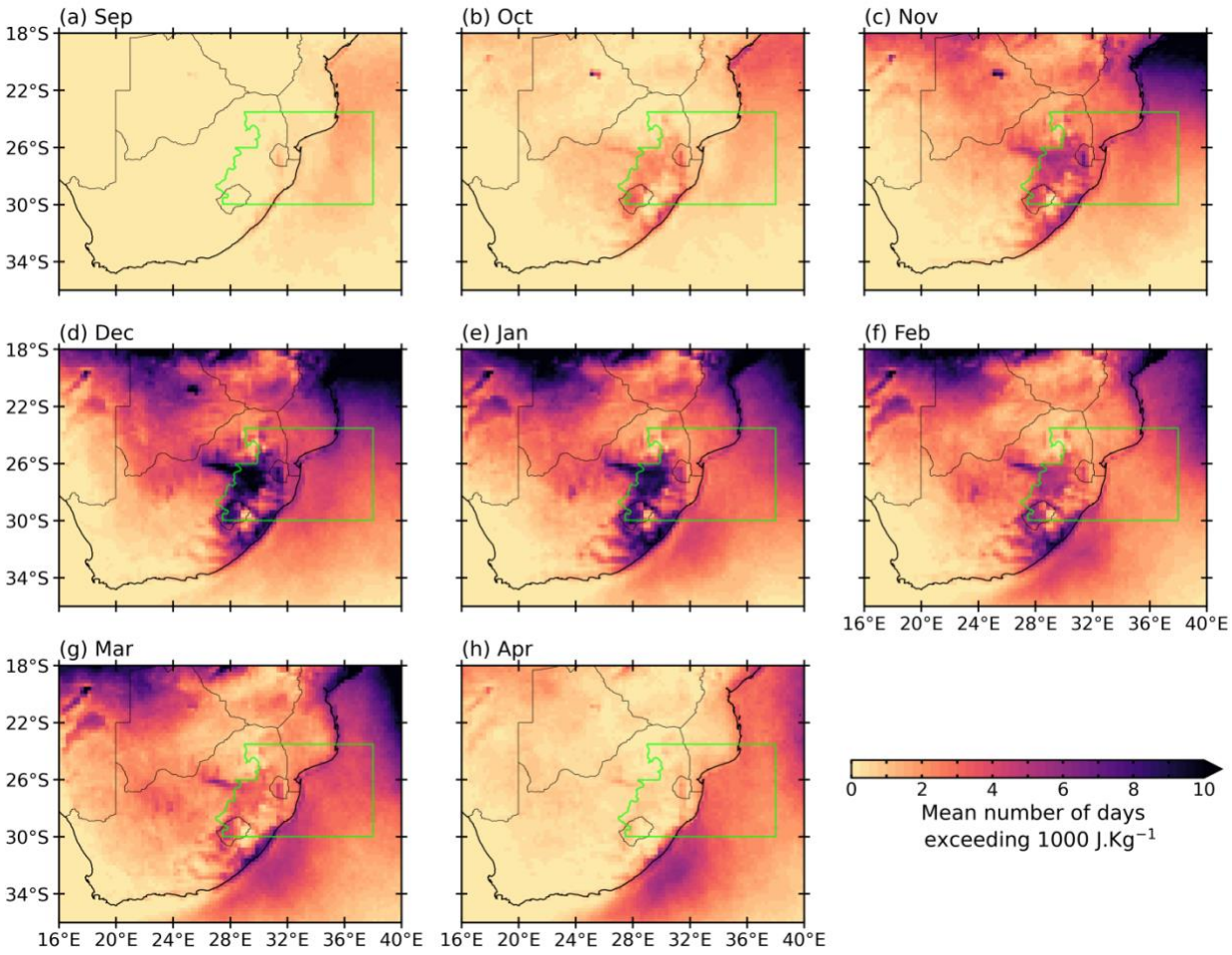

Figure 4.6: The monthly mean of the number of days with CAPE at 15h00 UTC (17h00 LST) exceeding 1000 J.kg^{-1} over the period 1985-2008. For reference, the green polygon illustrates the MCS domain used in the study.

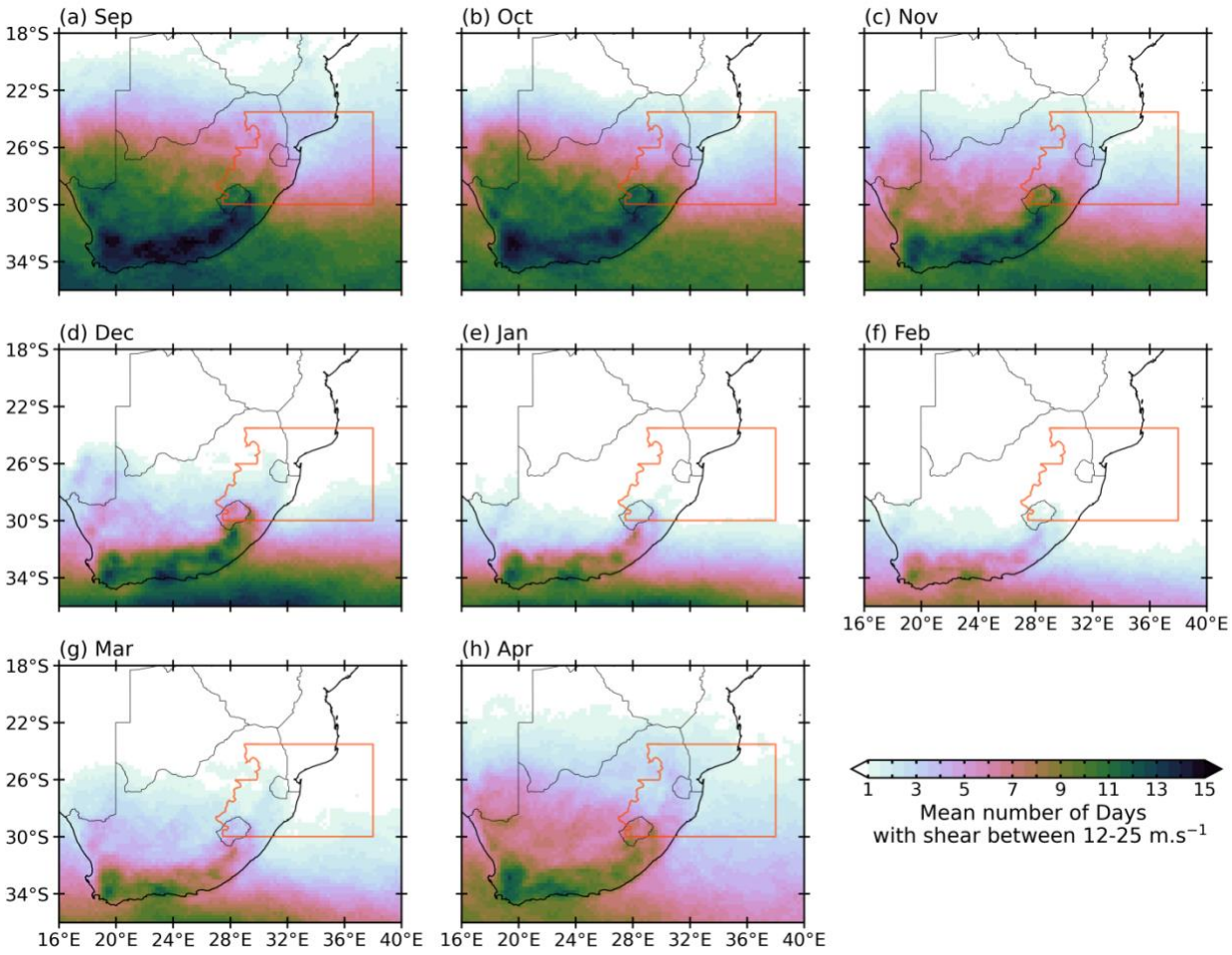

Figure 4.7: The monthly mean for the number of days (taken at 15h00 UTC) with the vertical wind shear between 12 - 25 m.s.$^{-1}$ across South Africa over the period 1985-2008. Here, deep layer vertical wind shear is calculated as the difference between winds at the 500-hPa pressure level with winds 100 m above ground level.

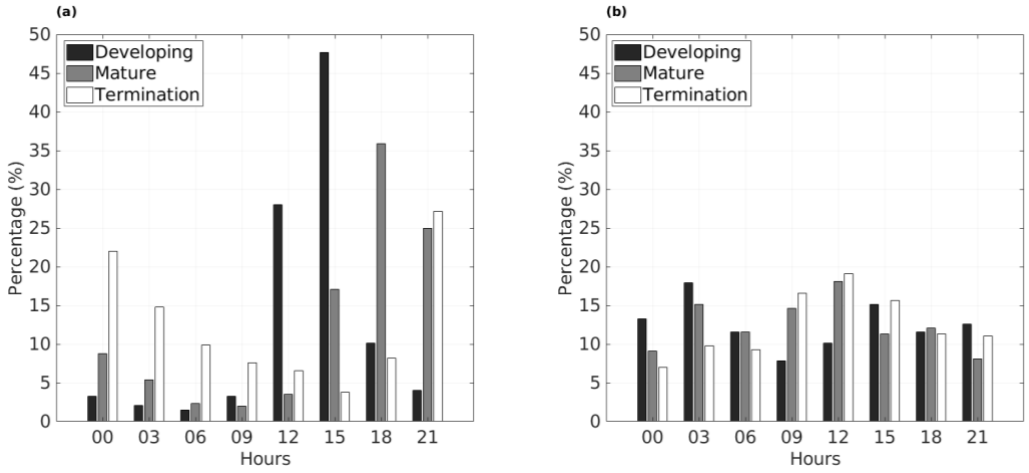

Figure 4. 8: As in **Fig. 4.2**, but for **(a)** continental and **(b)** oceanic systems (see text for definitions).

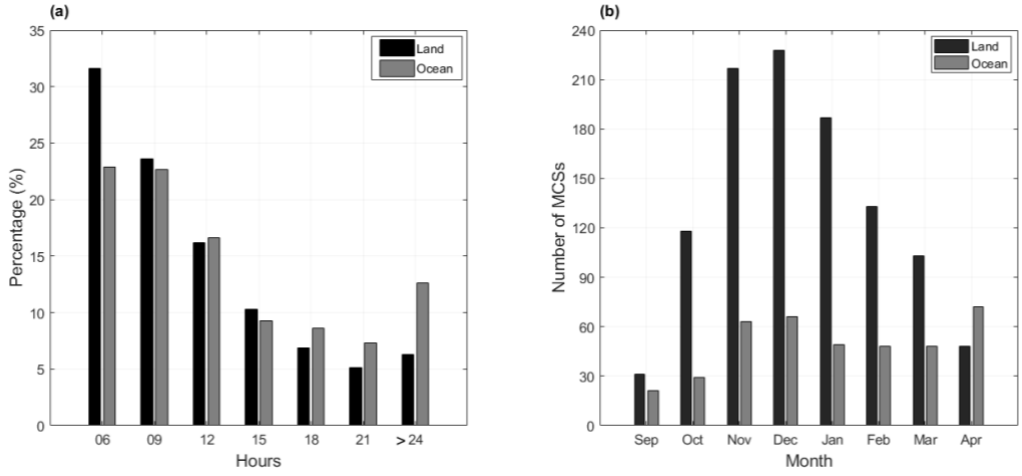

Figure 4.9: (a) As in **Fig. 4.3**, but for continental (black bars) vs oceanic systems (grey bars) and, **(b)** the total number of MCSs for each month for continental (black bars) and oceanic systems (grey bars).

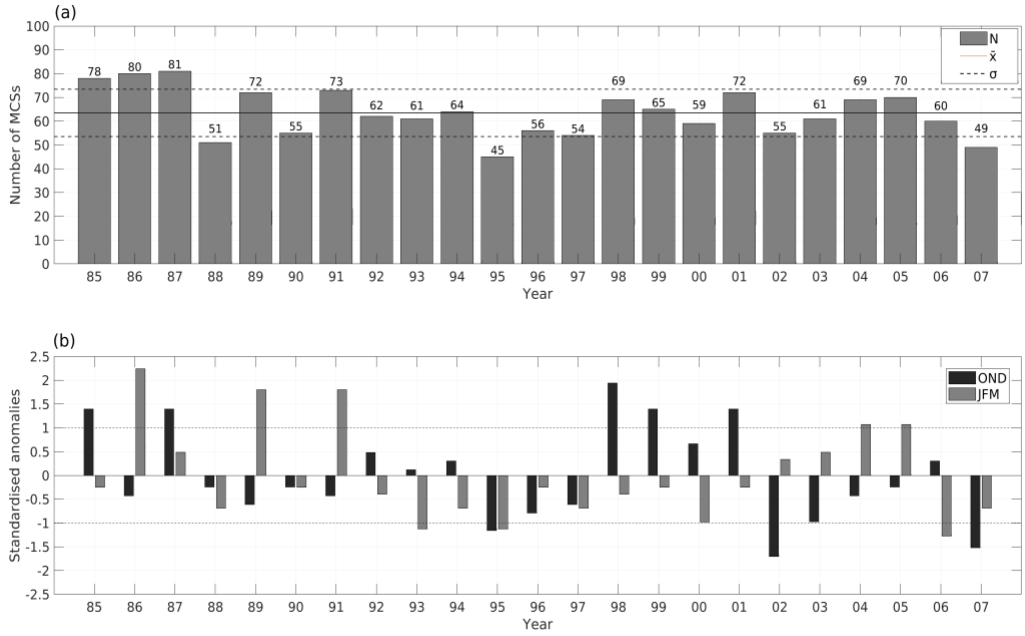

Figure 4.10: (a) Summer totals of MCSs of extended summer [SOND(0)JFMA(+1)] within the domain for period 1985-2008. The first bar is for the 1985/86 summer and the last is 2007/08. The numbers above each bar represent the total number of systems for each summer, while the horizontal line shows the summer mean, and the dashed lines are ±1 standard deviation. **(b)** The standardised anomalies for MCS frequency for the OND (black bars) and JFM (grey bars) periods. The first bars are for the OND of 1985 and JFM of 1986.

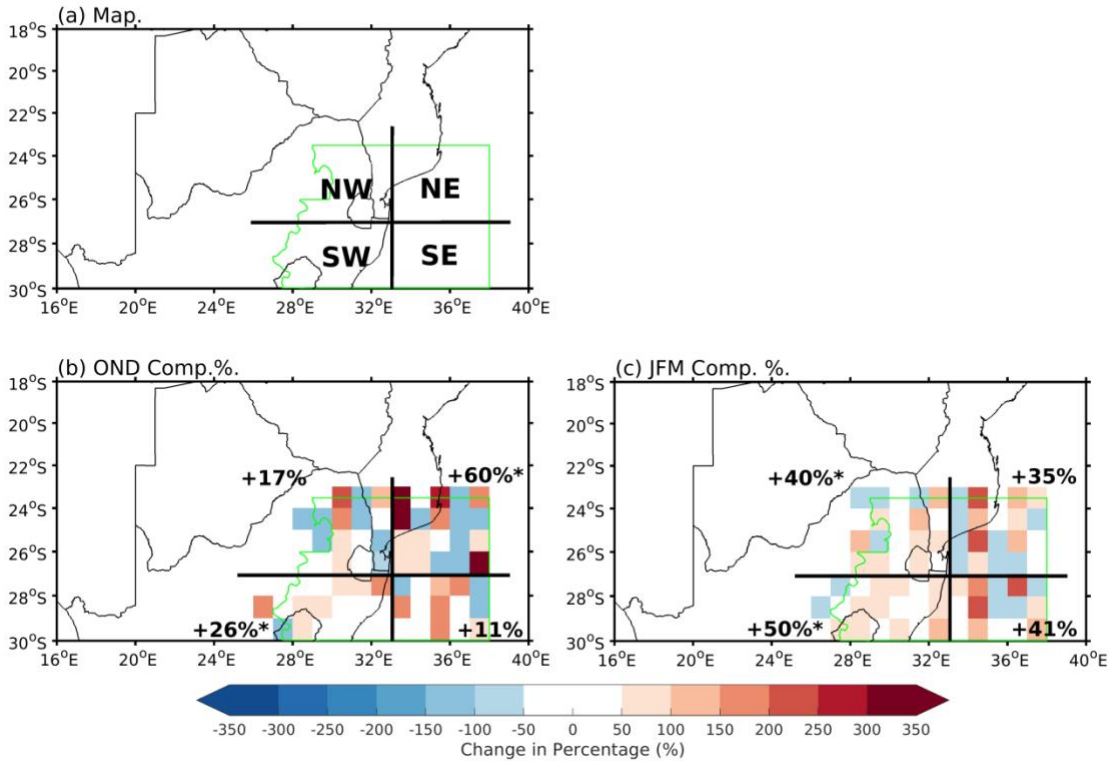

Figure 4.11: (a) shows the quadrants used when referring to the composite anomalies of the spatial distribution of number of MCSs during the developing phase for **(b)** OND and **(c)** JFM. Red (blue) values indicate an increase (decrease) in MCS activity (in percentage) within a given grid cell. The values in each corner represent the mean anomaly of the number of systems (given in percentage change from the mean) that occur across each quadrant (areas are divided up by the black lines). Values that are significant at the 95% confidence level are denoted by "*".

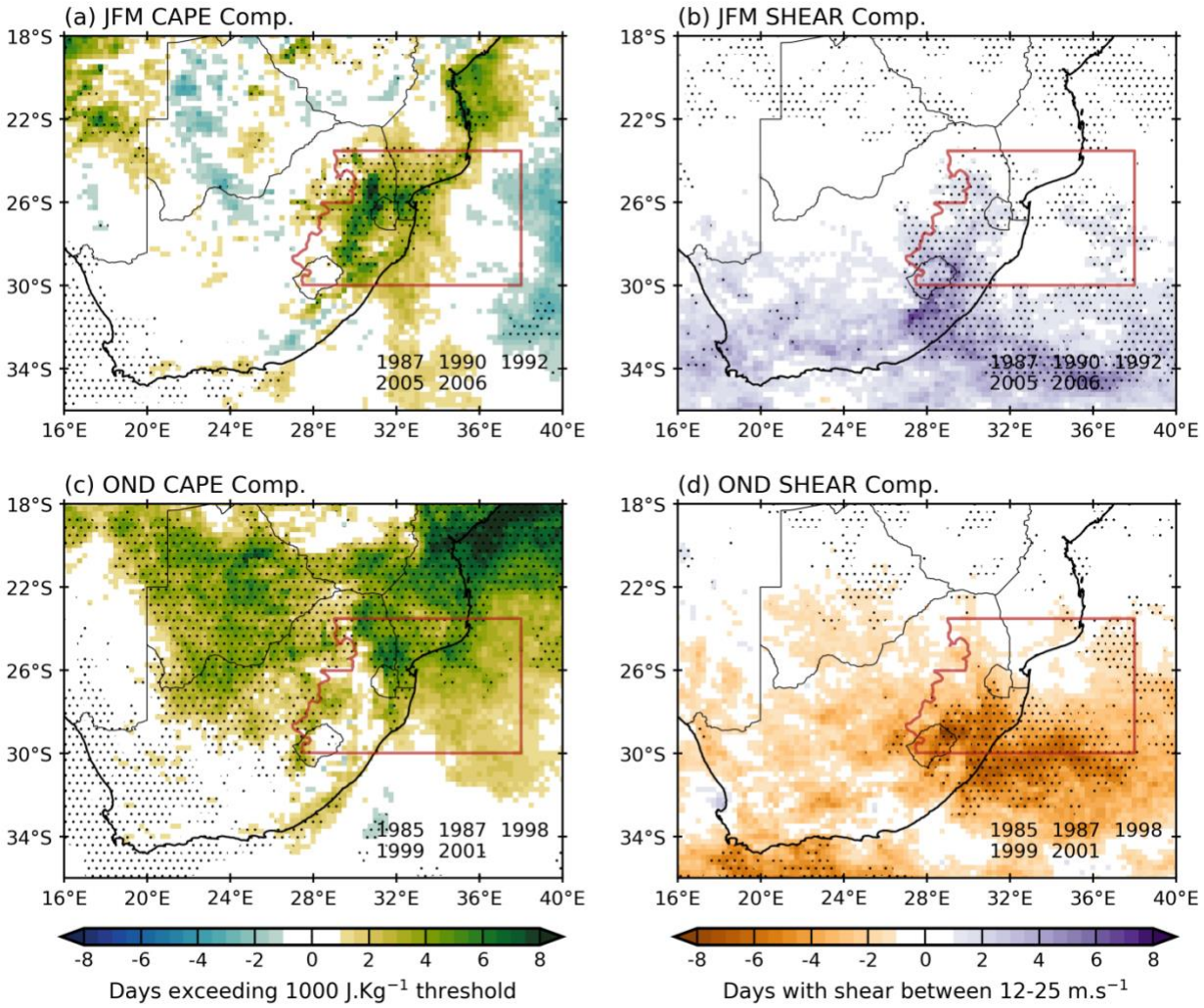

Figure 4.12: JFM composites anomalies for **(a)** days with CAPE exceeding 1000 J.kg^{-1} and **(b)** days with vertical wind shear between 12 - 25 m.s^{-1}. **(c)** and **(d)** same as **(a)** and **(b)** but for OND. The mean is based on ERA5 data from 1985-2008 and only from the 15h00 UTC time step. Stippling denotes values that are significant at or above 95% after applying a two-tailed nonparametric Monte Carlo bootstrap statistical significance test.

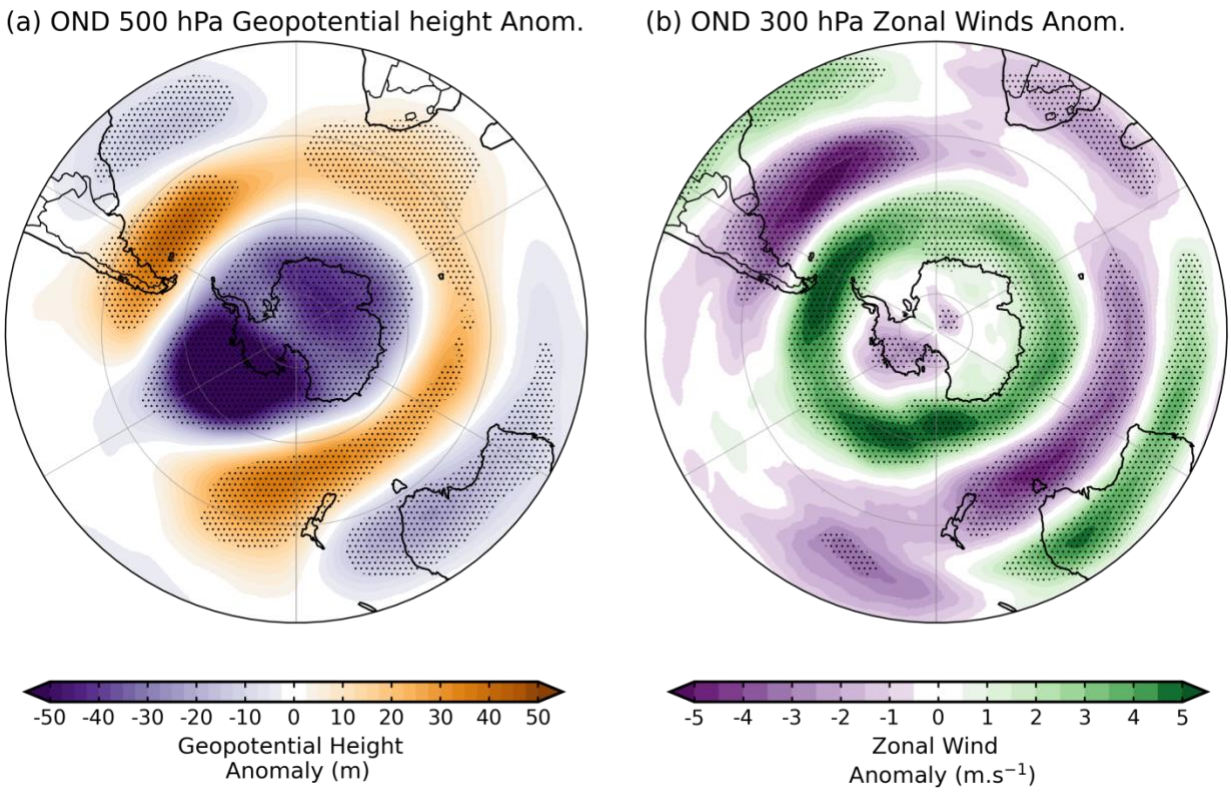

Figure 4.13: OND composites anomalies for **(a)** 500-hPa geopotential height and **(b)** 300-hPa zonal wind. The mean is based on monthly ERA5 data from 1985-2008. Stippling denotes values that are significant at or above 95% after applying a two-tailed nonparametric Monte Carlo bootstrap statistical significance test.

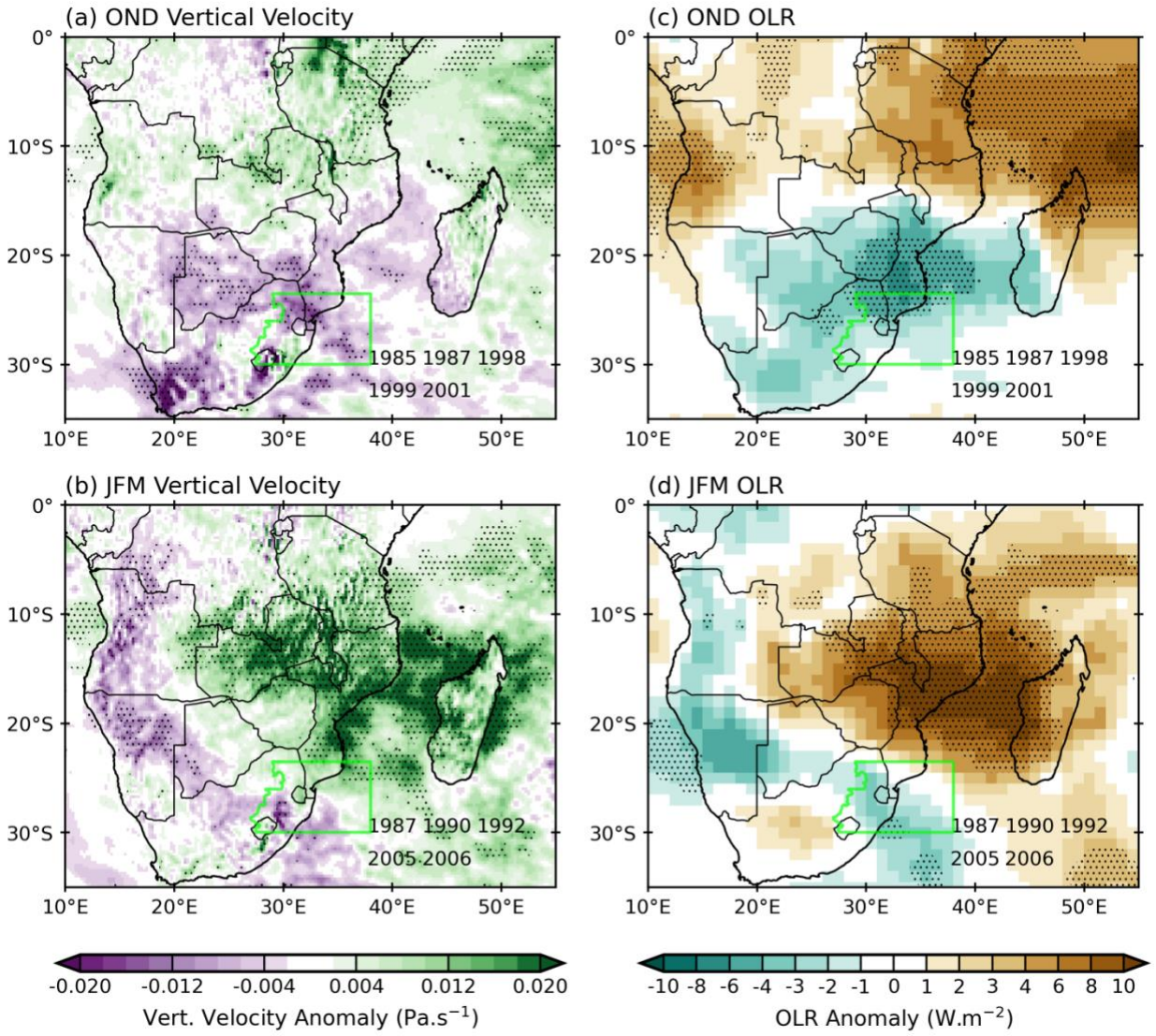

Figure 4.14: Composites anomalies of vertical velocity for **(a)** OND and **(b)** JFM. The mean is based on monthly ERA5 data from 1985-2008. The corresponding OLR anomalies, based on NOAA OLR, are shown in **(c)** OND and **(d)** JFM. Stippling denotes values that are significant at or above 95% after applying a two-tailed nonparametric Monte Carlo bootstrap statistical significance test.

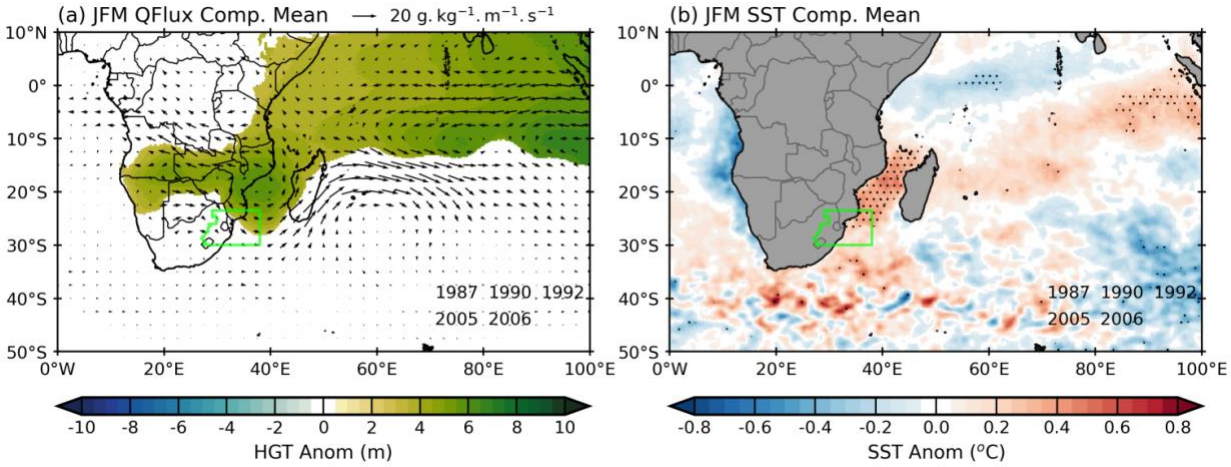

Figure 4.15: Composites JFM anomalies for **(a)** 850-hPa geopotential height (shaded; m) and moisture flux (vectors; $g.kg^{-1}$ $m.s^{-1}$) and **(b)** SST. The SST composite is based on monthly OISST data from 1985-2008. In (a), geopotential values that are not significant are masked out, while in (b) stippling denotes values that are significant at or above 95% after applying a two-tailed nonparametric Monte Carlo bootstrap statistical significance test.

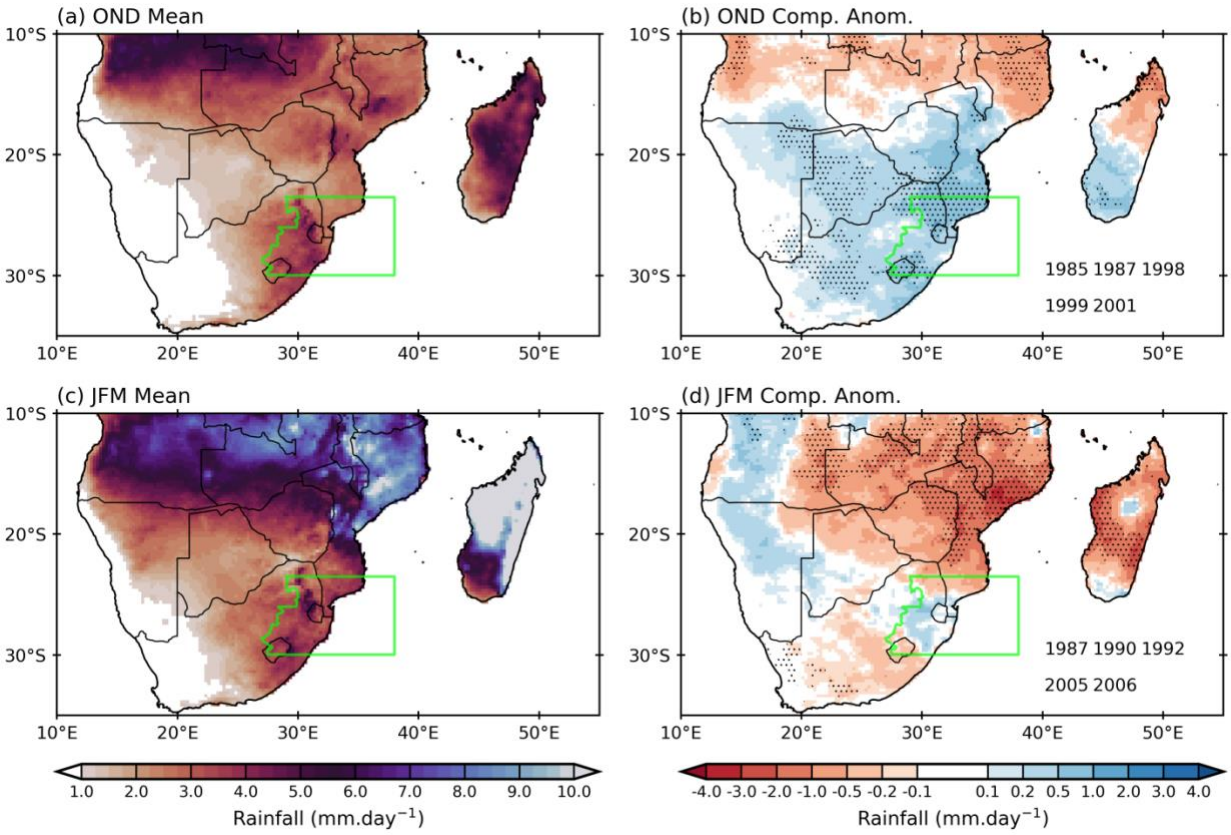

Figure 4.16: (a) Mean OND rainfall (shaded; mm.day^{-1}) and **(b)** OND composite anomaly of rainfall (shaded; mm.day^{-1}) for OND periods with high MCS activity (years given in bottom right-hand panel). The mean is based on CHIRPS daily data from 1985-2008. Stippling denotes values that are significant at or above 95% after applying a two-tailed nonparametric Monte Carlo bootstrap statistical significance test. **(c)** and **(d)** same as (a) and (b) but for JFM.

Chapter 5: Extreme rainfall events related to long-lived MCSs

This chapter investigates the rainfall impact of long-lived mesoscale convective systems (MCSs) over part of eastern South Africa where MCSs mostly have an impact on people's livelihoods and the regional economy. Most of the population here is poor and is dependent on rain-fed subsistence agriculture and the farming industry (e.g., sugar cane) that contributes to the national economy. We examine the links between MCSs and extreme rainfall events, and their contribution to two smaller domains that cover the KwaZulu-Natal (KZN) Province in South Africa and parts of Eswatini (green polygons in **Fig. 5.1**) during October-March. In the previous **Chapter 4**, it was revealed that an increase in rainfall often occurred in regions containing anomalously high MCS activity during OND and JFM. Thus, **Chapter 5** analysis of the impact of MCSs related to extreme rainfall events is based on these two summer seasons. The summer season is divided into two seasons, early summer [October-December (OND)], and late summer [January-March (JFM)]. In this chapter, the role of large long-lived MCSs in extreme rainfall events over eastern South Africa is assessed, together with the contribution of extreme rainfall events that are associated with large, long-lived MCSs towards seasonal and monthly rainfall totals. Most part of southeastern Africa receives its significant rainfall during austral summer (December-February, DJF), and most of rainfall over the east coast and also the interior of South Africa is of convective origin which is found to be predominantly a summer rainfall region (**Fig. 2.2**) (Tyson and Preston-Whyte, 2000).

5.1. MCSs and Extreme Rainfall

The Climate Hazards Infrared Precipitation with Stations (CHIRPS) rainfall dataset is used to identify the top 50 extreme daily rainfall events based on the amount of rainfall that occurred, and the areal extent of the rainfall. A subset of the top 50 extreme rainfall events is identified for each of the two domains. The MCSs associated with these ranked rainfall events are listed in **Table 5.1** (northern domain) and **Table 5.2** (southern domain). The MCSs associated with the extreme rainfall events were determined by matching MCS database developed in **Chapter 4** with that of

the ranked days of extreme rainfall. The northern domain and southern domain of KZN have shown to have local environmental factors that played a role in the increase in long-lived MCS activity between OND and JFM. It was illustrated in **Chapter 4** that the land-based southwest and northwest quadrants contained the largest increase in MCS frequency. For these reasons, this chapter focuses its place on the MCS related extreme rainfall events that occurred within these two small domains.

Out of the top 50 extreme daily rainfall events in the northern domain, 42% (21 events) are found to be linked to an MCS (**Table 5.1**). Seven of these 21 events are within the top 10 ranked rainfall events. For the southern domain, 34% (17 events) of the extreme rainfall events are linked to MCSs (**Table 5.2**). Other extreme rainfall producers during this period include cut-off lows, tropical lows, and tropical-extratropical cloud bands. No tropical cyclones occurred in the region during the period of analysis, but they are known to produce very large amounts of rainfall on the rare occasions that they make landfall near the region. For example, Tropical Cyclone Domoina produced 597 mm in rainfall in January-February 1984 which led to the then province of Natal being declared a disaster area (Grobler, 2003).

For the northern domain, it should be noted while 21 of these top 50 extreme rainfall events occur in October and March, only 9 of these 21 events are as a result of MCSs, consistent with the monthly climatology shown in **Fig. 4.5**. Similarly, the southern domain also contains a high portion (17 out of 50) of extreme rainfall events during October and March. However, only 6 of these 17 extreme events resulted from an MCS. Most of the remaining events during these months for both domains are cut-off lows consistent with previous studies on the climatology of these events over subtropical southern Africa, which show October and March/April to be when these systems typically occur (Singleton and Reason, 2007ab; Favre et al. 2012).

During the core summer months (DJF), MCSs are linked to 11 out of 21 of the extreme daily rainfall events in the northern domain. The peak in MCS activity for the northern KZN domain is typically NDJ. Surprisingly, only one MCS was responsible for the 7 out of the top 50 events which occurred in November since this is typically a month of frequent MCS activity. For the

southern domain, 7 out of the 17 events in DJF were linked to an MCS and November is now a bigger contributor with 4 out of 7 extreme daily rainfall events linked to an MCS.

There are no obvious similarities in MCS properties for the different extreme rainfall events in the two domains. Of the 38 MCS events, the duration ranges from 6 hours through to 51 hours, with 14 (9) of the events lasting longer than 12 hours for the northern (southern) domain. The size of the cloud shield of the MCS linked to extreme rainfall also varies from relatively small systems of around 28000 km^2 in size to large systems of over 700000 km^2. Exaggeration of the size of the MCSs (> 700000 km^2) is due to neighbouring clouds and it is apparent that occasionally events that are flagged as an MCS by the Huang et al. (2018) methodology appear to contain tropical-extratropical cloud band characteristics (i.e., an expanse of cloud cover and rainfall stretching diagonally northwest – southeast across southern Africa). The potential links between similarities in environmental conditions favouring MCS development, and that of cloud bands were noted by Blamey and Reason (2013). Although quasi-circular systems are present, with some reaching mesoscale convective complex (MCC) status, majority of the cases are either more linear systems or more disorganized. To highlight these different characteristics between MCSs, plotted in **Figure 5.2** are six of the heavy rainfall producing MCSs over the two domains. Although in general there is no clear pattern of favourable MCS initiation points that result in the heavy rainfall over the northern domain, many of the systems first reach MCS status further south along the coast before travelling northeastwards following the midlevel westerly flow (**Fig. 5.3**). The rainfall produced by these six MCSs is generally widespread across the two domains (**Fig. 5.2**). The maximum in rainfall produced over the land is located either along the eastern edge of the escarpment or near the coast. This typically occurs where convection, denoted by low BT, is at its strongest. There are some events where the daily rainfall totals are influenced by more than one system. For example, **Fig. 5.1c** contained an MCS during the early morning hours on 7 Feb 1991 within the northern sub-domain, while another system developed further to the west/southwest near Lesotho during the evening on the same day (**Fig. 5.1d**) and produced considerable rainfall inside the southern sub-domain.

In general, the northern domain has higher rainfall producing MCSs compared to the southern domain. Out of the 21 MCSs in the northern domain, 12 are estimated to have produced over 100

mm of rainfall whereas for the southern domain, only 5 out of 17 of the systems are estimated to have done so. To put this value into context, the mean annual rainfall for the northern domain ranges from about 600 mm inland to about 1000 mm near the coast, with the late summer (JFM) having a mean of around 300 mm to 400 mm (**Fig. 5.4**). Thus, these systems that produce over 100 mm in rainfall can be considerable contributors to seasonal or even annual rainfall totals, as documented by Blamey and Reason (2009) for a single MCS in February 2005. Given that many systems occur late at night/early morning (e.g., **Fig. 5.1a**) and hence spread over 2 days, it is likely that the daily values in **Table 5.1** and **Table 5.2** are not the complete rainfall total produced by each system listed.

Using CHIRPS rainfall data for period 1985-2008, seasonal rainfall anomalies for OND and JFM were created for the northern domain and the southern domain (**Fig. 5.5**). In the northern domain out of the 23 seasons, the OND of 1998, 1999, 2000, and 2001 experienced well above average rainfall, as well as contained the most MCS activity (**Fig. 4.10b**). While the driest summers, that of 1986, 1991, 2002, 2003, 2004, and 2005 experienced the lowest MCS frequency (**Fig. 4.10b**). However, in the southern domain, the OND of 1985, 1999, 2001, and 2006, experienced well above average rainfall, as well as contained the most MCS activity, while the driest summer (negative anomalies), that of 1990, 1992, 2002, and 2003, experienced the lowest MCS frequency (**Fig. 4.10b**). Meanwhile, the OND of 1987 and 2001 all contained similar frequency of MCS activity, yet low rainfall was produced over the two sub-domains during these summers (**Fig. 5.5a**).

For JFM 2004, 2005, and 2006 experienced well above average rainfall, as well as contained the most MCS activity, while the driest summer that of 1995, 2001, 2002, and 2007 experienced the lowest MCS frequency in the northern domain. For the southern domain, JFM of 1988, 2004, 2005, and 2006 experienced well above average rainfall, as well as contained the most MCS activity. While the driest summer, that of 1993, 2001, 2002, and 2007 experienced the lowest MCS frequency (**Fig. 4.10b**). However, the late summer seasons of 1987, 1990, and 1992 yielded lowest rainfall with the most MCS activity for both domains. However, it is difficult to evaluate whether the MCS activity or lack of MCS activity may influence the two regions having an above or a below average rainfall of the season. Other systems, such as tropical depression, cut-off lows and

cloud bands make considerable contribution to rainfall over the eastern South Africa (Hart el al. 2013; Rapolaki et al. 2019).

5.2. MCS Contribution to eastern South African summer rainfall

To determine the contribution of long-lived MCSs have on eastern South Africa summer rainfall, top 10 extreme daily rainfall events from each domain were selected based on maximum rainfall produced by each MCS related event. From the top 38 extreme rainfall events analysed in the previous section, 10 extreme rainfall event that produced the highest maximum rainfall from the two sub-domains were selected to be used to analyse here. A subset of MCSs that are associated with the 10 wettest extreme daily rainfall events identified from the top 38 extreme rainfall events are listed in **Table 5.1** (northern domain) and **Table 5.2** (southern domain) and are used here to quantify the average contribution of individual MCS rainfall events to seasonal and monthly rainfall totals. The contribution of long-lived MCSs to eastern South Africa rainfall is defined as the ratio of MCS related daily rainfall of the event towards the seasonal and monthly rainfall total at each grid point. For each event, the percentage of rainfall contribution at each grid point is calculated using daily rainfall of the MCS event and total rainfall of that particular season or month (see - **Equation 1**). Although this is calculated across the domain, only values within the small KZN domains are of interest and used for the statistics in the **Table 5.3** and **Table 5.4** to indicate how much that MCS contributed to the seasonal rainfall totals. In order to investigate the contribution of MCSs to the seasonal and monthly rainfall, extreme MCSs are used. Another approach to investigate the contribution of MCSs to the seasonal and monthly rainfall would be to examine the contribution from all MCSs.

The impact of the MCS that occurred in March 1990 is used to demonstrate the methodology described above in **Fig. 5.6**. This event is chosen because it is a system that is not affected by other cloud structures, positioned against the KZN coastline and is visually easy to explain the contribution totals. **Fig. 5.6a** shows the spatial extent of the MCS (through cloud top brightness temperature) on 24 March 1990 at 18h00, while the rainfall produced by the system is shown in **Fig. 5.6b**. This MCS produced a considerable amount of rainfall (exceeding 100 mm in many locations) along the central part of the KZN coastline, with a maximum rainfall of 203.9 mm. The

total rainfall for JFM in 1990 over the same region where this MCS occurred ranges from between 350 mm to 450 mm (**Fig. 5.6c**). It is then determined that the MCS contributed between 20% - 40% of the total JFM 1990 rainfall over large parts of KZN with a maximum contribution of 56% (**Fig. 5.6d**).

Extending the above methodology to all the MCSs, it is calculated that for the northern domain, MCSs accounted for maximum contribution between 20%–56%, with mean contribution between 9%-19% and median contribution between 8%-19% for the individual seasonal rainfall total (JFM/OND) (**Table 5.3**). If OND season is excluded from the analysis, then the contribution of MCSs to summer rainfall increases, with the systems' maximum contribution ranging between 24%-56% over the sub-domain. For the southern domain, MCSs showed maximum contribution between 17%-53%, with a mean contribution between 6%-14% and median contribution between 6%-14% (**Table 5.4**). While, for the southern domain if OND season is excluded in the analysis, the systems' maximum contribution doesn't change much to summer rainfall over the sub-domain. Maximum rainfall contribution is the grid point with the most rainfall contribution, mean rainfall contribution is a spatial mean across the domain and median rainfall contribution is a median between two grid points. The impact that MCS related extreme rainfall events have on eastern South Africa summer rainfall slightly decreases when one is looking at MCS contribution towards climatological seasonal mean rainfall of JFM and OND. However, even though MCSs in the northern domain produce a higher maximum rainfall than systems in the southern domain, the contribution of MCSs between the two domains is fairly similar. It is also clear that there is considerable interannual variability associated with the activity of MCSs and MCS related extreme rainfall events and contribution that these systems make to seasonal rainfall total.

The variety in spatial rainfall contribution of MCSs that are related to the 10 wettest extreme rainfall events is seen in **Fig. 5.7**, with these events showing maximum contribution between 24%-55% in the northern domain and between 21%-53% over the southern domain. There are some events where the daily rainfall totals are influenced by more than one system or one event making a widespread significant rainfall contribution for the two sub-domains (e.g., **Fig. 5.7d, Fig. 5.7b** and **Fig. 5.7d**). For example, the contribution in the two sub-domains in **Fig. 5.7d** and **Fig. 5.7b** were influenced by two separate MCSs that occurred at the same day, while for **Fig. 5.7d** one MCS

was responsible for the widespread rainfall contribution that contributed significantly for the two sub-domains. In addition, there is considerable spatial variability associated with MCS related extreme rainfall events contribution to summer rainfall over eastern South Africa. The rainfall contribution of long-lived MCSs over the northern domain is primarily confined to the eastern part off the east coast of South Africa near the moisture source (warm waters of Agulhas Current) and contained a higher maximum rainfall contribution during JFM (e.g., **Fig. 5.7a, Fig. 5.7b, Fig. 5.67c**), which is consistent with timing of MCSs over the region often at their maximum extent by the time they reach the coast (e.g., **Fig. 5.1**). The rainfall contribution of MCSs over the southern domain is confined along the east of the escarpment over the steep topography regions (e.g., **Fig. 5.7d, Fig. 5.7e, Fig. 5.7f**), which is more linked to favorable environmental conditions (e.g., days with favorable CAPE and wind shear) (**Fig. 4.12b and Fig. 4.12b**), particularly over the southwest quadrant during JFM which contained the largest increase in MCS frequency (**Fig. 4.11c**).

For monthly analysis, the northern domain MCSs showed maximum rainfall contribution of between 57%-100%, with mean contribution of between 21%-39% and median contribution of between 22%-39% towards monthly rainfall total (**Table A.5.1**). However, contribution of MCSs varies from month to month. For December, the maximum contribution is low (57%) compared to other months (**Table A.5.1**). During January, MCSs showed maximum contribution of 59% and 80%, with mean contribution of 23% and 31% and median contribution of 23% and 30% over the northern sub-domain. In February, maximum contribution of between 59%-100%, with mean contribution of between 21%-39% and median contribution of between 22%-39%. For March, all MCSs showed maximum contribution of 100% for their individual monthly rainfall total over the northern domain, with mean contribution between 33%-39% and median contributing of between 31%-39%.

For the southern domain, MCS related extreme rainfall events showed maximum contribution of between 28%-100%, with mean contribution between of 15%-43% and median contribution between of 14%-44% towards monthly rainfall totals (**Table A.5.2**). During November, MCSs accounted for maximum contribution of 28% and 100%, with mean contribution of 15% and 18%, and median contribution 15% and 18% respectively (**Table A.5.2**). For January, an individual MCS contributed up to 76%, with mean contribution 24% and median contribution of 23%. During

February, MCSs showed maximum contribution of between 66%-100%, with mean contribution of between 25%-43% and median contribution of between 23%-44%. For March, MCSs showed maximum contribution of between 67%-100%, with mean contribution of between 19%-30% and median contribution of between 14%-28%. Caution must be taken because these statistics are based only on 10 extreme events.

To help understand how long-lived MCSs that are related to extreme rainfall events influence seasonal rainfall over part of eastern South Africa, spatial standardised rainfall anomalies for OND and JFM were created using CHIRPS for the 10 of the wettest events (**Fig. 5.8** and **Fig. 5.9**, respectively). On average, 9 events (1 event) occurred during JFM (OND) summer months for the northern domain (**Fig. 5.8)**, highlighting that most MCSs with substantial rainfall occurred during JFM which is consistent with the largest increase in MCS frequency in the land-based northwest quadrant (**Fig. 4.11c**). For the most part, there is average or above average rainfall in the northern domain with JFM of 1985, 1991, 1995, 1996, 1997, 2000 and OND of 1995 experienced positive rainfall anomalies with most of MCSs occurring over the coast in the northwest and southwest quadrant during JFM (**Fig. 4.11c**). While JFM 1990 and 1989 experienced negative anomalies and normal conditions respectively over the small domain **(Fig. 5.8**), with summer of 1990 experiencing the lowest average number of MCSs (**Fig. 4.10a**) and 1989 experiencing the anomalously low seasonal number of long lived MCS over the region (**Fig. 4.10b**). For southern domain, 8 events (2 events) occurred during JFM (OND), with the southwest quadrant also showing a significant increase in number of MCSs in JFM. For the most part, there is an average or above average rainfall in the southern domain with JFM of 1988, 1991, 1996, 1998 and OND 1989 experiencing positive rainfall anomalies (**Fig. 5.9**). These results are consistent with the significant increase in JFM MCSs that occurred over the land-based southwest and northwest quadrant (**Fig. 4.11c**) and significant increase in environmental conditions that are favorable for MCS development over the region (**Fig. 4.12a and Fig. 4.12b**). While JFM of 1990, 1999 and OND of 1997 experiencing negative anomalies and normal conditions respectively over the southern domain (**Fig. 5.9**)**.**

5.3. Summary

This chapter investigated the role of large, long-lived MCSs in extreme rainfall events over the eastern half of southern Africa. Focus was placed on two sub-domains, namely; the northern part of the KZN province in South Africa/Eswatini and then a second covering the southern part of the KZN. Given the relatively strict MCS thresholds used in the study, extreme rainfall events for smaller, and short-lived, systems were excluded. Heavy rainfall events are frequently experienced over these two sub-domains and can result in substantial socio-economic impacts, including loss of life in some cases. However, long-term studies of extreme weather events for the region are generally limited by a lack of high spatial and temporal observation data. Results in this study show that just under 40% of the top 50 extreme daily rainfall events in these two regions during October-March are linked to these long-lived MCSs. Furthermore, for the northern domain, around 50% of the top extreme daily rainfall events during December-February are associated with an MCS. More than half of these MCSs produced over 100 mm, with a two of nocturnal MCSs, satisfying MCC criteria, producing over 200 mm within 24 hours. These results suggest that variability in the frequency and intensity of MCSs could have a considerable impact on regional rainfall totals during summer over this part of southeastern Africa, and further highlights the need to better understand local environmental factors that play a role in the frequency, intensity, and evolution of these systems.

The results presented here also show that there is considerable variability in the contribution of MCSs towards seasonal and monthly rainfall totals. Long-lived MCSs contributed significantly to individual seasonal and monthly totals over the most part of eastern South Africa when looking at the maximum rainfall contribution of MCS related extreme rainfall events. It is found that these long-lived MCSs can account for up to 56% of the seasonal rainfall total of that summer. Extreme rainfall events that are related to MCSs over northern domain of KZN accounted for maximum contribution of between 29%-54%. While for the southern domain MCSs contributed between 21%-48% towards seasonal rainfall total suggesting that MCS over the northern domain contribute higher than the southern domain. The rainfall contribution of MCS increases when looking at the month-to-month rainfall contribution, some months MCSs accounted for up to 100% of the individual monthly rainfall total. There is also noticeable interannual variability of seasonal rainfall

over the northern and the southern domain and considerable spatial variability in seasonal rainfall of MCS related extreme rainfall events over the two sub-domains.

In order to see the variety in spatial rainfall contribution of MCS related to extreme rainfall events, contribution of three MCSs extreme rainfall events to individual seasonal rainfall totals from two sub-domains were analysed. The results suggest that there is spatial variability in MCS related extreme rainfall events contribution toward individual season rainfall totals, with rainfall contribution over the northern domain is mostly confined along the east coast near the moisture source, while over the southern the rainfall contribution is most over the east of the escarpment following the high topography. Most of the MCS related extreme rainfall events occurred during the JFM compared to the OND, with JFM rainfall patterns confined along the east coast compared to the interior. However, both the OND and JFM seasonal rainfall from the MCS extreme rainfall events suggest that these MCS events played an important role in mitigating dry conditions in individual seasons, or in some cases resulted in seasons with above average rainfall across the region.

These results are consistent with previous studies investigating MCSs in South Africa. The case study of Blamey and Reason (2009) showed that an individual MCS in February 2005 contributed approximately 20% to DJF rainfall total at two weather stations in the northern parts of the KZN province. Similarly, the mean summer rainfall contribution of MCCs (based on TRMM rainfall data) for most part of the northern parts of the KZN province has been calculated as between 8% and 18% (Blamey and Reason, 2013).

Caution must be taken that some of the MCSs occurred late at night/early morning, their rainfall contribution would count as being spread over two days. The one-day extreme analysis does not take into account the total amount of rainfall such MCSs produced since these systems last longer than 24 hours. Nevertheless, the results here reinforce the suggestion that MCSs are important rainfall producers for the eastern South Africa region. The previous chapter highlighted that those years with above MCSs activity over eastern South Africa resulted in an increase in rainfall for that season. In this chapter, evidence has been presented indicating that a single MCS can have a considerable impact on the seasonal rainfall total. Thus, these are important results for this region

that has for the past two decades experienced a slow decline in the summer rainfall totals (Blamey et al. 2018).

Overall, MCSs are not considered the dominant contributor to South African summer rainfall. Previous findings have shown that cloud bands (TTTs) are the biggest contributors of summer rainfall, with these systems contributing between 30%-50% during all summer months (Hart et al. 2013). Another considerable contributor are cut-off lows, which have been shown to contribute between 25%-35 % of South African annual accumulative rainfall (Favre et al. 2013). However, cut-off lows tend to occur in the transition's seasons (Singleton and Reason, 2007ab).

Table 5.1: A subset of the top 50 ranked extreme rainfall events over northern domain in KwaZulu-Natal that are related with an MCSs over the eastern South Africa. The rank of the event within the top 50 is given in the first column, followed by the date of the event, and then various properties of the MCS (continued next page).

Rank	Date	MCS ID	Duration (hours)	Max. Size (km^2)	T_B min (^oC)	Max. Rain (mm)
1	17 Mar 00	1659	27	749,335.3	-83.1	202.1
2	23 Oct 96	2462	27	36,171.03	-65.7	89.1
3	01 Jan 00	49	12	145,451.8	-76.4	135.4
4	22 Dec 95	2320	21	521,914.1	-80.4	110.1
7	01 Jan 01	3	6	197,303.3	-70.4	95.9
9	07 Feb 85	781	6	715,02.98	-75.7	151.0
10	24 Mar 90	2634	51	440,075.1	-83.7	203.9
11	07 Feb 91	662	15	100,212.3	-83.7	145.6
17	28 Nov 89	2993	27	322,596.6	-78.4	97.3
19	18 Mar 00	1800	39	221,831.5	-82.4	139.5
21	11 Mar 04	1080	9	42,531.3	-67.7	108.5
28	27 Jan 96	2724	21	137,339.5	-88.4	96.9
29	03 Mar 96	245	18	45,973.7	-68.4	81.1
32	14 Feb 96	1458	18	229,481.4	-88.4	132.5
38	14 Feb 89	1380	15	150,580.1	-72.4	132.8
44	28 Dec 93	3094	9	290,661.3	-82.4	71.1
45	22 Jan 97	2086	6	112,874.2	-71.7	114.7

46	01 Mar 05	95	9	166,173.5	-66.3	101.1
47	12 Oct 87	1382	15	282,992.8	-67.7	53.9
49	29 Oct 85	3349	27	324,714.7	-68.4	86.9
50	05 Dec 90	494	24	262,984.8	-73.7	73.4

Table 5.2: Same as **Table 5.1** but for events over the southern domain in KwaZulu-Natal.

Rank	Date	MCS ID	Duration (hours)	Max. Size (km^2)	T_B min (°C)	Max. Rain (mm)
2	07 Feb 91	779	21	149,932.6	-77.7	196.1
6	28 Nov 89	2879	15	179,300.7	-75.0	83.9
9	03 Oct 07	474	12	290,864.1	-65.0	74.1
10	01 Oct 93	64	12	202,592.7	-69.0	81.8
12	24 Mar 90	2634	51	440,075.1	-83.7	154.2
13	26 Jan 96	2724	21	137,339.5	-88.4	99.7
17	11 Mar 08	1231	9	52,603.27	-71.0	75.8
26	01 Mar 88	72	6	39,914.88	-64.3	136.1
29	25 Dec 01	2550	45	432,158.9	-79.7	73.7
39	26 Nov 89	2792	18	712,457.9	-77.0	63.0
41	17 Nov 95	2792	15	75,158.59	-71.0	54.5
42	03 Feb 99	183	6	28,975.34	-59.0	87.5
45	06 Nov 97	535	9	100,633.8	-63.7	129.8
46	23 Dec 01	2208	18	148,708.7	-66.3	67.7
47	15 Feb 98	1269	6	66,052.2	-62.3	86.6
48	12 Mar 88	1197	30	132,807.2	-65.0	110.9
49	25 Feb 98	2249	6	68,210.63	-58.3	84.7

Table 5.3: A subset of 10 extreme rainfall events from the top 50 ranked extreme rainfall events over northern domain in KwaZulu-Natal that are related with an MCSs over the eastern South Africa. The rank of the event within the top 50 is given in the first column, followed by the date of the event, and then various properties of the MCS. The last two columns show the maximum rainfall contribution (%), mean rainfall contribution (%) and median rainfall contribution of each MCS event (per day) to seasonal rainfall total (JFM and OND). Maximum rainfall contribution is the grid point with the most rainfall contribution, mean rainfall contribution is a spatial mean across the domain and median rainfall contribution is a median between two grid points.

Rank	**Date**	**Duration (hours)**	**Max. Size (km^2)**	**T_B min (^oC)**	**Max. Rain (mm)**	**Max. Contri. (%)**	**Mean. Contri. (%)**	**Media. Contri. (%)**
1	17 Mar 00	27	749,335.3	-83.1	202.1	55	19	19
3	01 Jan 00	12	145,451.8	-76.4	135.4	24	9	8
4	22 Dec 95	21	521,914.1	-80.4	110.1	20	10	9
9	07 Feb 85	6	715,02.98	-75.7	151.0	34	14	14
10	24 Mar 90	51	440,075.1	-83.7	203.9	56	16	11
11	07 Feb 91	15	100,212.3	-83.7	145.6	24	11	11
19	18 Mar 00	39	221,831.5	-82.4	139.5	27	11	10
32	14 Feb 96	18	229,481.4	-88.4	132.5	25	10	10
38	14 Feb 89	15	150,580.1	-72.4	132.8	34	13	13
45	22 Jan 97	6	112,874.2	-71.7	114.7	24	9	8

Table 5.4: Same as **Table 5.3** but for events over the southern domain in KwaZulu-Natal.

Rank	Date	Duration (hours)	Max. Size (km^2)	T_B min (^oC)	Max. Rain (mm)	Max. Contri. (%)	Mean. Contri. (%)	Media. Contri. (%)
2	07 Feb 91	21	149,932.6	-77.7	196.1	32	13	14
6	28 Nov 89	15	179,300.7	-75.0	83.9	17	8	8
12	24 Mar 90	51	440,075.1	-83.7	154.2	53	10	6
13	26 Jan 96	21	137,339.5	-88.4	99.7	21	8	8
26	01 Mar 88	6	39,914.88	-64.3	136.1	26	10	9
42	03 Feb 99	6	28,975.34	-59.0	87.5	31	14	10
45	06 Nov 97	9	100,633.8	-63.7	129.8	49	8	8
47	15 Feb 98	6	66,052.2	-62.3	86.6	22	9	9
48	12 Mar 88	30	132,807.2	-65.0	110.9	20	6	6
49	25 Feb 98	6	68,210.63	-58.3	84.7	23	10	10

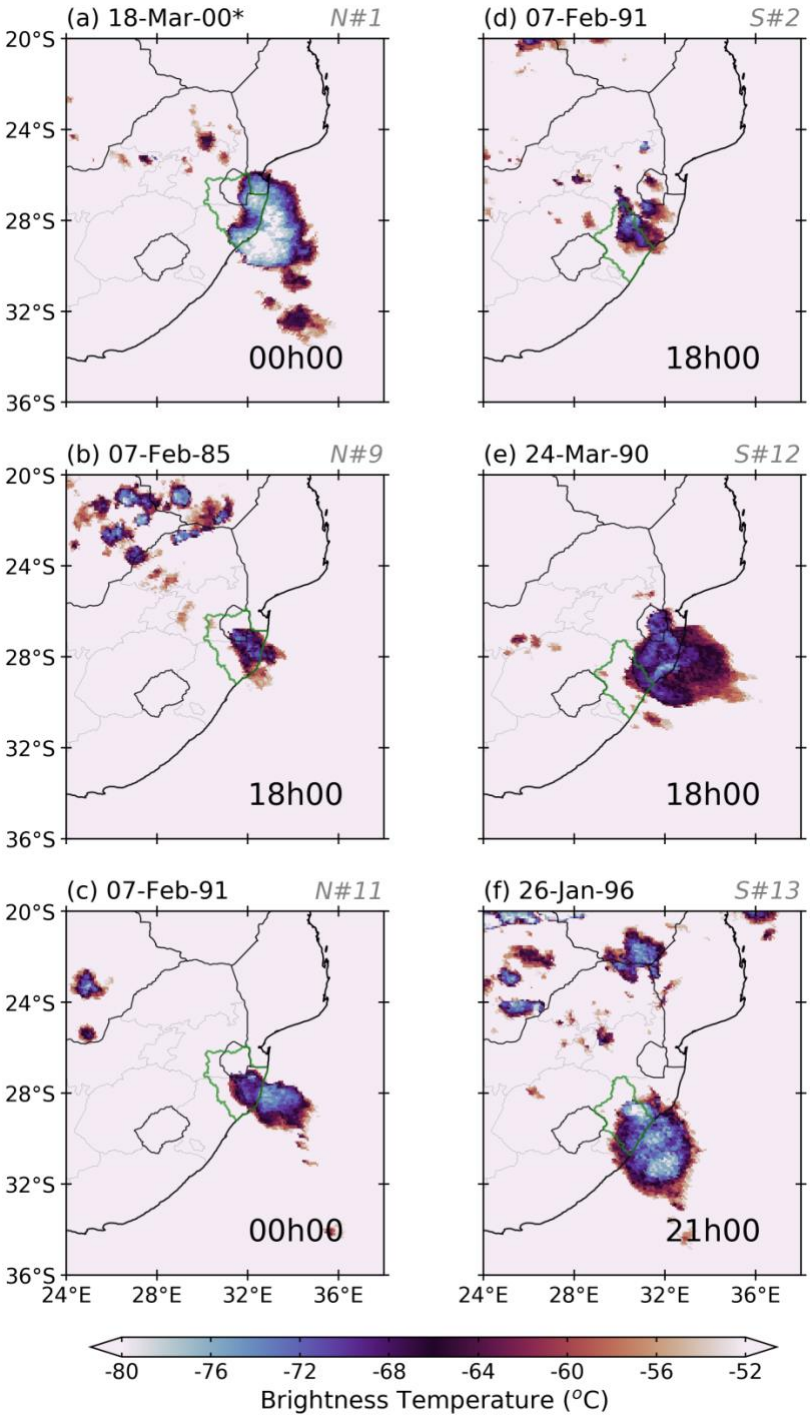

Figure 5.1: GRIDSAT cloud top temperatures (shaded; °C) of the three MCSs found within the top 15 extreme rainfall events for the northern (left panels) and southern (right panels) domains (green polygon). The dates of the events are given in the top left corner and the rank within the top 50 extreme rainfall events is in the top right. The time (in UTC) is shown in the bottom right-hand corner. * Showing MCS at maximum extent, which occurred at 00h00 on 18 March 2000.

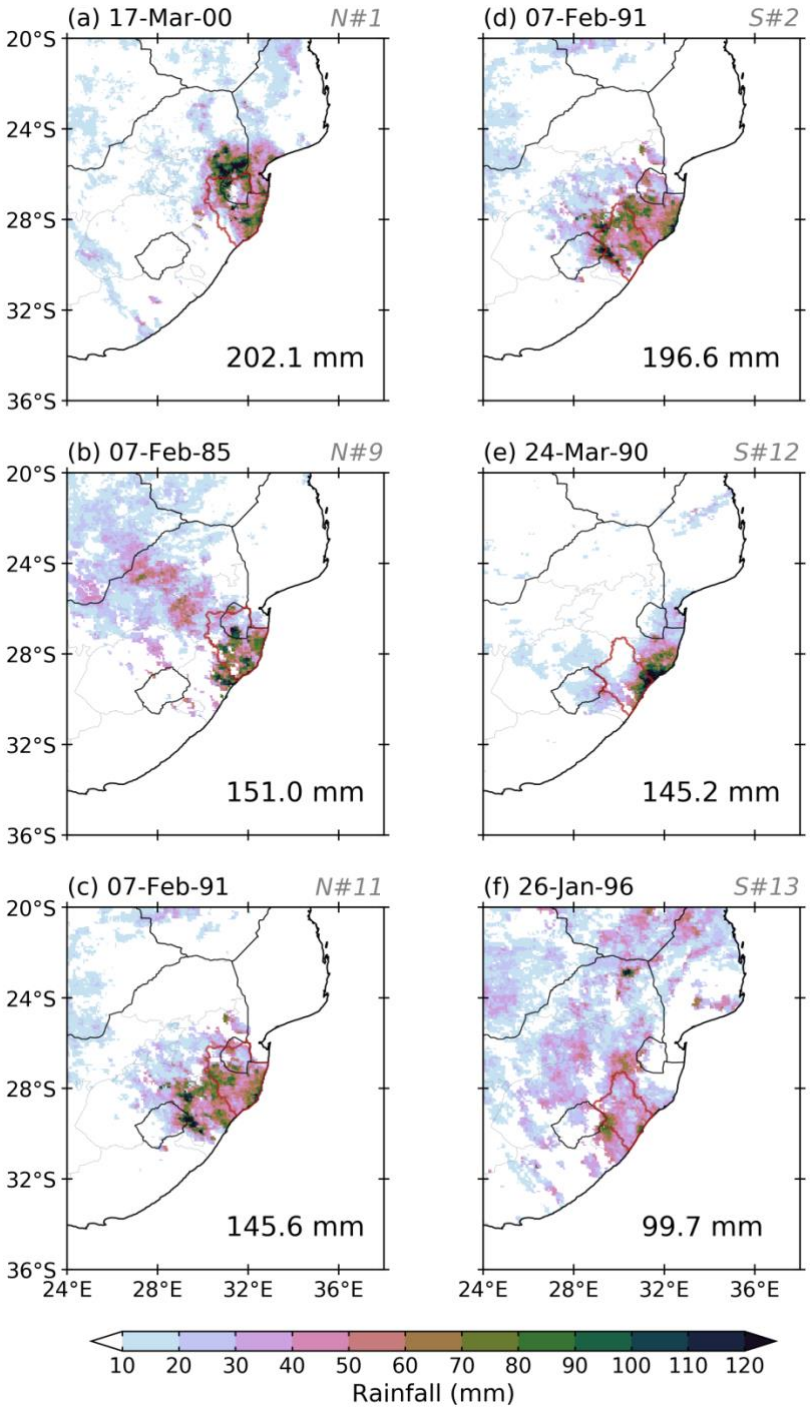

Figure 5.2: CHIRPS daily rainfall (shaded; mm) associated with the three MCS events from the northern (left panels) and southern (right panels) domain depicted in **Fig. 5.1**. The date of the event is given at the top left-hand corner, the rank within the top 50 extreme rainfall events is in the top right and the maximum in rainfall (from within the domain; red polygon) is shown in the bottom right-hand corner. Event in panel e (24-Mar-90) is also event #10 for the northern domain with a maximum of 203.9 mm.

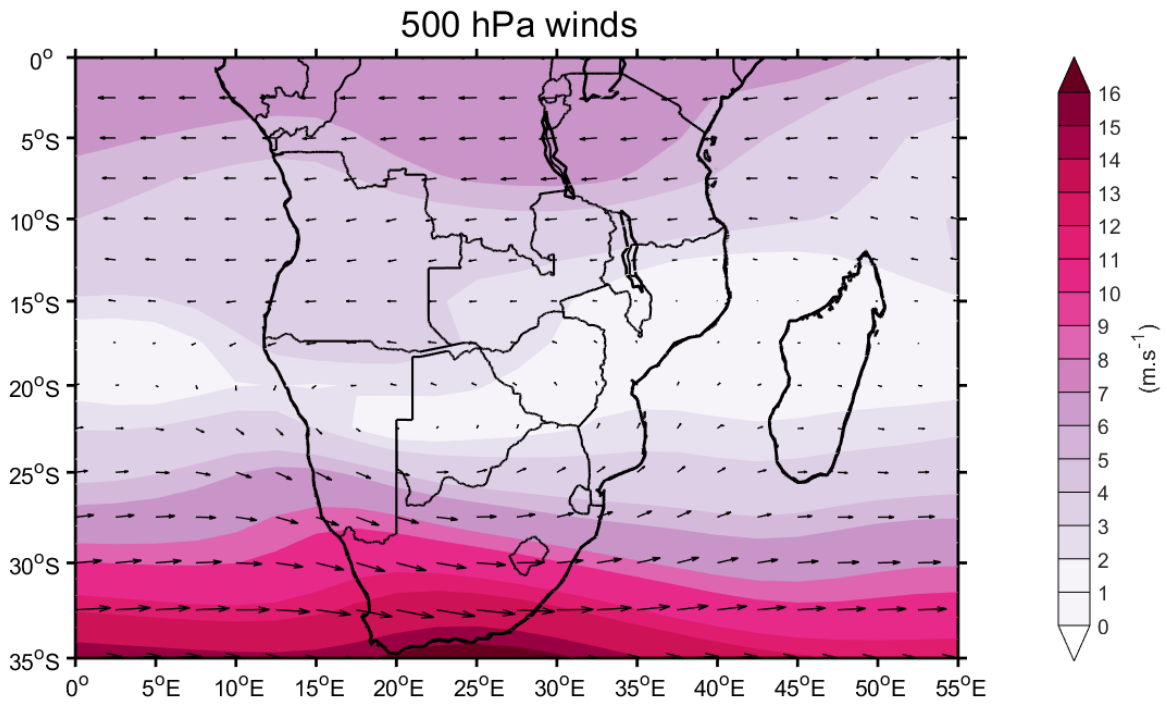

Figure 5.3: ONDJFM climatological mean wind flow at 500 hPa (shaded; $m.s^{-1}$). The climatology is based on NCEP reanalyses data from 1985-2008.

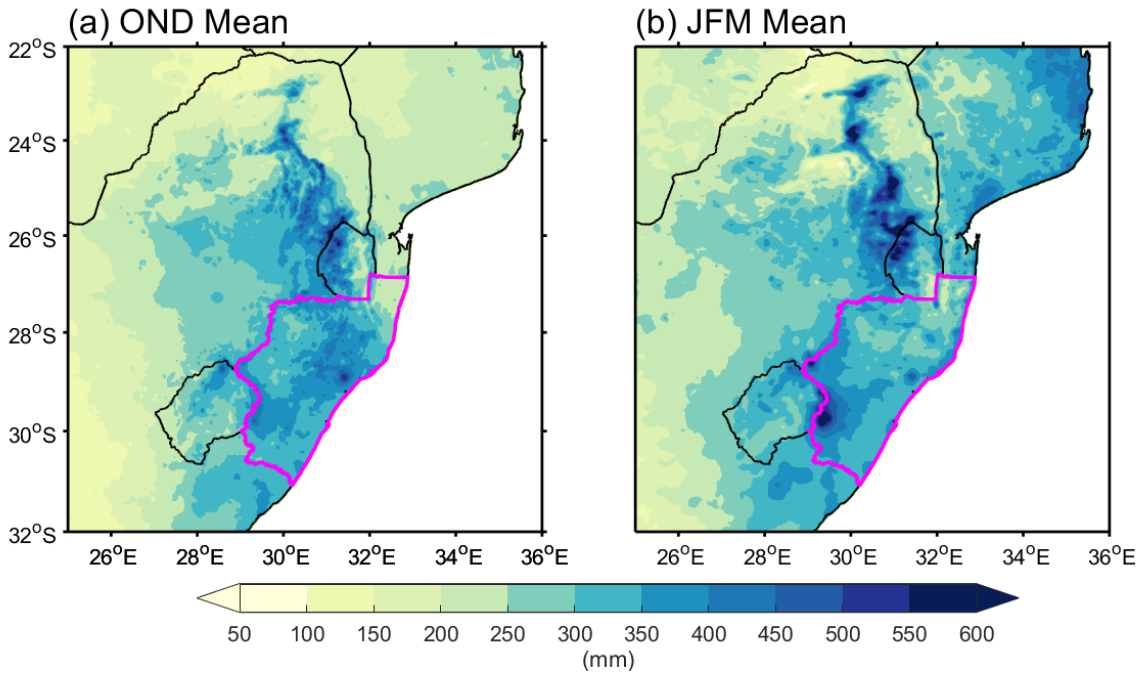

Figure 5.4: (a) OND seasonal Mean rainfall (shaded; mm) and **(b)** JFM seasonal Mean rainfall (shaded; mm). The mean is based on CHIRPS daily data from 1985-2008. For reference, pink polygon illustrates the KZN province (eastern South Africa).

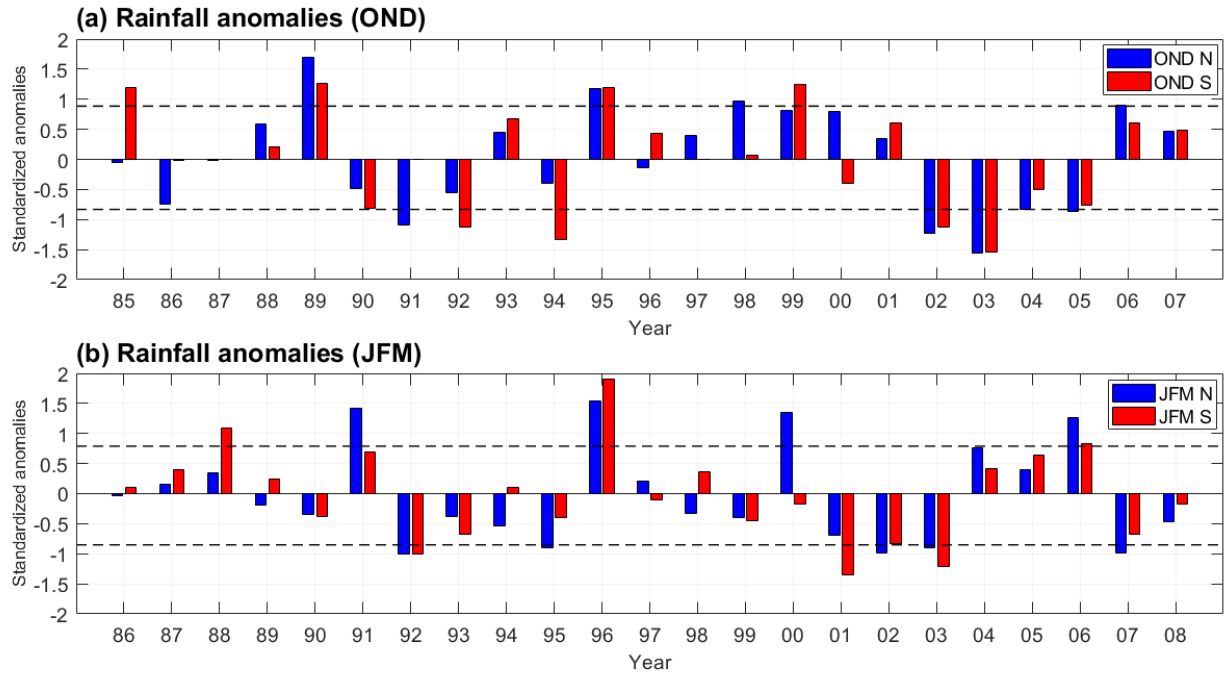

Figure 5.5: Comparison of **(a)** OND standardized rainfall anomalies over the (N) and southern (S) domains and **(b)** JFM standardized rainfall anomalies during the period 1985- 2008, dashed lines are ±1 standard deviation.

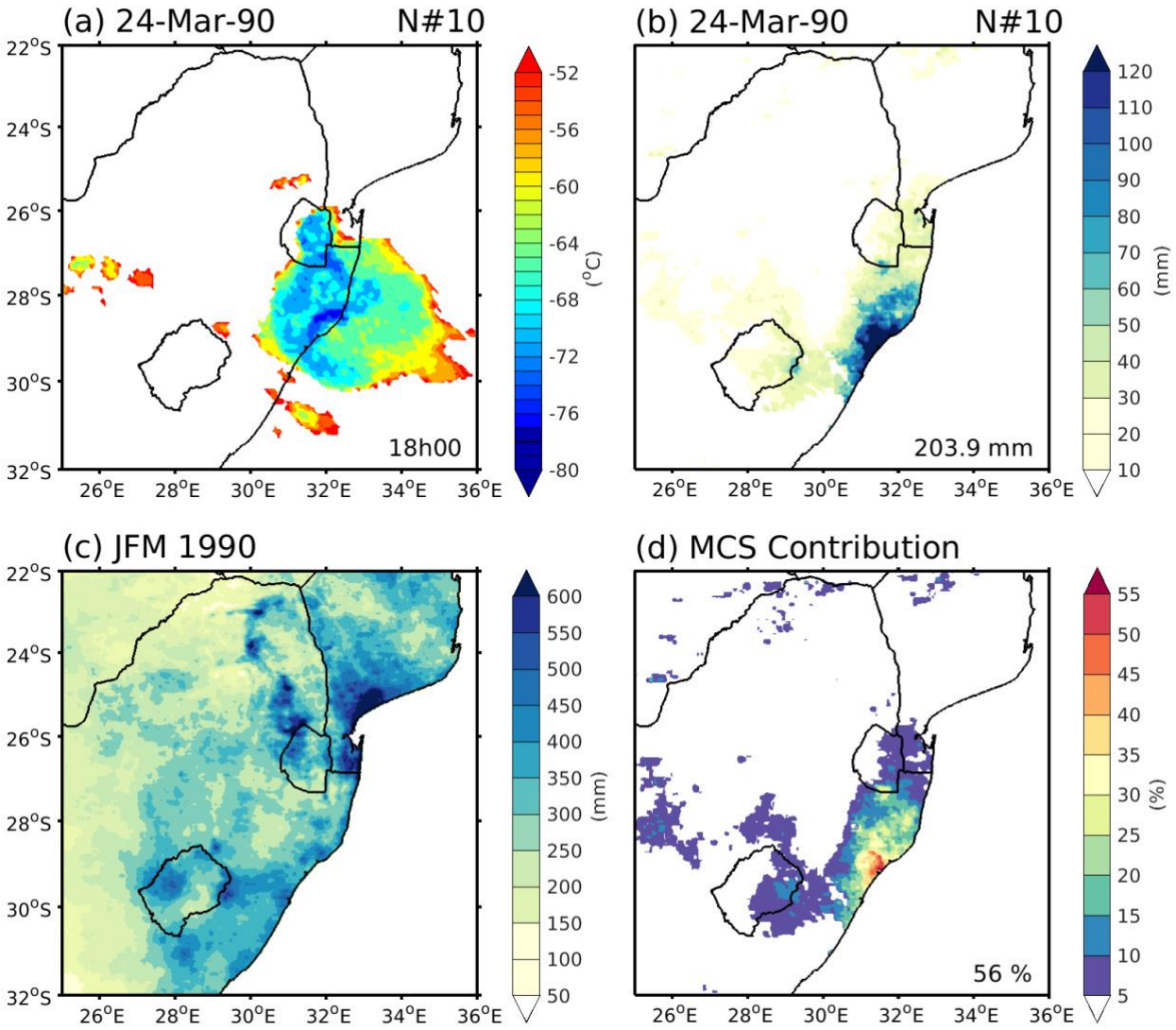

Figure 5.6: (a) GRIDSAT cloud top temperature (shaded; °C) of the MCS found within the top 10 extreme rainfall events on the 24th of March 1990 for the northern domain and **(b)** CHIRPS daily rainfall (shaded, mm) associated with the MCS event. The date of the event is given at the top left corner, the rank within the top 50 extreme rainfall events is in the top right and the maximum in rainfall is shown in the bottom right corner and **(c)** JFM 1990 total rainfall (shaded, mm), the mean is based on CHIRPS daily data from 1990 and **(d)** MCS rainfall contribution of event shown in **(a)** to JFM 1990 Mean Rainfall **(c).** The contribution is shown in the bottom right corner.

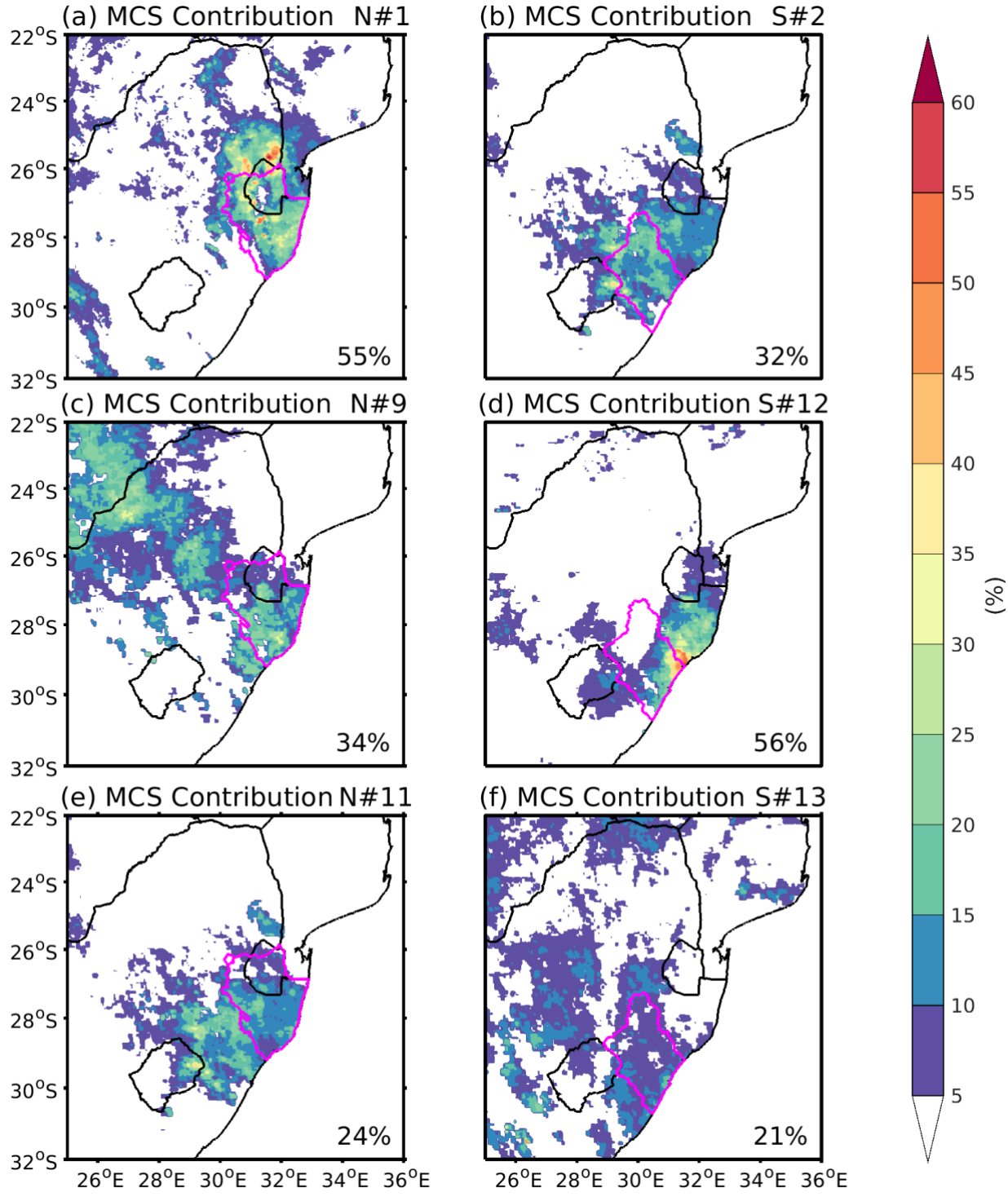

Figure 5.7: MCS maximum rainfall contribution of three MCS events from the northern (left panels) and southern (right panels) domain depicted in **Figure 5.2** to individual total seasonal (JFM) rainfall**.** The maximum contribution within the small domain is shown in the bottom right corner.

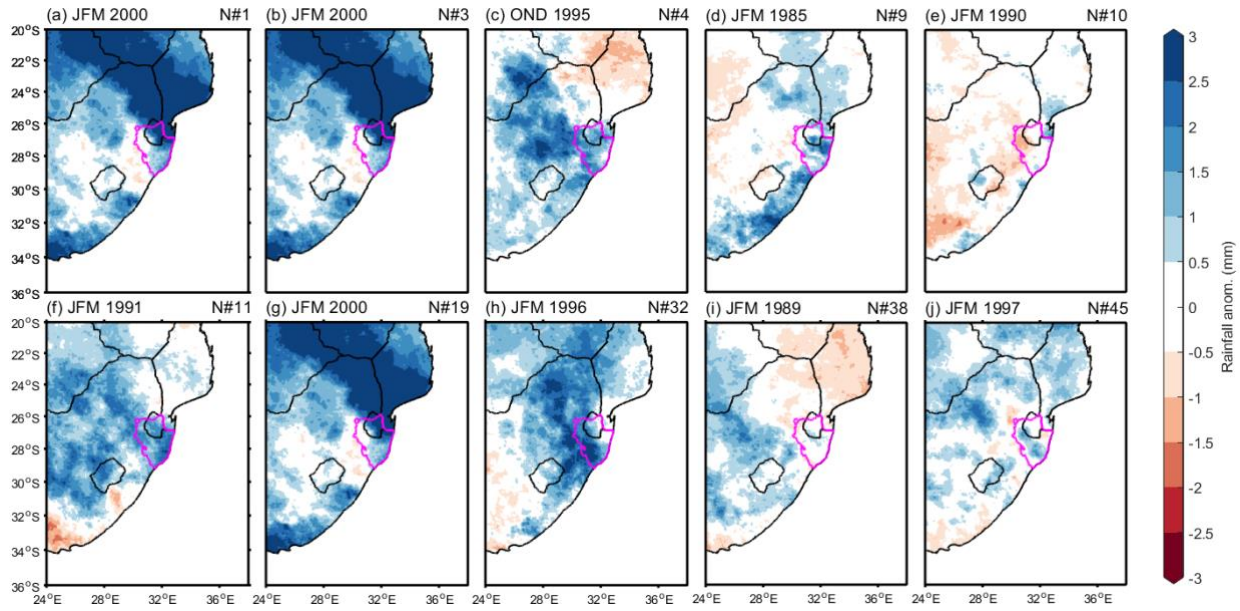

Figure 5.8: Seasonal rainfall anomalies (shaded; mm) for the years of the events listed in **Table 5.3** over the northern domain. The mean is based on CHIRPS daily data from 1985-2008.

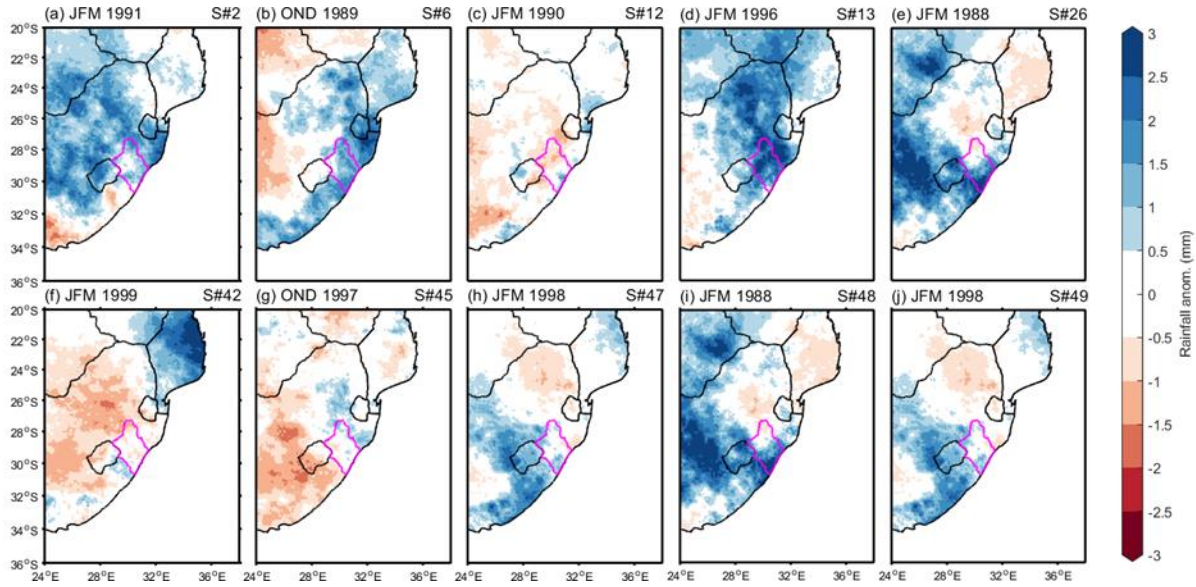

Figure 5.9: Same as **Fig. 5.8**, but for the southern domain.

Chapter 6: Summary and conclusion

The main objective of this thesis has been to develop a long-term climatology of long-lived mesoscale convective systems (MCSs) over eastern South Africa based on a longer period of data and a sub-group of MCSs that excludes shorter-lived MCSs in the region, with majority of which exist in the late afternoon / evening hours. It was also to understand their seasonal and interannual variability, to look at large-scale environmental conditions that are favorable for their development and the role that long-lived MCSs play in South Africa summer rainfall. The analysis focussed on the extended summer months (September – April).

Detailed climatology studies on organised convective systems have become more frequent since the advancement in technology. Over the past few decades, the identification and tracking of MCSs became more automated using infrared (IR) images, and a combination of IR images and visible images. The global distribution of favourable severe weather environments (e.g., Brook et al. 2003) and of intense thunderstorms (Zipser et al. 2006) have previously identified southeastern Africa and the Agulhas Current as a convective "hotspot". However, there have been very limited studies of MCSs over southern Africa compared to other regions around the world, likely due to the relatively low frequent occurrence of nature of these systems here and poor infrastructure. Apart from the climatology of MCCs developed by Blamey and Reason (2012, 2013), there are no long-term studies of MCSs over southern Africa. Two limitations to the Blamey and Reason (2012, 2013) analysis were that only a subset of MCSs, namely MCCs were considered and that it only covered a 9-year period (1998-2006). This resulted in no clear evidence of any relationship between MCCs and the main modes of climate variability.

To better understand spatial distribution, frequency, lifecycle, and seasonal cycle of long-lived MCSs over eastern South Africa, this thesis presented an analysis of MCS climatology in **Chapter 4** based on the quasi-tropical (30°N-30°S) MCSs dataset covering the period 1985-2008 developed by Huang et al. (2018). Over southern Africa between 15°S and 30°S there is a pronounced local maximum in frequent MCS activity over the relatively small region extending from the Drakensberg to the Agulhas Current. A total of 1461 long-lived MCSs were identified over eastern South Africa and the adjacent ocean for the extended summer months for 1985-2008. Overall, the number of systems identified in this region is less than that

compared to other regions such as North America, Europe, Asia and West Africa. It is near impossible to make direct comparisons between the regions given the much smaller domain used for this study, and the variation in the literature in MCS threshold criteria. However, it is clear that outside of the equatorial band of frequent MCS activity, eastern South Africa exhibits a local MCS maximum.

Long-lived mesoscale convective systems over eastern South Africa are predominately found to occur during November and January, with a peak during December. There are larger frequencies in the early summer months (November and December) particularly over land, compared to late summer (January-March, JFM). The frequencies are linked to the large-scale environmental conditions since temperature and moisture gradients over South Africa tend to be stronger in early summer (October-December, OND) than in late summer (Todd et al. 2004). The results also revealed that more favourable CAPE and wind shear profiles occur across the wider domain during early summer. The peak of MCS activity in the early summer months has been documented in other parts of the Southern Hemisphere, such as South America (Velasco and Fritsch, 1987; Durkee and Mote, 2009) and Australia (Pope et al., 2009). In the late summer months, CAPE and wind shear environments are more restricted to the southern parts of the east coast of South Africa and over the Agulhas Current. In general, the results are consistent with previous studies that highlighted the dominance of organised convection in early summer over eastern South Africa, for example through large-scale cloud bands (Hart et al. 2013), MCCs (Blamey and Reason 2012) and the frequency of days with favourable severe weather conditions (Blamey et al. 2017).

The systems generally showed a clear and common diurnal cycle with most systems reaching MCS status (i.e., developing phase) during the mid-afternoon, a maximum extent during the evening hours and subsequently terminate in the middle of the night. This MCS life cycle closely matches the diurnal cycle of rainfall over the east coast of South Africa (Rouault et al. 2013). Furthermore, the results presented here suggest that most of the MCSs initiated over land as opposed to over the adjacent ocean, with systems over eastern South Africa typically developing over land (near the escarpment), and then track eastward to adjacent warm ocean (Agulhas Current). A similar pattern was documented in the study of MCCs over southern Africa by Blamey and Reason (2012). The difference between continental versus ocean systems in the diurnal variation of convective systems revealed that MCSs over the ocean contain two favourable initiation times, one at about 0300 UTC, and the other occurring in the

afternoon 1500 UTC. Another difference appeared in the seasonal cycle, wherein land-based system revealed a single peak in December, whereas ocean-based systems reveal two intraseasonal peaks (December and April). A peak in December for oceanic systems arises because during this time circulation over South Africa is still influenced by midlatitude systems, which lead to relatively large airmass contrasts and baroclinicity in the environment. April is similar to the month March, which is a month of maximum SST as well as the time when midlatitude systems start to dominate over the tropics.

Chapter 4 also found a considerable interannual variability in the frequency of MCSs within the MCS domain, on average, 63 systems occur per season with the least in 1995/96 (45) and the most in 1987/88 (81). The results showed little to no evidence of any robust relationship between MCS frequency and the main climate modes of variability such as El Niño-Southern Oscillation (ENSO), the subtropical south Indian Ocean dipole (SIOD), and southern annular mode (SAM). The only significant correlation found was between MCS frequency and SAM during early summer and the SIOD in the late summer. Even though ENSO is considered the dominant driver of interannual rainfall variability over southern Africa during summer, there were no significant correlations with ENSO or the Indian Ocean dipole (IOD) found. The relationship between MCS frequency and the SIOD in JFM is linked through the strength of the Mascarene high and Mozambique Channel trough. It was also found that the increase in rainfall often occurred in regions containing anomalously high MCS activity during OND and JFM.

To demonstrate the importance of MCSs for regional rainfall, this thesis presented an analysis of extreme rainfall events associated with MCSs over the two sub-domains of KZN province (South Africa) in **Chapter 5** derived from high resolution Climate Hazards Infrared Precipitation with Stations (CHIRPS) data. Using the methodology of Ramos et al. (2014), the top 50 extreme daily rainfall events were identified for the two sub-domains in KZN, over 24-year period. The methodology is based on the amount of rainfall that occurred and the areal extent of rainfall. However, given the relatively strict MCSs thresholds used in **Chapter 4**, extreme rainfall events for smaller, and short-lived, systems were excluded. Out of the top 50 extreme daily rainfall events, just under 40% of the top 50 extreme daily rainfall events in these two regions during October-March were linked to large, long-lived MCSs. This was determined by matching MCSs from the MCS database developed in **Chapter 4** with that of ranked days of extreme rainfall. For the northern domain, around 50% of the top daily extreme

rainfall events during December - February were associated with long-lived MCSs and more than half of these MCSs produced rainfall over 100 mm. Two of these systems were nocturnal MCSs, satisfying MCC criteria and producing over 200 mm within 24 hours.

The results in **Chapter 5** also found no obvious similarities in long-lived MCS properties for the different extreme daily rainfall events in the two sub-domains. Of the 38 events, duration of these systems ranged from 6 hours through to 51 hours, with 14 (9) of the events lasting for longer than 12 hours for the northern (southern) domain. With the size of cloud shield of MCS that are associated with extreme daily rainfall varying from relatively small systems (28000 km^2) in size to large systems (over 700000 km^2). However, there is no general pattern of favourable MCS initiation points that results in the heavy rainfall over the northern domain. Many systems first reach MCS status positioned further south along the coast before they travel northeast in the prevailing mid-level westerly flow.

The results presented in **Chapter 5** also revealed that there is considerable variability in the contribution of long-lived MCSs make towards seasonal and monthly rainfall totals. The results found that long-lived MCS can account for up to 56% of the seasonal rainfall total. Extreme daily rainfall events that are related with MCSs over northern domain of KZN accounted for maximum rainfall contribution ranging between 29%-54%, whereas in the southern domain MCSs contributed between 21%-48% of associated seasonal rainfall totals. These results are consistent with previous studies investigating MCSs in South Africa. For example, the case study of Blamey and Reason (2009) showed that an individual MCS in February 2005 contributed approximately 20% to the summer season (DJF) rainfall total at two weather stations in the northern parts of the KZN province. These similarities suggest that the analysis presented here, based on high-resolution CHIRPS rainfall data, provides comparable results to the case study using station data of Blamey and Reason (2009) and using Tropical Rainfall Measuring Mission (TRMM) data for MCC work over the eastern South Africa by Blamey and Reason (2013). In general, these results suggest that variability in the frequency and intensity of MCSs could have a considerable impact on regional rainfall totals during summer over part of southeastern Africa, and further highlights the need to better understand local environment conditions that play a role in the frequency and intensity of these systems.

Lastly, this study arises from the reality that is faced over eastern South Africa where intense storms are frequent and the region is affected by the severe weather. Previous studies on severe

weather in South Africa often overlooked these convective storms. However, MCSs are known to produce severe weather, which includes significant amount of rainfall which at times can be very important for sustaining people's livelihoods and the regional economy over the region. Thus, it is of importance to better understand the seasonal and interannual variability and the large-scale circulations that are favourable for the development and intensification of long-lived MCSs in the region, and also on the role these systems play in eastern South Africa rainfall.

In conclusion, this work has contributed towards the knowledge of global population of MCSs by building a long-term climatology for eastern South Africa, and local understanding of large-scale environment of MCSs over eastern South Africa. Furthermore, the impact in which these systems have on eastern South Africa summer rainfall. The results presented here provided a basis for future research on a wider group of MCSs and better understanding of the synoptic and environmental conditions in which these systems develop and intensify. A subsequent study may provide further analysis on the impact and contribution that these systems have on regional rainfall. Such study may be to further explore the importance of MCSs on seasonal and monthly rainfall totals, this includes separating rainfall from MCS vs non-MCS rainfall.

However, it should be emphasised that the results presented in this study poses challenges for weather forecasting and seasonal prediction since these systems can be crucial for rainfall patterns. Monitoring and better understanding of these large convective systems is important and complements ongoing efforts to better forecast these systems, particularly with uncertainties related to frequency and intensity of these powerful systems under the climate change scenarios. Thus, an improved understanding of these systems and their variability should then help with large, long-lived MCS forecasting as well as with seasonal rainfall outlooks over eastern South Africa to facilitate improved disaster warning and mitigation.

References:

Alfaro, D.A., 2017: Low-tropospheric shear in the structure of squall lines: Impacts on latent heating under layer-lifting ascent. J. Atmos. Sci., **74**(1), 229-248.

Anderson, C. J. and R. W. Arritt, 1998: Mesoscale Convective Complexes and Persistent Elongated Convective Systems over the United States during 1992 and 1993. Mon. Wea. Rev., **126**, 578–599.

Anderson, C. J. and R. W. Arritt, 2001: Mesoscale convective systems over the United States during the 1997-98 El Niño. Mon. Wea. Rev., **129**, 2443-2457.

Ashley, W.S., T.L. Mote, P.G. Dixon, S.L. Trotter, E.J. Powell, J.D. Durkee and A.J. Grundstein, 2003: Distribution of mesoscale convective complex rainfall in the United States. Mon. Wea Rev., **131**(12), 3003-3017.

Ashley, S.T. and W.S. Ashley, 2008: The storm morphology of deadly flooding events in the United States. Int. J. Climatol., **28**(4), 493-503.

Augustine, J. A. and K. W. Howard, 1991: Mesoscale convective complexes over the United States during 1986 and 1987. Mon. Wea Rev., **119**(7), 1575-1589.

Barimalala, R., F. Desbiolles, R.C. Blamey and C. Reason, 2018: Madagascar influence on the south Indian Ocean convergence zone, the Mozambique channel trough and southern African rainfall. Geophys. Res. Lett., **45**(20), 11-380.

Behera, S.K. and T. Yamagata, 2001: Subtropical SST dipole events in the southern Indian Ocean. Geophys. Res. Lett., **28**, 327–330.

Blamey, R. C. and C. J. C. Reason, 2009: Numerical simulation of a mesoscale convective system over the east coast of South Africa, Tellus A: Dyn. Meteor. Oceanogr., **61**(1), 17–34.

Blamey, R.C. and C.J.C. Reason, 2012: Mesoscale convective complexes over southern Africa. J. Climate, **25**(2), 753-766.

Blamey, R.C. and C.J.C. Reason, 2013: The role of mesoscale convective complexes in southern Africa summer rainfall. J. Climate, **26**(5), 1654-1668.

Blamey, R. C., Middleton, C., Lennard, C. and C. J. C. Reason, 2017: A climatology of potential severe convective environments across South Africa. Climate Dyn., **49**(5-6), 2161-2178.

Blamey, R. C., S. R. Kolusu, P. Mahlalela, M. C. Todd, and C. J. C. Reason, 2018: The role of regional circulation features in regulating El Niño climate impacts over southern Africa: A comparison of the 2015/2016 drought with previous events. Int. J. Climatol., **38,** 4276-4295.

Bluestein, H. B., and M. H. Jain, 1985: Formation of mesoscale lines of precipitation: Severe squall lines in Oklahoma during the spring. J. Atmos. Sci., **42**, 1711–1732.

Boer, E. R. and V. Ramanathan, 1997: Lagrangian approach for deriving cloud characteristics from satellite observations and its implications to cloud parameterization. J. Geophys. Res: Atmos., **102**(17), 21383-21399.

Boulard, D., B. Pohl, J. Crétat, N. Vigaud, and T. Pham-Xuan, 2013: Downscaling large-scale climate variability using a regional climate model: the case of ENSO over Southern Africa. Climate Dyn., **40**(5-6), 1141-1168.

Brooks, H. E., J. W. Lee, and J. P. Craven, 2003: The spatial distribution of severe thunderstorm and tornado environments from global reanalysis data. Atmos. Res., **67**, 73-94.

Brooks, H. E. and N. Dotzek, 2008: The spatial distribution of severe convective storms and an analysis of their secular changes. In: H. F. Diaz, R. J. Murnane (eds) Climate extremes and society. Cambridge University Press, Cambridge, 35-53.

Carvalho, L. M. and C. Jones, 2001: A satellite method to identify structural properties of mesoscale convective systems based on the maximum spatial correlation tracking technique (MASCOTTE). J. Appl. Meteor., **40**(10), 1683-1701.

Cheeks, S. M., S. Fueglistaler and S. T. Garner, 2020: A satellite-based climatology of central and southeastern U.S. mesoscale convective systems. Mon. Wea. Rev.,**148**, 2607-2621

Chen, S. S. and R. A. Houze, 1997: Diurnal variation and life cycle of deep convective systems over the tropical Pacific warm pool. Quart. J. Roy. Meteor. Soc., **123**, 357–388.

Chen, S.S., R. A. Houze Jr, and B. E. Mapes, 1996: Multiscale variability of deep convection in realation to large-scale circulation in TOGA COARE. J. Atmos. Sci., **53**(10), 1380-1409.

Colberg, F., C.J.C. Reason, and K. Rodgers, 2004: South Atlantic response to El Niño–Southern Oscillation induced climate variability in an ocean general circulation model. J. Geophys. Res: Oceans., **109**(12).

Coniglio, M. C., D. J. Stensrud, and L. J. Wicker, 2006: Effects of upper-level shear on the structure and maintenance of strong quasi-linear mesoscale convective systems. J. Atmos. Sci., **63**, 1231–1252.

Coniglio, M. C., J. Y. Hwang, and D. J. Stensrud, 2010: Environmental factors in the upscale growth and longevity of MCSs derived from Rapid Update Cycle analyses. Mon. Wea. Rev., **138**, 3514–3539

Cook, K.H., 2001: A Southern Hemisphere wave response to ENSO with implications for southern Africa precipitation. J. Atmos. Sci., **58**(15), 2146-2162.

Cook, C., C. J. C. Reason, and B. C. Hewitson, 2004: Wet and dry spells within particularly wet and dry summers in the South African summer rainfall region. Climate Res., **26**(1), 17–31.

Copernicus Climate Change Service (C3S) (2017): ERA5: Fifth generation of ECMWF atmospheric reanalyses of the global climate. Copernicus Climate Change Service Climate Data Store (CDS), 2020. https://cds.climate.copernicus.eu/cdsapp#!/home

Cotton, W. R., M. S. Lin, R. L. McAnelly and C. J. Tremback, 1989: A composite model of mesoscale convective complexes. Mon. Wea Rev., **117**(4), 765-783.

Cotton, W.R. 2000: An overview of mesoscale convective systems. Storms, Vol. II, RA Pielke Jr., and RA Pielke Sr., Eds., Routledge, 3-25.

Cifelli, R. and S. A. Rutledge, 1998: Vertical motion, diabatic heating, and rainfall characteristics in north Australia convective systems. Quart. J. Roy. Meteor. Soc., **124**(548), 1133-1162.

Crétat, J., Vizy, E.K. and Cook, K.H., 2015. The relationship between African easterly waves and daily rainfall over West Africa: Observations and regional climate simulations. Climate Dyn., **44**(1-2), 385-404.

Crimp, S. J., and S. J. Mason, 1999: The extreme precipitation event of 11 to 16 February 1996 over South Africa. Meteor. Atmos. Phys., **70**, 29–42, https://doi.org/10.1007/s007030050023.

Grobler, R.R., 2003: A framework for modelling losses arising from natural catastrophes in South Africa (Doctoral dissertation, University of Pretoria).

De Coning, E., G. S. Forbes, and E. Poolman, 1998: Heavy precipitation and flooding on 12-14 February 1996 over the summer rainfall regions of South Africa: Synoptic and isentropic analyses. Natl. Wea. Dig., **22**(3), 25-36.

Dias, J., S. N. Tulich, and G. N. Kiladis, 2012: An object-based approach to assessing the organization of tropical convection. J. Atmos. Sci., **69**(8), 2488-2504.

Dong, W., Y. Lin, J. S. Wright, Y. Ming, Y. Xie, B. Wang, Y. Luo, W. Huang, J. Huang, L. Wang, and L Tian, 2016: Summer rainfall over the southwestern Tibetan Plateau controlled by deep convection over the Indian subcontinent. Nat. Commun., **7**(1), 1-9.

Doswell, C. A., III, H. E. Brooks, and R. A. Maddox, 1996: Flash flood forecasting: An ingredients-based methodology. Wea. Forecasting, **11**, 560–581

Dieppois, B., B. Pohl, M. Rouault, M. New, D. Lawler, and N. Keenlyside, 2016. Interannual to interdecadal variability of winter and summer southern African rainfall, and their teleconnections. J. Geophys. Res: Atmos., **121**(11), 6215-6239.

Durkee, J. D. and T. L. Mote, 2009: A climatology of warm-season mesoscale convective complexes in subtropical South America. Int. J. Climatol., **30** (3), 418–431

Durkee, J. D., T. L. Mote, and J. M. Shepherd, 2009: The contribution of mesoscale convective complexes to rainfall across subtropical South America. J. Climate, **22**(17), 4590-4605.

Driver, P., B., Abiodun, and C. J. C. Reason, 2019: Modelling the precipitation response over southern Africa to the 2009/2010 El Niño using a stretched grid global atmospheric model. Climate Dyn., **52**(7-8), 3929-3949.

Dyson, L.L. and J. Van Heerden, 2001: The heavy rainfall and floods over the northeastern interior of South Africa during February 2000. *S. Afr. J. Sci.*, **97**, 80-86.

Dyson, L. L., J. Van Heerden, and P. D. Sumner, 2015: A baseline climatology of sounding-derived parameters associated with heavy rainfall over Gauteng, South Africa. Int. J. Climatol., **35**(1), 114-127.

Dyson L., 2015: A heavy rainfall sounding climatology over Gauteng South Africa, using self-organising maps. Climate Dyn., **45**, 3051–3065.

Driver, P., and C. J. C. Reason, 2017: Variability in the Botswana High and its relationships with rainfall and temperature characteristics over southern Africa, Int. J. Climatol., **37**, 570-581.

Engelbrecht, C. J., W. A. Landman, F. A. Engelbrecht and J. Malherbe, 2015: A synoptic decomposition of rainfall over the Cape south coast of South Africa. Climate Dyn., **44**, 2589-2607.

Evans, J. L. and R. E. Shemo, 1996: A procedure for automated satellite-based identification and climatology development of various classes of organized convection, J. Appl. Meteor., **35**(5), 638-652.

Fauchereau, N., B. Pohl, C.J.C. Reason, M. Rouault, and Y. Richard, 2009: Recurrent daily OLR patterns in the Southern Africa/Southwest Indian Ocean region, implications for South African rainfall and teleconnections. Climate Dyn., **32**(4), 575-591

Favre, A., B. Hewitson, M. Tadross, C. Lennard, and R. Cerezo-Mota, 2012: Relationships between cut-off lows and the semiannual and southern oscillations. Climate Dyn., **38**(7-8), 1473-1487.

Favre, A., Hewitson, B., Lennard, C., Cerezo-Mota, R. and Tadross, M., 2013. Cut-off lows in the South Africa region and their contribution to precipitation. Climate Dyn., **41**(9-10), 2331-2351.

Feng, Z., R. A. Houze Jr, L. R. Leung, F. Song, J. C. Hardin, J. Wang, W. I. Gustafson Jr, and C. R. Homeyer, 2019: Spatiotemporal characteristics and large-scale environments of mesoscale convective systems east of the Rocky Mountains. J. Climate, **32**(21), 7303-7328.

Fiolleau, T. and R. Roca, 2013: An algorithm for the detection and tracking of tropical mesoscale convective systems using infrared images from geostationary satellite. IEEE Trans. Geosci. Remote Sens., **51**(7), 4302-4315.

Fitzpatrick, R.G., D.J. Parker, J.H. Marsham, D.P. Rowell, F.M. Guichard, C.M. Taylor, K.H. Cook, E.K. Vizy, L.S. Jackson, D. Finney, and J. Crook, 2020: What drives the intensification of mesoscale convective systems over the West African Sahel under climate change?. J. Climate, **33**(8), 3151-3172.

Fritsch, J. M., R. J. Kane, and C. R. Chelius, 1986: The contribution of mesoscale convective weather systems to the warm-season precipitation in the United States. J. climate. Appl. Meteor., **25**(10), 1333-1345.

Fritsch, J. M., and G. S. Forbes, 2001: Mesoscale Convective Systems. Severe Convective Storms, Meteor. Monogr., No. 50, Amer. Meteor. Soc., 323–357.

Funk, C., P. Peterson, M. Landsfeld, D. Pedreros, J. Verdin, S. Shukla, G. Husak, J. Rowland, L. Harrison, A. Hoell, and J. Michaelsen, 2015: The climate hazards infrared precipitation with stations-a new environmental record for monitoring extremes, Sci. Data, **2**, 150066, https://doi.org/10.1038/sdata.2015.66

García-Herrera, R., E. Hernández, D. Paredes, D. Barriopedro, J. F. Correoso, and L. Prieto, 2005: A MASCOTTE-based characterization of MCSs over Spain, 2000–2002. Atmos. Res., **73**(3-4), 261-282.

Garstang, M., B. E. Kelbe, G. D. Emmitt, W. B. London, 1987: Generation of convective storms over the escarpment of northeastern South Africa. Mon. Wea. Rev., **115**, 429-443.

Gillett, N. P., T. D. Kell, and P. D. Jones, 2006: Regional climate impacts of the Southern Annular Mode. Geophys. Res. Lett., **33**(23). L23704, doi:10.1029/2006GL027721

Goyens, C., D. Lauwaet, M. Schröder, M. Demuzere, and N. P. Van Lipzig, 2012: Tracking mesoscale convective systems in the Sahel: relation between cloud parameters and precipitation. Int. J. Climatol., **32**(12), 1921-1934.

Gray, W. M., and R. W. Jacobson, 1977: Diurnal Variation of Deep Cumulus Convection, Mon. Wea. Rev., **115**, 429-443.

Groisman, P.Y., Knight, R.W., Easterling, D.R., Karl, T.R., Hegerl, G.C. and V.N. Razuvaev, 2005: Trends in intense precipitation in the climate record. J. climate, **18**(9), 1326-1350.

Haberlie, A. M. and W. S. Ashley, 2019: A Radar-Based Climatology of Mesoscale Convective Systems in the United States. J. Climate, **32**(5), 1591-1606.

Harrison, M. S. J., 1984: A generalized classification of South African summer rain-bearing synoptic systems, Int. J. Climatol., **4**,547-560.

Hart, N. C. G., C. J. C. Reason, and N. Fauchereau, 2010: Tropical–extratropical interactions over southern Africa: Three cases of heavy summer season rainfall. Mon. Wea. Rev., **138**, 2608–2623.

Hart, N. C. G., C. J. C. Reason, and N. Fauchereau, 2013: Cloud bands over southern Africa: seasonality, contribution to rainfall variability and modulation by the MJO. Climate Dyn., **41**(5-6), 1199-1212.

Hart, N.C., R. Washington, and C. J. Reason, 2018: On the likelihood of tropical–extratropical cloud bands in the south Indian convergence zone during ENSO events. J. Climate., **31**(7), 2797-2817.

Hu, H., Z. Feng, and Ruby Leung, L., 2021: Linking flood frequency with mesoscale convective systems in the US. Geophys. Res. Lett., p. e2021GL092546.

Hartman, A. T. 2020: Tracking mesoscale convective systems in central equatorial Africa. Int J. Climatol., **41**, 469-482

Hartmann, D.L., and F. Lo, 1998: Wave-driven zonal flow vacillation in the Southern Hemisphere. J. Atmos. Sci., **55**(8), 1303-1315.

Hermes, J.C., and C.J.C. Reason, 2005. Ocean model diagnosis of interannual coevolving SST variability in the South Indian and South Atlantic Oceans. J. Climate, **18**(15), 2864-2882.

Hodges, K.I., and C.D. Thorncroft, 1997: Distribution and statistics of African mesoscale convective weather systems based on the ISCCP Meteosat imagery. Mon. Wea. Rev., **125**(11), 2821-2837.

Hodges, K. I., D. W. Chappell, G. J. Robinson, and G. Yang, 2000: An improved algorithm for generating global window brightness temperatures from multiple satellite infrared imagery. J. Atmos. Oceanic. Technol., **17**(10), 1296-1312.

Hope, A.C.A., 1968: A Simplified Monte Carlo Significance Test Procedure. J. Royal Statistical Soc., B, 30, 582–598.

Houze, R. A., 2018: 100 years of research on mesoscale convective systems. A Century of Progress in Atmospheric and Related Sciences: Celebrating the American Meteorological Society Centennial, Meteor. Monogr., No. 59, Amer. Meteor. Soc., 17.11–17.54,

Houze Jr, R. A., 2004: Mesoscale convective systems. Rev. Geophys., **42**(4).

Howard, E., R. Washington, and K.I. Hodges, 2019: Tropical lows in southern Africa: Tracks, rainfall contributions, and the role of ENSO. J. Geophys. Res: Atmos., 124(21),11009-11032.

Huang, X., 2017: A comprehensive Mesoscale Convective System (MSC) dataset, links to files in MatLab and plain text format. Tsinghua University, Beijing, PANGAEA, accessed 12 October 2019. doi: https://doi.org/10.1594/PANGAEA.877914.

Huang, X., C. Hu, X. Huang, Y. Chu, Y. H. Tseng, G. J. Zhang and Y. Lin, 2018: A long-term tropical mesoscale convective systems dataset based on a novel objective automatic tracking algorithm. Climate Dyn., **51**(7-8), 3145-3159.

Hsieh, J.S. and K.H. Cook, 2007: A study of the energetics of African easterly waves using a regional climate model. J. Atmos. Sci., **64**(2), 421-440.

Jirak, I.L., W.R. Cotton, and R.L. McAnelly, 2003: Satellite and radar survey of mesoscale convective system development. Mon. Wea. Rev., **131**(10), 2428-2449.

Johnson, J. T., P. L. MacKeen, A. Witt, E. D. W. Mitchell, G. J. Stumpf, M.D. Eilts, and K. W. Thomas, 1998: The storm cell identification and tracking algorithm: An enhanced WSR-88D algorithm. Wea. Forecasting, **13(**2), 263-276.

Kiladis, G.N. and H.F. Diaz, 1989: Global climatic anomalies associated with extremes in the Southern Oscillation. J. Climate, **2**(9), 1069-1090.

Klein, C., and C.M. Taylor, 2020: Dry soils can intensify mesoscale convective systems. Proceedings of the National Academy of Sciences, **117**(35), 21132-21137.

Knapp, K.R., 2008: Scientific data stewardship of International Satellite Cloud Climatology Project B1 global geostationary observations. J. Appl. Meteor. Remote Sens., **2**(1), 023548.

Knapp, K.R., S. Ansari, C.L. Bain, M.A. Bourassa, M.J. Dickinson, C. Funk, C.N. Helms, C.C.

Kolios, S., and H. Feidas, 2010: A warm season climatology of mesoscale convective systems in the Mediterranean basin using satellite data. Theor. Appl. Climatol., **102**(1), 29–42. doi: 10.1007/s00704-009-0241-7.

Kruger, A.C., 2006: Observed trends in daily precipitation indices in South Africa: 1910–2004. Int. J. Climatol.: A J. Roy. Meteor. Soc., **26**(15), 2275-2285.

Hennon, C.D. Holmes, G.J. Huffman, and J.P. Kossin, 2011: Globally Gridded Satellite observations for climate studies, Bull. Amer. Meteor. Soc., **92**(7), 893-907, doi: 10.1175/2011BAMS3039.1.

Lennard, C., Coop, L., Morison, D. and Grandin, , 2013: Extreme events: Past and future changes in the attributes of extreme rainfall and the dynamics of their driving processes. Climate Systems Analysis Group University of Cape Town.

Landman, W.A., J. Malherbe, and F. Engelbrecht, 2017: South Africa's present-day climate. In Understanding the social and environmental implications of global change, 7-12. Africa Sun Media.

Laing, A. G., and J. M. Fritsch, 1993a: Mesoscale convective complexes in Africa. Mon. Wea. Rev., **121**, 2254–2263.

Laing, A. G., and J. M. Fritsch, 1993b: Mesoscale convective complexes over the Indian monsoon region. J. Climate, **6**, 911-919.

Laing, A. G., and M. J. Fritsch, 1997: The global population of mesoscale convective complexes. Quart. J. Roy. Meteor. Soc., **123**, 389–405.

Laing, A. G., J. M. Fritsch, and A. J. Negri, 1999: Contribution of mesoscale convective complexes to rainfall in Sahelian Africa: Estimates from geostationary infrared and passive microwave data. J. Appl. Meteor., **38**(7), 957-964.

Laing, A. G., and J. M. Fritsch, 2000: The large-scale environments of the global populations of mesoscale convective complexes. Mon. Wea. Rev., **128**, 2756-277.

Laing, A.G., R. Carbone, V. Levizzani, and J. Tuttle, 2008: The propagation and diurnal cycles of deep convection in northern tropical Africa. Quart. J. Roy. Meteor. Soc., **134**(630), 93-109.

Laurent, H., N. D'Amato, and T. Lebel, 1998: How important is the contribution of the mesoscale convective complexes to the Sahelian rainfall? Phys. Chem. Earth, **23**, 629-633, doi: 10.1016/S0079-1946(98)00099-8.

Lima, D.C., P.M. Soares, A. Semedo, and R.M. Cardoso, 2018: A global view of coastal low-level wind jets using an ensemble of reanalyses. J. Climate. **31**(4), 1525-1546.

Lindesay, J. A. 1988: South African rainfall, the Southern Oscillation and a Southern Hemisphere semi-annual cycle. J. Climatol.,**8**, 17-30, doi: 10.1002/joc.3370080103.

Liu, C. and E. Zipser, 2013: Regional variation of morphology of organized convection in the tropics and subtropics. J. Geophys. Res: Atmos., **118**(2), 453–466. doi: 10.1029/2012JD018409.

Liu, W., K. H. Cook, and E. K. Vizy, 2019: The role of mesoscale convective systems in the diurnal cycle of rainfall and its seasonality over sub-Saharan Northern Africa. Climate Dyn.,**52**, 729-745, doi: 10.1007/s00382-018-4162-y.

Liu, Y., X. Yao, J. Fei, X. Yang, and J. Sun, 2021: Characteristics of mesoscale convective systems during the warm season over the Tibetan Plateau based on FY-2 satellite datasets. Int. J. Climatol., **41**(4), 2301-2315.

Lyon, B. and S. J. Mason, 2007: The 1997-98 summer rainfall season in Southern Africa. Part I: Observations. J. Climate, **20**(20), 5134–5148. doi: 10.1175/JCLI4225.1.

Machado, L. A. T., W.B. Rossow, R.L. Guedes, and A.W. Walker, 1998: Life cycle variations of mesoscale convective systems over the Americas. Mon. Wea. Rev., **126**(6), 1630–1654. doi: 10.1175/1520-0493(1998)126<1630:LCVOMC>2.0.CO;2.

Maddox, R.A., 1980: Mesoscale convective complexes. Bull. Amer. Meteor. Soc., **61**, 1374-1387.

Maddox, R.A., K.W. Howard, D.L. Bartels, and D.M. Rodgers, 1986: Mesoscale Convective Complexes in the Middle Latitudes. Mesoscale Meteorology and Forecasting, American Meteorological Society, 390-413.

Mahlalela, P. T., R. C. Blamey, and C. J. C. Reason, 2019: Mechanisms behind early winter rainfall variability in the southwestern Cape, South Africa. Climate Dyn., **53**(1), 21-39. doi: 10.1007/s00382-018-4571-y.

Marshall, G. J. 2003: Trends in the Southern Annular Mode from observations and reanalyses. J. Climate, **16**, 4134-4143, doi: 10.1175/1520-0442(2003)016<4134:TITSAM>2.0.CO;2.

Mason, S. J. and M. R. Jury, 1997: Climatic variability and change over southern Africa: A reflection on underlying processes. Progress in Physical Geography, **21**(1), 23–50.

Matarira C.H., 1990: Drought over Zimbabwe in a regional and global context. Int. J. Climatol., **10**, 609–625.

Mathon, V., and H. Laurent, 2001: Life cycle of Sahelian mesoscale convective cloud systems. Quart. J. Roy. Meteor. Soc., **127**, 377–406, https://doi.org/10.1002/qj.49712757208.

Mathon, V., Laurent, H. and T. Lebel, 2002: Mesoscale convective system rainfall in the Sahel. J. Appl. Meteor., **41**, 1081–1092.

Mawren, D., J. Hermes, and C. J. C. Reason, 2020: Exceptional Tropical Cyclone Kenneth in the Far Northern Mozambique Channel and Ocean Eddy Influences. Geophys. Res. Lett., **47**(16), p.e2020GL088715.

Midgley, G.F., Chapman, R.A., Hewitson, B., Johnston, P., De Wit, M., Ziervogel, G., Mukheibir, P., Van Niekerk, L., Tadross, M., Van Wilgen, B.W. and B. Kgope, 2005: A status quo, vulnerability and adaptation assessment of the physical and socio-economic effects of climate change in the Western Cape.

Miller, D., and J. M. Fritsch, 1991: Mesoscale convective complexes in the western Pacific region. Mon. Wea. Rev., **119** (12), 2978-2992.

Mohr, K. I., and E. J. Zipser, 1996: Mesoscale convective systems defined by their 85-GHz ice scattering signature: Size and intensity comparison over tropical oceans and continents, Mon. Wea. Rev., **124**, 2417-2437.

Morel, C., and S. Senesi, 2002: A climatology of mesoscale convective systems over Europe using satellite infrared imagery. I: Methodology. Quarter. J. Roy. Meteor. Soc., **128**(584), 1953-1971.

Mulholland, J. P., S. W. Nesbitt, and R. J. Trapp, 2019: A case study of terrain influences on upscale convective growth of a supercell. Mon. Wea. Rev., **147**, 4305-4324.

Munday, C., and R. Washington, 2017: Circulation controls on southern African precipitation in coupled models: The role of the Angola Low. J. Geophys. Res: Atmos. **122**(2), 861–877.

Munday, C., R. Washington, and N. Hart, 2021: African Low-Level Jets and Their Importance for Water Vapor Transport and Rainfall. Geophys. Res. Lett., **48**(1), p. e2020GL090999.

Ndarana, T., M.J. Bopape, D. Waugh, and L. Dyson, 2018: The influence of the lower stratosphere on ridging Atlantic Ocean anticyclones over South Africa. J. Climate, **31**(15), 6175-6187.

Ndarana, T., T.S. Rammopo, H. Chikoore, M.A. Barnes, and M.J. Bopape, 2020: A quasi-geostrophic diagnosis of the zonal flow associated with cut-off lows over South Africa and surrounding oceans. Climate Dyn., **55**(9), 2631-2644.

Nesbitt, S. W., R. Cifelli, and S. A. Rutledge, 2006: Storm morphology and rainfall characteristics of TRMM precipitation features. Mon. Wea. Rev., **134**, 2702-2721.

Nguyen, H., and J. P. Duvel, 2008: Synoptic wave perturbations and convective systems over equatorial Africa. J. Climate, **21**, 6372-6388, doi: 10.1175/2008JCLI2409.1.

Nicholson, S.E., and D. Entekhabi, 1987: Rainfall variability in equatorial and southern Africa: Relationships with sea surface temperatures along the southwestern coast of Africa. J. climate. Appl. Meteor. Climatol., **26**(5), 561-578.

Nicholson, S. E., 2009: A revised picture of the structure of the "monsoon" and land ITCZ over West Africa. Climate Dyn., **32**(7–8), 1155–1171. doi: 10.1007/s00382-008-0514-3.

Núñez Ocasio, K. M., J. L. Evans, and G. S. Young, 2020: Tracking mesoscale convective systems that are potential candidates for tropical cyclogenesis. Mon. Wea. Rev., **148**, 655–669, https:// doi.org/10.1175/MWR-D-19-0070.1.

Nuryanto, D. E., H. Pawitan, R. Hidayat, and E. Aldrian, 2019: Characteristics of two mesoscale convective systems (MCSs) over the Greater Jakarta: Case of heavy rainfall period 15–18 January 2013. Geosci. Lett., **6**, 1, https://doi.org/10.1186/s40562-019-0131-5.

Omar, S.A., and B.J. Abiodun, 2020: Characteristics of cut-off lows during the 2015–2017 drought in the Western Cape, South Africa. Atmos. Res., **235**, 104772.

Parker, M. D., and R. H. Johnson, 2000: Organizational modes of midlatitude mesoscale convective systems. Mon. Wea. Rev., **128**, 3413-3436

Parker, M. D., and R. H. Johnson, 2004: Simulated convective lines with leading precipitation. Part II: Evolution and maintenance. J. Atmos. Sci.,**61,** 1656-1673.

Perrin, G. M., and C. J. C. Reason, 2000: Monsoonal influences on a mesoscale convective system over midlatitude South Australia. Meteor. Atmos. Phys., **74**, 63–82.

Pope, M., C. Jakob, and M.J. Reeder, 2009: Objective classification of tropical mesoscale convective systems. J. Climate, **22**(22), 5797-5808.

Preston-Whyte, R. A., 1970: Land breezes and rainfall on the Natal coast. South African Geographical Journal, **52**(1), 38–43.

Preston-Whyte, R.A., and P.D. Tyson, 1988: Atmosphere and weather of southern Africa. Oxford University Press.

Púčik, T., and Coauthors, 2017: Future changes in European severe convection environments in a regional climate model ensemble. J. Climate, **30**, 6771–6794.

Rafati, S. and M. Karimi, 2017: Assessment of mesoscale convective systems using IR brightness temperature in the southwest of Iran. Theor. Appl. Climatol., **129**, 539-549, doi: 10.1007/s00704-016-1797-7.

Ramos, A. M., R., M. Trigo, and M. L. R. Liberato, 2014: A ranking of high-resolution daily precipitation extreme events for the Iberian Peninsula. Atmos. Sci. Lett., **15**(4),328-334. doi: 10.1002/asl2.507.

Rapolaki R. S and C. J. C. Reason, 2018: Tropical storm Chedza and associated floods over south-eastern Africa. Nat. Hazards, **93**,189–217.

Rapolaki, R. S., R. C. Blamey, J. C. Hermes, and C. J. C. Reason, 2019: A classification of synoptic weather patterns linked to extreme rainfall over the Limpopo River Basin in southern Africa. Climate Dyn., **53**, 2265–2279, https://doi.org/10.1007/s00382-019-04829-7.

Rasmussen, K. L., M. M. Chaplin, M. D. Zuluaga, and R. A. Houze, Jr., 2016: Contribution of extreme convective storms to rainfall in South America. J. Hydrometeor., **17**, 353–367, https://doi.org/10.1175/JHM-D-15-0067.1

.

Ratna S.B, S. Behera, J.V. Ratnam, K. Takahashi, T. Yamagata, 2013: An index for tropical temperate troughs over southern Africa. Clim. Dyn. **41**, 421–441.

Reason, C. J. C., H. Mulenga, 1999: Relationships between South African rainfall and SST anomalies in the southwest Indian Ocean. Int. J. Climatol., **19**, 1651–1673.

Reason, C.J.C., R.J. Allan, J.A. Lindesay, and T.J. Ansell, 2000: ENSO and climatic signals across the Indian Ocean basin in the global context: Part I, Interannual composite patterns. Int. J. Climatol., **20**(11), 1285-1327.

Reason, C. J. C., 2001a: Subtropical Indian Ocean SST dipole events and southern African rainfall. Geophys. Res. Lett., **28**, 2225–2227, https://doi.org/10.1029/2000GL012735.

Reason, C.J.C., 2001b: Evidence for the influence of the Agulhas Current on regional atmospheric circulation patterns. J. Climate, **14**, 2769-2778.

Reason, C. J. C., 2002: Sensitivity of the southern African circulation to dipole sea surface temperature patterns in the south Indian Ocean. Int. J. Climatol., **22**, 377–393.

Reason, C. J. C., and A. Keibel, 2004: Tropical cyclone Eline and its unusual penetration and impacts over the southern African mainland. Wea. Forecasting, **19**, 789–805,

Reason, C. J. C., and D. Jagadheesha, 2005: A model investigation of recent ENSO impacts over southern Africa. Meteor. Atmos. Phys., **89**, 181–205, https://doi.org/10.1007/s00703-005-0128-9.

Reason, C. J. C., W. Landman, and W. Tennant, 2006: Seasonal to decadal prediction of southern African climate and its links with variability of the Atlantic Ocean. Bull. Amer. Meteor. Soc., **87**, 941–956, https://doi.org/10.1175/BAMS-87-7-941.

Reason, C.J.C., 2016: The Bolivian, Botswana, and Bilybara Highs and Southern Hemisphere drought/floods. Geophys. Res. Lett., **43**(3), 1280-1286.

Reason, C.J.C., and M. Rouault, 2005: Links between the Antarctic Oscillation and winter rainfall over western South Africa. Geophys. Res. Lett., **32**(7).

Rehbein, A., T. Ambrizzi, and C.R. Mechoso, 2018: Mesoscale convective systems over the Amazon basin. Part I: climatological aspects. Int. J. Climatol., **38**(1), 215-229.

Reynolds, R. W., T. M. Smith, C. Liu, D. B. Chelton, K. S. Casey, and M. G. Schlax, 2007: Daily high-resolution-blended analyses for sea surface temperature. J. Climate, **20**, 5473–5496,https://doi.org/10.1175/2007JCLI1824.1.

Rife, D.L., J.O. Pinto, A.J. Monaghan, C.A., Davis, and J.R. Hannan, 2010: Global distribution and characteristics of diurnally varying low-level jets. J. Climate, **23**(19), 5041-5064.

Rocha, A., and I. Simmonds, 1997: Interannual variability of southeastern African summer rainfall. Part 1: Relationships with air–sea interaction processes. Int. J. Climatol., **17**, 235–265, https://doi.org/10.1002/(SICI)1097-0088(19970315)17:3,235::AID-JOC123.3.0.CO;2-N.

Ropelewski, C.F. and M.S. Halpert, 1986: North American precipitation and temperature patterns associated with the El Niño/Southern Oscillation (ENSO). Mon. Wea. Rev., **114**(12), 2352-2362.

Rossow, W. B., and R. A. Schiffer, 1999: Advances in understanding clouds from ISCCP. Bull. Amer. Meteor. Soc., **80**, 2261–2287.

Rouault, M., S. A. White, C. J. C. Reason, J. R. E. Lutjeharms, and I. Jobard, 2002: Ocean–atmosphere interaction in the Agulhas Current region and a South African extreme weather event. Wea. Forecasting, **17**, 655–669.

Rouault, M., C. J. C. Reason, J. R. E. Lutjeharms, and A. C. M. Beljaars, 2003: Underestimation of latent and sensible heat fluxes above the Agulhas Current in NCEP and ECMWF analyses. J. Climate, **16**, 776–782.

Rouault, M., S. Sen Roy, and R. C. Balling, 2013: The diurnal cycle of rainfall in South Africa in the austral summer. Int. J. Climatol., **33**, 770–777, https://doi.org/10.1002/joc.3451.

Russell, J.O., Aiyyer, A., White, J.D. and W. Hannah, 2017: Revisiting the connection between African easterly waves and Atlantic tropical cyclogenesis. Geophys. Res. Lett., **44**(1), 587-595.

Salio, P., M. Nicolini, and E.J. Zipser, 2007: Mesoscale convective systems over southeastern South America and their relationship with the South American low-level jet. Mon. Wea. Rev., **135**(4), 1290-1309.

Schubert, W. H., , P. E. Ciesielski, , D. E. Stevens, , and H. C. Kuo, 1991: Potential vorticity modeling of the ITCZ and the Hadley circulation. *J. Atmos. Sci.*, **48 ,** 1493–1509.

Simpson, L-A and L. L. Dyson, 2018: Severe weather over the Highveld of South Africa during November 2016. Water SA, **44**, 75-85.

Singleton, A. T., and C. J. C. Reason, 2006: Numerical simulations of a severe rainfall event over the eastern Cape coast of South Africa: Sensitivity to sea surface temperature and topography. Tellus, **58A**, 335–367, https://doi.org/10.1111/j.1600-0870.2006.00180.x.

Singleton, A. T., and C. J. C. Reason, 2007: Variability in the characteristics of cut-off low pressure systems over subtropical southern Africa. Africa. Int. J. Climatol., **27**, 295–310, https://doi.org/10.1002/joc.1399.

Taszarek, M., H. E. Brooks, B. Czernecki, P. Szuster, and K. Fortuniak, 2018: Climatological aspects of convective parameters over Europe: A comparison of ERA-Interim and sounding data. J. Climate, **31**, 4281–4308, https://doi.org/10.1175/JCLI-D-17-0596.1.

Taylor, C. M., A. H. Fink, C. Klein, D. J. Parker, F. Guichard, P. P. Harris, and K. R. Knapp, 2018: Earlier seasonal onset of intense mesoscale convective systems in the Congo basin since 1999. Geophys. Res. Lett., **45**, 13 458–13 467, https://doi.org/10.1029/2018GL080516.

Thompson, D. W. J., and J. M. Wallace, 2000: Annular modes in the extratropical circulation. Part II: Trends. J. Climate, **13**, 1018–1036.

Thompson, R. L., B. T. Smith, J. S. Grams, A. R. Dean, and C. Broyles, 2012: Convective modes for significant severe thunderstorms in the contiguous United States. Part II: Supercell and qlcs tornado environments. Wea. Forecasting, **27**, 1136–1154.

Todd, M. C., R. Washington, and P. I. Palmer, 2004: Water vapour transport associated with tropical–temperate trough systems over southern Africa and the southwest Indian Ocean. Int. J. Climatol., **24**, 555–568, https://doi.org/10.1002/joc.1023.

Tofighi, D., and D.P. MacKinnon, 2016: Monte Carlo confidence intervals for complex functions of indirect effects. *Structural Equation Modeling: A Multidisciplinary J.*, **23**(2), 194 205.

Trier, S. B., and D. B. Parsons, 1993: Evolution of environmental conditions preceding the development of a nocturnal mesoscale convective complex. Mon. Wea. Rev., **121**(4), 1078-1098.

Tsakraklides, G. and Evans, J. L. 2003: Global and regional diurnal variations of organized convection. J. Climate, 16(10), 1562-1572. doi: 10.1175/1520-0442-16.10.1562.

Tyson, P.D., M. Garstang, R. Swap, P. Kallberg, and M. Edwards, 1996: An air transport climatology for subtropical southern Africa. Int. J. Climatol., **16**(3), 265-291.

Tyson, P. D., and R. A. Preston-Whyte, 2000: Weather and Climate of Southern Africa. Oxford University Press, 396 pp.

Tyson, P. D., and R. A. Preston-Whyte, 2015: The Weather and Climate of Southern Africa (2 ed.)., Cape Town. Oxford University Press Southern Africa.

Ukkonen, P., and A. Mäkelä, 2019: Evaluation of machine learning classifiers for predicting deep convection. J. Adv. Model. Earth Syst., **11**, 1784–1802.

Velasco, I., and J. M. Fritsch, 1987: Mesoscale convective complexes in the Americas. J. Geophys. Res., **92**, 9591–9613, https://doi.org/10.1029/JD092iD08p09591.

Vemado, F. and A.J. Pereira Filho, 2021: Convective Rainfall in Lake Victoria Watershed and Adjacent Equatorial Africa. Atmos. Climate Sci., **11**(3), 373-397.

Vizy, E.K., and K.H. Cook, 2018: Mesoscale convective systems and nocturnal rainfall over the West African Sahel: Role of the inter-tropical front. Climate Dyn, 50(1), 587-614.

Virts, K. S., and R. A. Houze, Jr., 2016: Seasonal and intraseasonal variability of mesoscale convective systems over the South Asian monsoon region. J. Atmos. Sci., **73**, 4753–4774, https://doi.org/10.1175/JAS-D-16-0022.1.

Wallace, J.M., and D.S., Gutzler, 1981: Teleconnections in the geopotential height field during the Northern Hemisphere winter. Mon. wea. Rev., **109**(4), 784-812.

Weisman, M. L., and J. B. Klemp, 1982: The dependence of numerically simulated convective storms on vertical wind shear and buoyancy. Mon. Wea. Rev., **110**, 504–520,

Weisman, M. L., and J. B. Klemp, 1984: The structure and classification of numerically simulated convective storms in directionally varying wind shears. Mon. Wea. Rev., **112**, 2479–2498.

Weldon, D., and C. J. C. Reason, 2014: Variability of rainfall characteristics over the South Coast region of South Africa. Theor. Appl. Climatol., **115**, 177–185.

Whitehall, K., and Coauthors, 2015: Exploring a graph theory based algorithm for automated identification and characterization of large mesoscale convective systems in satellite datasets. Earth Sci. Inform., **8**, 663–675, https://doi.org/10.1007/s12145-014-0181-3.

Williams, M., and R. A. Houze, Jr., 1987: Satellite-observed characteristics of winter monsoon cloud clusters. Mon. Wea. Rev., **115**, 505–519.

Xing, J., Ai, H., and S. Lao, 2009: June. Multi-object tracking through occlusions by local tracklets filtering and global tracklets association with detection responses. In 2009 IEEE Confer. Comput. Vision Patt. Recogn., 1200-1207.

Yan, Y.Y., 2005: Intertropical convergence zone (ITCZ). Encyclopedia of World Climatology, J.E. Oliver, Ed., Springer, 429-432.

Yang, Q., R. A. Houze, Jr., L. R. Leung, and Z. Feng, 2017: Environments of long-lived mesoscale convective systems over the central United States in convection permitting climate simulations. J. Geophys. Res., **122**, 13 288–13 307, https://doi.org/10.1002/2017JD027033.

Yang, R., Y. Zhang, J. Sun, S. Fu, and J. Li, 2019: The characteristics and classification of eastward-propagating mesoscale convective systems generated over the second-step terrain in the Yangtze River Valley. Atmos. Sci. Lett., **20**, e874, https://doi.org/10.1002/asl.874.

Zhao, Y., C. Liu, Y. Wang, and M. W. Moncrieff, 2020: Quasistationary extreme rain produced by mesoscale convective system on the Mei-Yu front. Meteor. Atmos. Phys., 132, 721–742, https://doi.org/10.1007/s00703-019-00717-1.

Zipser, E. J., 1982: Use of a conceptual model of the life cycle of mesoscale convective systems to improve very-short-range forecasts. Nowcasting, K. Browning, Ed., Academic Press, 191–204.

Zipser, E. J., D. J. Cecil, C. Liu, S. W. Nesbitt, and D. P. Yorty, 2006: Where are the most intense thunderstorms on Earth? Bull. Amer. Meteor. Soc., **87**, 1057–1072.
BAMS-87-8-1057.

Yuan, J., and R.A. Houze, 2010: Global variability of mesoscale convective system anvil structure from A-Train satellite data. J. Climate, **23**(21), 5864-5888.

Zunckel, M., Held, G., Preston-Whyte, R.A. and Joubert, A., 1996. Low-level wind maxima and the transport of pyrogenic products over southern Africa. J. Geophys. Res. Atmos., **101**(D19), 23745-23755.

Appendices

Appendix A – Tables of a subset of 10 extreme rainfall events from the top 50 ranked extreme rainfall events over the two sub-domains.

Table 5.1A: A subset of 10 extreme rainfall events from the top 50 ranked extreme rainfall events over northern domain in KwaZulu-Natal that are related with an MCSs over the eastern South Africa. The rank of the event within the top 50 is given in the first column, followed by the date of the event, and then various properties of the MCS. The last two columns show the maximum rainfall contribution (%), mean rainfall contribution (%) and median rainfall contribution of each MCS event (per day) to monthly rainfall total.

Rank	**Date**	**Dur. (hours)**	**Max. Size (km^2)**	**T_B min (^oC)**	**Max. Rain. (mm)**	**Max. Contri. (%)**	**Mean. Contr. (%)**	**Media. Contri. (%)**
1	17-Mar-00	27	749,335.3	-83.1	202.1	100	39	39
3	01-Jan-00	12	145,451.8	-76.4	135.4	80	31	30
4	22-Dec-95	21	521,914.1	-80.4	110.1	57	24	23
9	07-Feb-85	6	715,02.98	-75.7	151.0	65	28	29
10	24-Mar-90	51	440,075.1	-83.7	203.9	100	37	31
11	07-Feb-91	15	100,212.3	-83.7	145.6	100	39	36
19	18-Mar-00	39	221,831.5	-82.4	139.5	100	33	33
32	14-Feb-96	18	229,481.4	-88.4	132.5	59	21	22
38	14-Feb-89	15	150,580.1	-72.4	132.8	66	22	23
45	22-Jan-97	6	112,874.2	-71.7	114.7	59	23	23

Table 5.1A: Same as **Table 5.1A** but for events over the southern domain in KwaZulu-Natal.

Rank	Date	Dur. (hours)	Max. Size (km^2)	T_B min (°C)	Max. Rain (mm)	Max. Contri. (%)	Mean. Contri. (%)	Media. Contri. (%)
2	07-Feb-91	21	149,932.6	-77.7	196.1	100	43	44
6	28-Nov-89	15	179,300.7	-75.0	83.9	28	15	15
12	24-Mar-90	51	440,075.1	-83.7	154.2	87	19	14
13	26-Jan-96	21	137,339.5	-88.4	99.7	76	24	23
26	01-Mar-88	6	39,914.88	-64.3	136.1	100	30	28
42	03-Feb-99	6	28,975.34	-59.0	87.5	100	37	30
45	06-Nov-97	9	100,633.8	-63.7	129.8	100	18	18
47	15-Feb-98	6	66,052.2	-62.3	86.6	66	25	23
48	12-Mar-88	30	132,807.2	-65.0	110.9	67	20	28
49	25-Feb-98	6	68,210.63	-58.3	84.7	77	27	25